

THE EFFECT OF CATALYST, HYDROGEN PRESSURE, AND SOLVENT IN COAL LIQUEFACTION UNDER SIMULATED PREHEATER CONDITIONS

J. P. Ferrance, R. P. Warzinski, and B. Bockrath
Federal Energy Technology Center
P. O. Box 10940
Pittsburgh, PA 15236

Keywords: Coal liquefaction preheater simulation, NMP extraction, Thermogravimetric analysis

INTRODUCTION

The purpose of a preheater in a coal liquefaction plant is to raise the temperature of a coal slurry to the reaction temperature before entering the reactor chain. In practice, the preheater actually serves as the first reactor because significant chemical and physical changes take place in the coal slurry as it heats to the reaction temperature. Investigations of these changes were carried out at the Fort Lewis and HRI pilot plants.¹⁻³ In addition to the actual preheaters, microautoclave experiments were used to simulate the HRI preheater as well as the preheater at the Wilsonville pilot plant.^{2,4} These studies have shown that much of the conversion of the coal into initial products is complete by the time the slurry exits the preheater.

All of the preheater studies described above were carried out in the absence of dispersed catalysts; the coal did not contact the catalyst until it entered the first packed-bed reactor. In this arrangement, the slurry was at reaction temperature when it contacted a preactivated catalyst. With dispersed catalysts, the catalyst precursor is added to the initial slurry and travels through the preheater with the coal. For the precursor used in this investigation, no work has been performed which shows whether the short time in the preheater is sufficient to form an active catalyst. If the catalyst did activate, would it have any effect on the coal breakdown reactions taking place in the preheater? The purpose of this study was to look at these issues. Microautoclave experiments were employed in which the loadings of coal, solvent, hydrogen, and catalyst were similar to those used in large-scale coal liquefaction preheaters and in which the heat-up was performed in a manner that reasonably approximated the time/temperature histories of the large units. In addition to routine microautoclave liquefaction product characterization procedures, extraction with N-methyl-pyrrolidone and thermogravimetric analysis were used to gain more insight into the reactions occurring as coal dissolves and begins to liquefy.

EXPERIMENTAL

The reactor used in these experiments was a previously described microautoclave system modified to allow controlled submersion of the reactor into the heated sand bath.⁵ This was accomplished by restricting the airflow to the pneumatic lift on the sand bath. A fairly reproducible internal time/temperature profile was obtained that resembled the available data from the Fort Lewis and Wilsonville pilot plant preheaters. A comparison of these data is shown in Figure 1. The solids concentration of 36.6% and slurry fraction loading of 0.4 used in these experiments were also representative of values used in these preheaters. For the microautoclaves used in these experiments, 7.0 g of coal and 11.0 g of solvent were used. In experiments without solvent, only 7.0 g of coal was placed in the reactor.

The coal used in this study was DECS-17 (Blind Canyon) coal, a bituminous coal from the Penn State Sample bank. The solvent used was a coal-derived vacuum gas oil (VGO) produced by Exxon in its bench-scale coal liquefaction reactor; this material had a boiling range of 274 - 510°C and was 100% soluble in cyclohexane.⁶ The catalyst used in this study was a dispersed MoS₂ formed by the decomposition of Mo(CO)₆ in the presence of H₂S.⁵ The precursor was added at a concentration of 1000 ppm Mo relative to the daf coal in the catalytic experiments. A H₂/3%H₂S gas mixture was used in most experiments at a cold pressure of 7.1 MPa (6.9 MPa hydrogen). One experiment was performed with an equivalent pressure of nitrogen. Also, thermal and catalytic experiments were carried out without solvent at higher (13.8 MPa) and lower (3.4 MPa) hydrogen pressures.

Experiments consisted of filling the reactor then raising the temperature to 425°C, along the profile given in Figure 1, followed by an immediate quench. Several experiments were performed in which the reactor was held at 425°C for 60 minutes following heat-up before being quenched. The products were initially fractionated by sequential extraction with THF and cyclohexane. The THF-insoluble fractions were further fractionated using a modification of published NMP extraction procedures.^{7,8} Small amounts (0.6-0.7 g) of the THF insolubles were refluxed under nitrogen with 90 ml of NMP (BASF) for 1 hour. The solution was centrifuged at

500xg for 60 minutes. The supernatant was collected and the residue resuspended in 90 ml of fresh NMP. The refluxing/centrifugation was repeated 4 times. The combined supernatants were filtered through a 5 μm Mitrex Teflon filter. The residue was washed onto the filter paper with acetone then the filter cake was washed with water and dried overnight in a vacuum oven. The filtrate was concentrated to about 20 ml volume by rotary evaporation. Acidified water (500 ml of 0.002 N) was then added dropwise overnight with stirring to precipitate the NMP-soluble material. This solution was filtered through a second Teflon filter, which was then washed with acetone and dried overnight in a vacuum oven.

TGA experiments were carried out on the cyclohexane-insoluble, NMP-soluble, and NMP-insoluble fractions using a DuPont 951 TGA. An open quartz pan was suspended from the end of the balance arm and filled with 10-15 mg of sample. The TGA was purged with nitrogen then held at 150°C to remove adsorbed water. The temperature was then raised to 900°C at a rate of 10°C/min. At that point, air was introduced into the TGA and the temperature held at 900°C until a constant weight was achieved. The amount of volatile material in the sample was equal to the weight lost as the sample was heated to 900°C. The weight loss following the introduction of air represented the loss of fixed carbon from the sample through oxidation. The weight of the material remaining in the pan following oxidation was the ash content of the sample. Figure 2 shows a typical curve generated by the TGA from an NMP-insoluble fraction.

RESULTS

The list of experiments, conditions, and conversions is given in Table 1. Cyclohexane, THF, and NMP conversion results are reported on a %daf coal basis. The TGA results for the NMP insoluble fractions are also given in Table 1. Because of the differences in conversions and the presence or absence of catalyst, there are large differences in ash contents of the NMP insoluble fractions. For easier comparisons the percentages of volatile matter and fixed carbon are reported on an ash-free basis.

Catalyst Activation Experiments

The $\text{Mo}(\text{CO})_6$ precursor has been extensively investigated in the microautoclave system. Under slow heat-up conditions (approximately 1 h), hydrogen transfer to the DECS-17 coal was shown by a corresponding increase in THF conversion. This occurred at temperatures as low as 325°C, with a pronounced increase in activity at 370°C.⁵ These experiments were performed without an added solvent, which would tend to mask the effect of the catalyst. Whether similar activation occurs under preheater simulation conditions was addressed by performing both thermal and catalytic experiments, again in the absence of solvent.

Solvent-free/Thermal Experiments The first series of experiments listed in the table are the solvent-free experiments. Hydrogen for the liquefaction reactions could only come from either the coal structure or the hydrogen gas phase in these experiments. Since coal conversion is known to be dependent on the amount of available hydrogen, the results should be dependent on the hydrogen pressure in the reactor if hydrogen gas is used in the reactions. For the thermal case, increasing (JF449) or decreasing (JF451) the hydrogen pressure in the reactor had no effect on conversions over the base pressure experiments (JF412, JF450). The fixed carbon content of the NMP insolubles was also the same in all three cases, further indicating that the reactions taking place are independent of hydrogen pressure. Holding the reactor at the reaction temperature for an additional 60 minutes (JF420) resulted in no additional conversion to NMP soluble material, showing that the initial coal decomposition takes place rapidly. The slower secondary reactions continue to take place during the additional time at reaction temperature with a minor increase in THF conversion and a significant increase in cyclohexane conversion. The fixed carbon content of the NMP insolubles increases as these secondary reactions take place, again showing that hydrogen from the coal structure is used in these reactions rather than gas-phase hydrogen.

Solvent-free/Catalytic Experiments The corresponding set of experiments in which $\text{Mo}(\text{CO})_6$ was included in the reaction show much different results from the thermal set. At the base hydrogen pressure, experiments JF413 and JF447 show greater conversion to NMP, THF, and cyclohexane soluble products compared with the thermal experiments. This immediately indicates that the catalyst precursor has become at least partly active when exposed to only this short heat-up profile. This is important, because it shows that a preactivation step may not be needed for certain dispersed catalysts in large-scale liquefaction processes. The large disparity between the NMP and THF conversions for these two experiments carried out under identical conditions has not yet been resolved.

In addition to determining if the catalyst was activated, the hypothesis that the role of the catalyst was to make gas-phase hydrogen available for the liquefaction reactions was also tested. This was accomplished by performing experiments at both a lower (3.4 MPa, JF448) and a higher (13.8 MPa, JF445) hydrogen pressure. The drastic increases in NMP and THF conversion in going to the higher pressure indicate that this hypothesis is probably correct, but the wide variance in the intermediate pressure experiments must be considered. Even at the lowest pressure, however, the NMP conversion is greater than those found in all thermal experiments.

The presence of the catalyst continues to have an effect on conversions, as seen from the 60-minute catalytic experiment (JF417). The NMP conversion has been affected by the longer reaction time showing a small increase; this was not seen in the thermal experiments. As was seen in the thermal 60-minute experiment, however, there is an increase in the fixed carbon content of the NMP insoluble fraction and greatly increased THF and cyclohexane conversions.

One additional insight can be gained by comparing the TGA results of the thermal and catalytic experiments. The fixed carbon content of the NMP insolubles was $58\% \pm 2\%$ regardless of the amount of NMP conversion. This shows that the volatile matter in the NMP insolubles is not preferentially broken down into soluble product, but that the more condensed structures are equally reactive.

Microautoclave Simulations of a Preheater

The second set of experiments listed in Table 1 are those performed using the VGO solvent. These experiments represent the actual simulations of a liquefaction preheater, where a slurry of coal and a coal-derived solvent are in contact with a hydrogen gas phase as the mixture is pumped through the preheater. In an initial set of experiments, not reported in the table, the VGO was tested under thermal and catalytic conditions without coal present. Elemental analysis, average molecular weights, ^1H NMR, and ^{13}C NMR of the treated and untreated VGO showed no differences, indicating that the VGO itself is not reactive under these conditions. As discussed below, however, there is adduction of the VGO to the coal material in some of the coal plus solvent experiments.

The solvent serves as an additional source of hydrogen for the liquefaction reactions. The dramatic increases in NMP and THF conversions over both the thermal and catalytic solvent-free experiments show how important this source of hydrogen is for these reactions. The importance of having good hydrogen transferring solvents during the heat-up phase of the coal liquefaction process has long been recognized.

Thermal Simulations Thermal experiments were carried out under three sets of conditions in which VGO solvent was used. The baseline preheater simulations (JF410, JF415, JF453, JF455) had an average of 88% conversion to NMP solubles and 68% conversion to THF solubles within the five minute heat-up to 425°C. Cyclohexane conversions for these experiments are lower than those for the solvent free experiments, however. The reason for this is that the amount of VGO present is subtracted out of the cyclohexane solubles collected at the end of the experiment. Some of the VGO solvent adducts to larger molecular weight coal molecules, however, and becomes insoluble in cyclohexane. This type of solvent behavior has been reported before with complex solvents.⁹

Performing the same experiment under 6.9 MPa of nitrogen, with no hydrogen gas present (JF414), produces the same NMP and THF conversions. This again shows that the presence of the hydrogen gas is not important in the thermal experiments. An experiment was also performed holding the coal and solvent at 425°C under 6.8 MPa of hydrogen for 60 minutes following the heat-up (JF459). A disproportionation occurs over time, with retrograde reactions causing a decrease in the NMP conversion while secondary reactions increase the THF and cyclohexane conversions. The cyclohexane conversion, however, remains lower than that achieved in the solvent-free experiments held for 60 minutes due to reaction of the solvent with the coal. The NMP insoluble material is also becoming more condensed, with the fixed carbon content increasing almost 20%.

Catalytic Simulations From the previous solvent-free results, it is presumed that the catalyst makes hydrogen gas more readily available for liquefaction reactions. Interestingly, however, this has no effect on the NMP conversion catalytic preheater simulation experiments (JF452, JF454, JF456). The presence of the solvent alone provides sufficient hydrogen for this phase of coal dissolution. The additional hydrogen provided by the catalyst does increase the THF and cyclohexane conversions. The catalyst, however, does not prevent solvent adduction reactions because the solvent-free experiments had greater cyclohexane conversions. Fixed carbon

contents of the NMP insolubles from the catalytic and thermal experiments are the same, indicating that the presence of the catalyst does not change the amount of hydrogen extracted from the coal structure during the liquefaction reactions.

In the 60-minute experiment with catalyst present (JF460), the retrograde reactions which took place without catalyst are prevented. There remains some use of hydrogen from the NMP insoluble material, because the amount of fixed carbon in this fraction still increases. In terms of conversion relative to the zero-minute experiment, there is a slight increase in the NMP solubles with larger increases in both the THF and cyclohexane solubles when the reaction is continued for 60 minutes.

CONCLUSIONS

This study confirmed two conclusions from earlier preheater and preheater simulation experiments: 1) The initial coal breakdown reactions occur very rapidly, and 2) greater than 90% of the total conversion for a system is achieved in the preheater.

For its own objectives, this study showed that dispersed catalyst precursor added to the slurry becomes active as it passes through the preheater. Experiments under different hydrogen pressures indicate that hydrogen gas does not participate in liquefaction reactions under thermal conditions, but seem to indicate that the molybdenum catalyst makes hydrogen from the gas phase available for these reactions. Hydrogen provided by the solvent is more easily used than hydrogen supplied by the catalyst, but the coal itself remains a significant source of hydrogen.

The use of NMP extraction to determine conversion is a valuable method for analyzing liquefaction results. NMP's ability to solubilize more of the coal material than THF gives insights into the formation and breakdown of this material. Especially important is the fact that no NMP-soluble material is formed above what would be produced in the preheater even after 60 minutes of additional reaction. The occurrence of retrograde reactions is also easily detected by increases in the NMP insoluble material.

The usefulness of thermogravimetric analysis to characterize solid products from the liquefaction reactions is also demonstrated. Determination of the fixed carbon contents showed that volatile material in the insoluble fraction is not preferentially converted to lighter products in the initial reactions. The use of hydrogen from the coal structure in the initial and secondary reactions was also identified through the TGA work.

Further work needs to be performed, first to determine the cause of the large variation between experiments JF413 and JF447, and second to apply this analysis to coals of lower rank, which would be more susceptible to retrograde reactions.

ACKNOWLEDGMENTS

Support for one of the investigators (JPF) was provided by an ORISE Fellowship through the Department of Energy's Oak Ridge National Laboratory. We also wish to thank J. Foster for his work on the microautoclave reactions.

REFERENCES

1. DOE/ET/10104-46 1981, 1 & 2
2. Yu, R.K., Comolli, A.G., Johanson, E.S., Hippo, E.J., *Proc. 17th, Inter. Ener. Conv. Eng. Conf.*, 1982, 844
3. DOE/ET/10152-86, 1982.
4. Brandes, S.D., Lancet, M.S., Robbins, G.A., Winschel, R.A., Burke, F.P., DOE/PC/89883-53, 1992.
5. Warzinski, R.P.; Bockrath, B.C. *Energy & Fuels*, 1996, 10, 612.
6. Coless, L.A., Poole, M.C., Wen, M.Y., Exxon Report, 1995, ERLA.2KW.95.
7. Renganathan, K., Zondlo, J.W., Stiller, A.H., Phillips, G., Mintz, E.A., *Int'l. Conf. Coal Sci.*, 1987, 367.
8. Cagniant, D., Gruber, R., Lacordaire-Wilhelm, C., Schulten, H.R., *Fuel*, 1990, 69, 902.
9. McNeil, R.I., Young, D.C., Cronauer, D.C., *Fuel*, 1983, 62, 806.

Table 1
Preheater Simulation Experiments - Conditions and Results

ID	SOLVENT	GAS	COLD		CATALYST PRECURSOR	TIME (min)	CONVERSION			NMP INSOLUBLES (daf%)	TGA RESULTS	
			PRESSURE (MPa)	TIME			Cyclohexane (daf%)	THF (daf%)	NMP (daf%)		Volatiles	Fixed
JF412	NONE	H ₂ /3% <i>H</i> 2S	7.1	NONE	NONE	0	20.3	35.4				Carbon
JF450	NONE	H ₂ /3% <i>H</i> 2S	7.1	NONE	NONE	0	15.1	28.4	44.3	55.7	39.2	60.8
JF451	NONE	H ₂ /3% <i>H</i> 2S	3.4	NONE	NONE	0	17.8	29.4	39.8	60.4	39.3	60.7
JF449	NONE	H ₂ /3% <i>H</i> 2S	13.8	NONE	NONE	0	14.7	27.6	40.7	59.3	42.9	57.1
JF420	NONE	H ₂ /3% <i>H</i> 2S	7.1	NONE	NONE	60	31.8	33.6	40.2	59.8	31.7	66.3
JF413	NONE	H ₂ /3% <i>H</i> 2S	7.1	Mo(CO) ₆	NONE	0	22.5	34.1	55.3	44.7	42.6	57.2
JF447	NONE	H ₂ /3% <i>H</i> 2S	7.1	Mo(CO) ₆	NONE	0	22.4	45.7	64.6	15.4	44.2	55.8
JF448	NONE	H ₂ /3% <i>H</i> 2S	3.4	Mo(CO) ₆	NONE	0	17.6	36.8	50.6	49.4	39.8	60.2
JF445	NONE	H ₂ /3% <i>H</i> 2S	13.8	Mo(CO) ₆	NONE	0	22	52.4	81.7	18.3	44.4	55.6
JF417	NONE	H ₂ /3% <i>H</i> 2S	7.1	Mo(CO) ₆	NONE	60	47.9	63.5	75.4	24.8	32.6	67.4
JF410	VGO	H ₂ /3% <i>H</i> 2S	7.1	NONE	NONE	0	11.7	67	90.3	9.7	45.4	54.6
JF415	VGO	H ₂ /3% <i>H</i> 2S	7.1	NONE	NONE	0	7.4	68.9	91.3	8.7	52.0	48.0
JF453	VGO	H ₂ /3% <i>H</i> 2S	7.1	NONE	NONE	0	2	68.4	89.6	10.4	50.0	50.0
JF455	VGO	H ₂ /3% <i>H</i> 2S	7.1	NONE	NONE	0	4.1	68.6	81.7	18.3	47.4	52.6
JF414	VGO	N ₂	6.9	NONE	NONE	0	18.9	66.5	89.5	10.5	49.8	50.2
JF459	VGO	H ₂ /3% <i>H</i> 2S	7.1	NONE	NONE	60	24.7	71.4	82	18	32.0	68.0
JF452	VGO	H ₂ /3% <i>H</i> 2S	7.1	Mo(CO) ₆	NONE	0	9.2	69.7	84.9	15.1	43.7	56.3
JF454	VGO	H ₂ /3% <i>H</i> 2S	7.1	Mo(CO) ₆	NONE	0	13.6	71.4	92.6	7.4	49.7	50.3
JF456	VGO	H ₂ /3% <i>H</i> 2S	7.1	Mo(CO) ₆	NONE	0	7.1	73.8	87.9	12.1	48.6	51.4
JF460	VGO	H ₂ /3% <i>H</i> 2S	7.1	Mo(CO) ₆	NONE	60	38.4	84.8	91.5	8.5	36.6	63.4

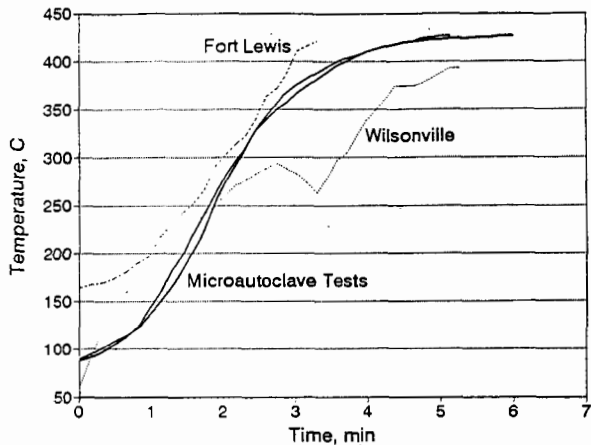


Figure 1. Comparison of microautoclave heating profiles with those from the Fort Lewis and Wilsonville pilot plants.

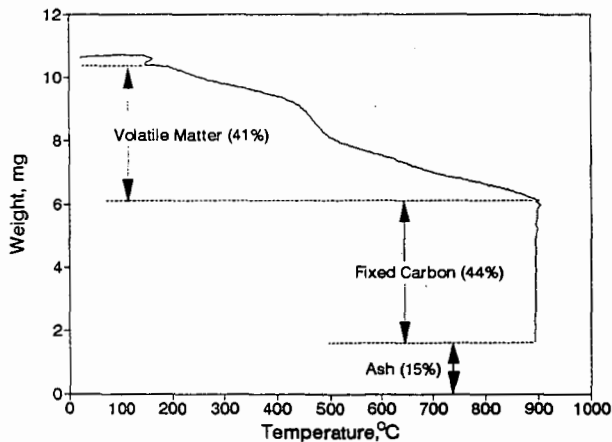


Figure 2. TGA curve of the NMP-insoluble material from experiment JF456 which contained both solvent and catalyst.

ACID CATALYZED DEPOLYMERIZATION OF COAL UNDER MILD CONDITIONS WITH SUPERACID HF/BF₃

Kiyoyuki Shimizu*, Ikuo Saito, Hiroyuki Kawashima
National Institute for Resources and Environment, AIST.
16-3 Onogawa, Tsukuba, Ibaraki 305-8569, Japan.

Shinsuke Sasaki, Akira Suganuma
Science University of Tokyo, Noda, Chiba 278-8510, JAPAN

Keywords: Coal solubilization, Superacid, Depolymerization

1. INTRODUCTION

Acid-catalyzed coal depolymerization has been widely studied as a way to liquefy coal under milder conditions^{1,4}. However, it is usually very difficult to recover completely the acid catalyst from solids or products. HF/BF₃, which has been recognized as a Bronsted/Lewis superacid catalyst for Friedel-Crafts reactions: isomerization and separation of m-xylene, and formylation of aromatic compounds on an industrial scale (Mitsubishi Gas Chemical Co., Ltd.). HF/BF₃ mixtures are fully recoverable from the product by distillation only, and can be reused, because their boiling points are very low (HF: 19.9°C, BF₃: -101°C). Olah studied coal liquefaction using the HF-BF₃-H₂ system and HF-BF₃-isopentane⁵. We also reported that HF and HF/BF₃ in the presence of toluene depolymerized coal more efficiently at 100-150°C through the acid-catalyzed transalkylation reaction of coal⁶.

In the present study, solubilization of coals of different rank were carried out at 50-150°C in order to evaluate recyclable superacid HF/BF₃ as catalyst for efficient depolymerization of coal of different rank via an ionic reaction. The depolymerization of coals in the acid-catalyzed reaction process was considered in terms of the chemical structure of coals and behaviors of oxygen containing functional groups.

Table 1 Elemental analyses of the treated coals.

Run	Elemental analyses (wt%, daf base)				ash (wt%)
	C	H	N	O _{air}	
Yallourn	65.6	4.6	0.6	29.20	1.3
Taiheiyo	73.3	6.4	1.2	19.1	13.7
Miike	82.0	6.7	1.2	10.1	14.7

2. EXPERIMENTAL

Yallourn lignite, Taiheiyo subbituminous and Miike bituminous coal were used, ground to a diameter of 0.25mm less and dried in a vacuum at 110°C for 24h (Table 1). The liquefaction was carried out in a hastelloy-C microautoclave of 100 ml capacity. Coal (5 g) and toluene or isopentane (20ml) were placed in the dry ice-methanol cooled autoclave. First, the reactor of autoclave was evacuated by vacuum pump; then the HF (0.582 g/g-coal) and BF₃ (0.219 g/g-coal) were introduced to the coal-solvent slurry while dry ice-methanol cooling continued. Gaseous hydrogen (5.1 MPa) was introduced to autoclave after BF₃ when instead of toluene or isopentane. The autoclave was then heated to 50-150°C at a heating rate of 1.5°C/min for 3 h under autogenous pressure with vigorous stirring. After the reaction, gaseous HF/BF₃, solvent and volatile fraction from toluene in the autoclave were depressurized and absorbed into ice-water at 90-110°C under flowing nitrogen gas (100-150 mL/min) with stirring (300rpm) for 2h. The contents of the autoclave were slowly poured into cool water, and then were gradually neutralized with an cool aqueous solution (5 wt%) of Na₂CO₃. The products were filtered and washed in water with sonication. Washing with an aqueous methanol solution (30-50 vol%) was repeated 3 times in order to remove small

amount of neutralized product NaF and dimer of toluene. The solid product was vacuum-dried at 110°C for 24h. Reaction conditions are summarized in Table 2. Calculation to obtain the yield of solubles and weight increase has been described in detail elsewhere⁵.

The products were extracted with benzene, THF and pyridine in a sequential Soxhlet extractor. Oxygen-containing functional groups were determined by the method of Hatami et al. This determination has been described in detail elsewhere⁶.

The ¹³C-CP/MAS solid-state NMR spectra were measured with a chemagnetics at 75.58 MHz. The following operating parameters were used: a spectral width of 30 kHz, a 90 proton pulse of 5 μs, an acquisition time of 34.130 ms, a pulse repetition time of 4 s and an accumulation of 4000 scans.

3. RESULTS AND DISCUSSION

3.1 Effects of reaction temperature

The effects of reaction temperature on coals solubilization in the presence of HF/BF₃ (7 mol%) are shown in Figure 1. The reaction at even 50°C showed higher extractability than original coals. The reaction at 100°C greatly increased extractability, especially Miike bituminous coal could solubilize almost completely. The reaction at 150°C resulted in high extractability as described. Pyridine soluble yield in the treated coals at the lower reaction temperature of 50 and 100 °C was increased with increasing of carbon content in coal. However, the extractability of product from any coal was not changed at the reaction temperature of 150°C.

3.2 Effects of stabilizer

The extractability of the products treated with different kinds of stabilizer are shown in Figure 2. Extractability of products from Yallourn lignite depend very much upon the kinds of stabilizer. Although it can solubilize nearly completely by the reaction with toluene isopentane and hydrogen showed lower extractability such as 49 and 20 wt%, respectively. Differences of extractability in the case of Taiheiyō subbituminous coal was smaller than Yallourn lignite. And the products from Miike bituminous coal was not significantly changed with kind of stabilizer.

3.3 Oxygen containing functional groups

The distribution of oxygen-containing functional groups in the original coals and the treated coals is summarized in Table 3. Oxygen-containing functional groups were divided into 4 groups (carboxylic, hydroxyl, carbonyl group and Orest). Orest is mostly ascribed to ether groups such as Ar-CH₂-O-R, Ar-O-Ar and Ar-O-R. Most of the oxygen-containing functional groups decreased after the reaction. Decreasing of ether bonds, carboxylic and hydroxyl groups were increased with increasing of reaction temperature. This highly deoxygenation during reaction at 150°C would be cause of high extractability of products. The reaction with isopentane under HF/BF₃ at 150 °C retained more hydroxyl groups and ether bond in the products than did the reaction with toluene, indicating that these oxygen containing functional groups remained restricted extractability, leading that lower coal depolymerization. In contrast, Miike bituminous coal inherently have small amount of oxygen containing functional groups, and their decreasing after reaction was substantially small, therefore behaviours of oxygen containing functional groups in Miike coal did not contribute the solubilization reaction.

These results indicated that Miike bituminous coal comparatively easy to produce highly soluble products even at any reaction conditions because of small amount of oxygen containing functional groups. In contrast, Yallourn lignite which have more amount of their functional groups and its content in products depend on the reaction condition such as kind of stabilizer and reaction temperature.

3.4 CP/MAS-¹³C NMR spectra

Table 4 summarizes the carbon distributions of original coals and treated coal from the reaction with HF/BF₃ under gaseous hydrogen. The carbon atoms were classified into

7 categories as shown. Original Yallourn lignite have more aromatic carbons bound to oxygen (phenolic-OH), oxygen functional groups C=O, COOH and other bond (-O-CH₂-), but less methylene bridges and terminal CH₃ content when compared with those of Taiheiyo subbituminous and Miike bituminous coal. After the reaction, decreasing of methylene bridges in the Yallourn treated coal was the lowest by less 5%. In contrast, Taiheiyo and Miike coal showed more reduction of methylene bridge. The Yallourn treated coal have more aromatic carbons bound to oxygen and oxygen containing functional groups than those of products from others. These results indicated that the improvement of extractability of Taiheiyo and Miike coal was ascribed to the cleavage of methylene and other bridges in their coal, while lower extractability of Yallourn treated coal was caused by small cleavage of methylene bridge and a significant amount of oxygen containing functional groups.

4. CONCLUSIONS

1. Solubilization of higher-rank coals, Miike bituminous coal, by any reaction conditions was almost higher than those of lower rank coals.
2. Solubilization of lignite, Yallourn coal, depend upon reaction conditions, it was greatly changed by the stabilizer and reaction temperature.
3. The reaction with toluene as stabilizer significantly solubilized even Yallourn lignite coal because of more cleavage of ether groups and deoxygenation.

5. REFERENCES

1. Heredy, L.A. and Neuworth, M.B. Fuel 1962, 41, 21
2. Larsen, J.W. and Kuemmerle, E.W. Fuel 1976, 55, 162
3. Kumagai, H., Shimomura, M. and Sanada, Y. Fuel Process. Technol. 1986, 13, 97
4. Farasiu, M. Fuel Process. Technol. 1986, 14, 161
5. Olah, G.A., Bruce, M.R., Edelson, E.H. and Husain, A. Fuel 1984, 63, 1130
6. Shimizu, K. and Saito, I. Energy & Fuels, 1997, 11, 115.

Table 2 Reaction condition of the treated coals.

Run	Temp. (°C)	HF (g)	BF ₃ (g)	solvent	W1 (%)
Y-1	50	5.8	1.10	toluene	37
Y-2	100	5.8	1.18	toluene	44
Y-3	150	5.8	1.26	toluene	97
Y-4	150	5.8	1.24	isopentane	32
Y-5	150	5.4	1.38	H ₂	-7
T-1	50	5.10	1.38	toluene	18
T-2	100	4.92	1.28	toluene	35
T-3	150	5.8	1.39	toluene	71
T-4	150	5.5	1.38	isopentane	24
T-5	150	5.82	1.38	H ₂	-14
M-1	50	5.46	1.4	toluene	11
M-2	100	5.46	1.4	toluene	9
M-3	150	5.82	1.4	toluene	113
M-4	150	6.06	1.25	H ₂	-3

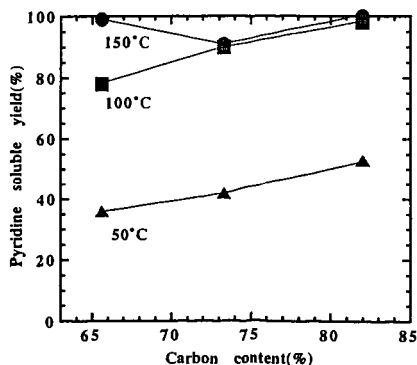


Figure 1 Effect of reaction temperature on extractability of treated coal with HF/BF₃.

Reaction condition: 3 h, toluene

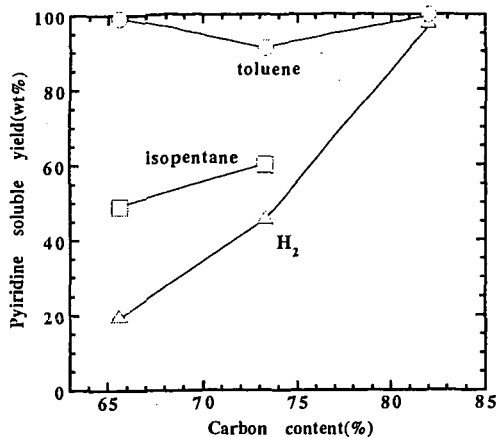


Figure 2 Effect of stabilizer on extractability of treated coal with HF/BF₃.

Reaction condition: 150°C, 3h

Table 3 Distribution of oxygen containing functional group in original coal and the treated coals.

Run	Reaction conditions				wt%				
	Temp. (°C)	HF (g)	BF ₃ (g)	solvent	COOH	OH	C=O	O _{rest}	Total
Yallourn					4.1	5.7	4.5	14.9	29.2
Y-1	50	5.8	1.10	toluene	1.9	5.0	2.8	12.8	22.5
Y-2	100	5.8	1.18	toluene	2.3	2.9	4.2	8.4	17.8
Y-3	150	5.8	1.26	toluene	0.6	1.8	4.5	6.5	13.4
Y-4	150	5.8	1.24	isopentane	0.8	3.9	4.5	9.0	18.0
Taiheiyō					0.6	5.3	3.4	9.8	19.1
T-1	50	5.10	1.38	toluene	1.0	5.1	2.8	3.7	12.6
T-2	100	4.92	1.28	toluene	0.5	6.1	2.9	3.0	12.5
T-3	150	5.8	1.39	toluene	0.7	3.4	2.8	1.7	8.6
T-4	150	5.5	1.38	isopentane	1.2	4.6	3.4	4.3	13.5
Miike					0.1	3.3	1.1	3.6	8.1
M-2	100	5.46	1.4	toluene	-	1.7	1.9	3.8	7.4
M-3	150	5.82	1.4	toluene	-	0.7	2.5	3.4	6.6

Content of oxygen functional groups and total oxygen were corrected with weight increase.

O_{rest}: ether or ester groups

Table 4 Carbon distribution in original and treated coals by NMR.

(ppm)	COOH, C=O (220-171)	Phenolic C-O (171-149)	Ar-C (149-128)	Ar-H (128-93)	-CH ₂ -O- (75-50)	-CH ₂ -CH (55-22)	-CH ₃ (22-0)
Yallourn	7.1	12.9	17.2	27.2	9.4	22.3	3.9
Y-5	8.5	14.6	18.7	26.0	6.6	18.8	6.8
Taiheiyō	4.3	8.2	15.3	24.4	7.0	34.1	6.7
T-5	3.7	9.6	18.4	29.7	7.8	22.9	7.9
Miike	4.3	8.3	15.7	24.4	5.9	32.5	8.9
M-4	3.6	10.0	21.7	31.5	6.5	18.6	8.1

PYROLYSIS OF COAL WITH HYDROGEN ATOMS

J. Bi, T. Kamo, Y. Kodera, H. Yamaguchi, and Y. Sato

Energy Resources Department,
National Institute for Resources and Environment
16-3 Onogawa, Tsukuba-city, Ibaraki, 305-8569 Japan

Keywords: coal hydrolysis, hydrogen atom, low pressure

ABSTRACT

The reactions of coal directly with hydrogen atoms are very important for understanding the mechanisms of coal liquefaction and coal hydrogasification. In the present study, Taiheiyō coal was reacted in a low pressure TG with hydrogen atoms (induced by microwave discharge cavity) and hydrogen gas under a pressure range of 1.0 - 50.0 torr, and a temperature range of 20 - 1000°C, with heating rates of 5-20 °C/min. The yields of char, gas and liquid were measured and analyzed by TG-MS and GC-MS respectively. The results showed that the conversion of coal with hydrogen atoms was higher than that under low pressure of hydrogen gas. More liquid and gas products were obtained in the reaction with hydrogen atoms. It was observed that in the presence of hydrogen atoms, CO was more produced at a relative low temperature. Alkylated naphthalene compounds in the liquid yield were less produced in the reaction with hydrogen atoms than in the atmosphere of hydrogen gas.

INTRODUCTION

It is recognized that reactions of coal hydrolysis has a significant effect on the yield and distribution of end products such as coal-derived liquids, gases, coke, or pollutant emissions in the processes of coal liquefaction and coal hydrogasification under various conditions. In usual coal hydrolysis, thermal decomposition of coal occurs first and tar and some light carbonhydrogen compounds release at/around 400-500 °C. After the temperature is increased to that hydrogen decomposes, then the hydrogen atoms react with coal, coal-derived pyrolysates and char, yielding products with a rather wide molecular distribution. Therefore the mechanism in hydrolysis is much more complex comparing with in pyrolysis. To investigate the reactions of coal directly with hydrogen atoms are very important for understanding the mechanism of hydrolysis. However, the information on reaction of coal directly with hydrogen atoms is limited. Amano et al.¹⁾ investigated reactions between carbonized coal and hydrogen atoms using a discharge flow apparatus in a temperature range of 130-250 °C under 1Torr pressure. They found that oil yielded in the presence of hydrogen atoms has a different composition from that in the absence of hydrogen atoms, while a similar composition with that of middle fraction of petroleum distillate. In their another study²⁾, it was found that the liquid products contain more monocyclic alkanes, which is rather different from the liquid products yielded in conventional coal liquefaction. In addition, the liquid products contain little compounds of heteroatoms.

Hydrolysis require more detailed chemical information to predict the distribution of final products. Especially the reactions of coal directly with hydrogen atoms are needed to be further investigated under a wide conditions. The present study investigated coal reactions in the presence and absence of hydrogen atoms by means of vacuum TG/MS. Gas components of CH₄, CO and CO₂ were quantitatively measured and their variations with temperature were observed. The liquid products obtained at different temperatures were analyzed and compared in different atmospheres.

EXPERIMENTAL

A vacuum thermogravimetry(TG, Rigaku, Thermo plus TG8120) was used to observe the variation of coal weight, as shown in Figure 1. About 4.0 mg(-100 mesh) of Taiheiyō coal was placed in a quartz pan(φ5mm) which was inserted into a quartz tube reactor. The pan was heated from ambient temperature to 1000 °C at a linear heating rate of 5 °C/min. The oven temperature was measured and controlled at the bottom of the pan by using a thermocouple. The pressure in the TG balance chamber was evacuated and controlled at less than 1.0 torr by a rotary vacuum pump and an adjustable valve.

Ultimate analysis data of Taiheiyō coal are 74.1 C, 6.4 H, 1.3 N, 18.0 O (by difference), 0.2 S(wt%, daf) and 14.2% ash(dry base).

Hydrogen gas was introduced to the TG chamber at a flow rate of $1.0\text{cm}^3/\text{min}$ (standard temperature and pressure, STA). Hydrogen atoms were induced by passing hydrogen gas through a microwave discharge cavity (2450 MHz). The discharge cavity was located at an introduction tube which was 10 cm above the quartz reactor. Total distance between the discharge cavity and the coal sample was about 20 cm which ensured the influence of plasma and UV from the discharge on the coal sample could be negligible. To prevent recombination of the hydrogen atoms, boric acid solution was coated in the inner surface of the reactor. For comparison, helium gas was also used under the same conditions as hydrogen gas was used.

The produced gas were analyzed by a mass spectrometer (MS, Balzers QMG112A). A turbomolecular pump (Balzers TMH/U 260) was used for evacuating the MS chamber up to 10^{-7} torr. MS conditions were set as follows: electron ionization voltage 70 eV, mass range scanned 1-110 amu, scan sweeping time 52 s. Each spectrum scanned was recorded and stored by computer through a MS interface (VTI, Aero Scan 1600MS/RGA).

Argon gas at a flow rate of $0.01\text{cm}^3/\text{min}$ (STA) was used as internal standard. Relation between ion intensity and flow rate of CH_4 , CO and CO_2 was calibrated. Therefore the gas products could be quantitatively measured through the ion intensity ratios of argon to CH_4 , CO and CO_2 . Before the experiment began, the background ion intensity was recorded and then subtracted during data treatment.

The liquid products were collected in a sample tube packed by Tenax powder. The sample tube was inserted in a U-tube immersed in a dry ice trap. Using a flash thermal desorption cold trap injector, the liquid products were analyzed by a gas chromatography (GC, HP-6890).

RESULTS AND DISCUSSION

1) Coal conversion

Coal weight variations with temperature in different atmospheres are described in Figure 2. It can be seen that the differences of weight variations in hydrogen gas, helium gas and discharged helium gas atmospheres are not so significant, where the weights decrease rapidly at around $400\text{ }^\circ\text{C}$ and the coal conversions at $800\text{ }^\circ\text{C}$ are about 50%. It reflects that hydrogen gas almost does not affect the pyrolysis reactions under low pressure. It also reflects that the discharge has scarce effect on pyrolysis in the present experiment, comparing the profiles between in the helium gas and in the discharged helium gas. However, the weight decreases rapidly at around $300\text{ }^\circ\text{C}$ in the hydrogen atom atmosphere and remarkable higher coal conversion, more than 60% at $800\text{ }^\circ\text{C}$, is observed with temperature increase. This result suggests that hydrogen atoms promote significantly the pyrolysis reaction at a lower temperature.

2) Gas products

CH_4 , CO and CO_2 gas yield rate profiles with temperature in the absence and presence of hydrogen atoms are shown in Figure 3. In the hydrogen atmosphere, as shown in Figure 3(a), CH_4 reaches the maximum at around $500\text{ }^\circ\text{C}$, CO has an increase tendency with temperature and CO_2 increases to the maximum before $400\text{ }^\circ\text{C}$ then decreases. In the reaction with hydrogen atoms, as shown in Figure 3(b), the profile patterns are quite different comparing with Figure 3(a). CH_4 has two peaks at around $200\text{ }^\circ\text{C}$ and $400\text{ }^\circ\text{C}$. In particular, CO has a sharp increase at $200\text{ }^\circ\text{C}$ then a small peak at $400\text{ }^\circ\text{C}$. CO_2 increases to the maximum at $200\text{ }^\circ\text{C}$ then decreases.

Mechanism is not exactly understood why CO increases so much. It is not likely that the shift reaction should be responsible for much CO yielded, since CO_2 increases not so dramatically as CO in the present experiment. The clarification of the mechanism is needed.

3) Liquid products

Figure 4 shows total amounts of BTX or monocyclic hydrocarbon compounds obtained at different temperatures in the absence and presence of hydrogen atoms. It can be seen that the amounts in the reaction with hydrogen atoms are much more than those in the hydrogen atmosphere with temperature increase. Comparing the amounts at $400\text{ }^\circ\text{C}$ and $600\text{ }^\circ\text{C}$ in different atmospheres, the amount increases about 5 times at $400\text{ }^\circ\text{C}$ while about 2 times at $600\text{ }^\circ\text{C}$. Combining the gas yields produced before $300\text{ }^\circ\text{C}$ as shown in Figure 3(b), this reflects partly that why coal weight decreases rapidly at $300\text{ }^\circ\text{C}$ in the reaction with hydrogen atoms as shown in Figure 2. It can also be seen that relatively more BTX compounds are produced at $800\text{ }^\circ\text{C}$ in the reaction with hydrogen atoms. From the liquid product distribution, more monocyclic compounds and less naphthalene compounds were yielded in the reaction with hydrogen atoms than in the hydrogen atmosphere.

In the reaction of coal with hydrogen atoms, it was observed that tar was less produced comparing with in hydrogen atmosphere under the same conditions.

Exact amount of hydrogen atoms generated are not known. It was estimated¹⁾ about 10% of the hydrogen was in atomic state near the discharge cavity when 2450 MHz microwave discharge was applied. Even less amount of hydrogen atoms exist, the impact on the pyrolysis is profound from the present experiment.

4) Effects of pressure and heating rate

Pyrolysis was also carried out in a wider experimental conditions in the hydrogen atmosphere. Increasing the pressure from 1 torr to 10, 20 and 45 torr showed a decrease in gas products. Increasing the heating rate from 5 °C/min to 10 and 20 °C/min resulted in an increase in gas products. It implies that the effect of heating rate on the gas products of small molecules is probably different from the effect on the larger molecular compound products (amu values larger than 50) as observed by Yun' et al.³⁾ where they found that the pyrolysate distributions of primary pyrolysis reactions in Pittsburgh No. 8 coal are independent of heating rate over a magnitude of 10^{-2} - 10^4 °C/s when monitoring the 50-200 amu mass range.

CONCLUSIONS

Pyrolysis of Taiheiyō coal in the reaction with hydrogen atoms was investigated and compared with pyrolysis in the hydrogen atmosphere. The result showed that the conversion of coal with hydrogen atoms was higher than that with hydrogen gas, and more liquid and gas products were obtained in the former case. It was observed that in the presence of hydrogen atoms, CO was more produced at a relative low temperature. More monocyclic compounds and less naphthalene compounds were yielded in the reaction with hydrogen atoms than in the hydrogen atmosphere.

REFERENCES

- 1) Amano, A., Yamada, M., Shindo, T., Akakura, T., Yotsusuji, S., *Inst. of Chem. Soc. of Jpn*, 1984, No. 10, 1648-1655
- 2) Amano, A., Yamada, M., Shindo, T., Akakura, T., *Fuel*, 1984, Vol. 63, May
- 3) Yun, Y., Maswadeh, W., Meuzelaar, H.L.C., Simmleit, N., Schulten, H.R., *Energy & Fuels*, 1991, 5, 22-29

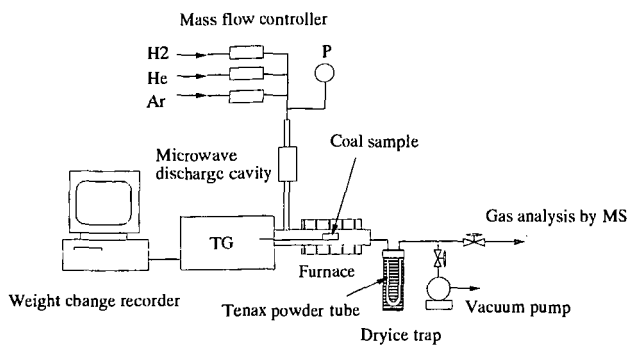


Figure 1. Experimental apparatus

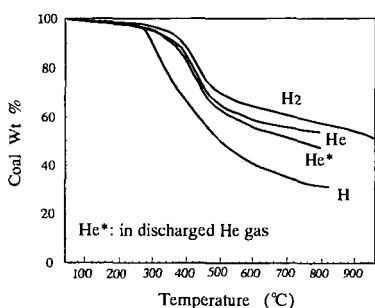


Figure 2. Coal weight decrease with temperature in various gas atmospheres

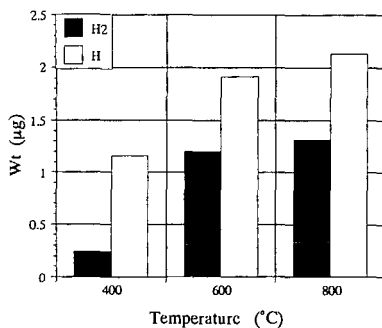
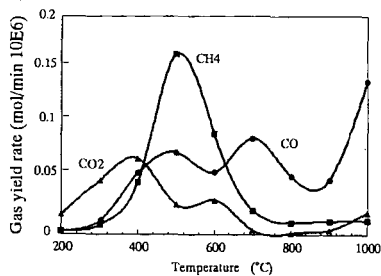
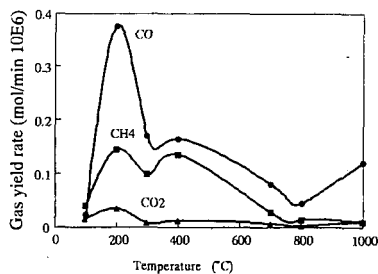


Figure 4. Weight variation of BTX compounds with temperature



(a) In H₂ atmosphere



(b) In H atmosphere

Figure 3. Main gas yield rate with temperature

STUDY ON INTERACTION BETWEEN COAL AND MODEL PLASTICS DURING LIQUID-PHASE CATALYTIC COLIQUEFACTION

H. Yamaguchi^a, Y. Okuyama^a, K. Matsubara^b, J. Bi^c, Y. Kodera^c, T. Kamo^c and Y. Sato^c

^a NKK Corp., 1-1 Minamiatarida-cho, Kawasaki, 210 Japan

^b NK Techno Service, 1-1 Minamiatarida-cho, Kawasaki, 210 Japan

^c National Institute for Resources and Environment, 16-3 Onogawa, Tsukuba, 305 Japan

ABSTRACT

Coliquefaction of Tanitoharum coal with PP, PS, high-density PE was carried out using red mud plus sulfur as the catalyst, at 430 °C for 60 min under 7 MPa initial pressure of hydrogen. There existed almost linear relationship of coal concentration in coal/plastics mixture with conversion to THF-soluble (THFS) or oil yield for the mixture of coal/PP, coal/PS or coal/PE in case of tetralin. Observed oil yield at 75 % of coal concentration for any coal/plastics mixture was slightly larger than that calculated. The use of decalin gave lower values of conversion, yields of THFS in VR and oil, particularly at coal concentration of 75% for the coal/PE mixture, compared to those calculated, while a similar tendency as to interaction in respect of conversion, yields of THFS in VR, oil, and gas was observed for the mixture of coal/PP and coal/PS. However, when the coal was reacted with mixed plastics of PP, PS and PE at coal concentration of 50 %, the interaction observed for the coal/PE mixture disappeared, and higher oil yield than that calculated was obtained. The results suggested interaction between PE and the other plastics (PP, PS) is larger than that between coal and PE. It is also suggested from the results for the coal/PP mixture that radicals from PP cracking was used for stabilization of radicals from the coal and PP, instead of hydrogen donated from gas and solvent. Higher values of conversion and oil yield for the use of decalin were obtained, compared to tetralin. The results indicated that a good hydrogen donor solvent would not be necessary in case of the use of catalyst for coliquefaction of coal with waste plastics.

Keywords: coal liquefaction, model compounds, waste plastics

1. INTRODUCTION

Under conventional direct coal liquefaction process, large amount of hydrogen gas is consumed to stabilize radical fragments from thermal cracking of coal. At present the price of produced coal liquid does not compete with that of crude oil, due to not only the severe operating conditions, but also the expensive production cost of hydrogen gas. Coprocessing of coal with heavy oil containing high concentrations of sulfur and heavy metals, has been investigated to improve the economical feasibility¹⁾. On the other hand, large amounts of waste plastics is being generated in Japan, mostly not recycled. The shortage of landfilling site has become more serious in recent years. Thus, coliquefaction of coal with heavy oil and waste plastics would be an attractive process of overcoming environmental problems and further enhancing economical feasibility. However, few studies have reported on this reaction, due to the complicated reaction system²⁾. We have conducted a model experiment of coliquefaction of coal with waste plastics using dibenzyl as a coal model compound to clarify the reaction mechanism, and investigated interactions between coal and plastics, and between the plastics, in respect of conversion, product distribution and composition of distillate oil³⁾.

In this study, catalytic coliquefaction of coal with model plastics was conducted under the same reaction conditions as those for the model experiment. Interaction between the coal and plastics was investigated in respect of conversion, product distribution, and H₂ transferred from gas or solvent, and the reaction mechanism involved was discussed.

2. EXPERIMENTAL

Catalytic coliquefaction of Tanitoharum coal (-100 mesh, C 75.91, H 5.66, N 1.62, S 0.37, O 16.44 (wt% daf (dry ash free) base)) with model plastics (PP, PS, high-density PE) and their mixture (1/1/1 by weight) was carried out at 430 °C for 60 min in a 500-ml magnetically stirred autoclave. Tetralin or decalin was used as the solvent. Red mud (total Fe 28.37 wt%) plus sulfur (1/1 by weight) was used as the catalyst. Weight ratio of (daf coal + plastics)/solvent/red mud was 100/150/3/3. Gas atmosphere was 7 MPa initial pressure of hydrogen gas. After the reaction, the measurement of gas volume and GC analysis were conducted for the product gas. Main part of the product liquid (plus any unconverted solid reactant and catalyst) was separated into distillate oil (-538 °C) and vacuum residue (+538 °C, VR) by vacuum distillation. The product liquid in part was subjected to Soxhlet extraction with hexane, tetrahydrofuran (THF) sequentially. Conversion to hexane & THF-soluble (THFS), yields of oil, hexane & THF-soluble in vacuum residue (THFS in VR), gas, and hydrogen gas consumption were measured, based on the weight of daf coal plus plastics by conventional methods. The composition of the distillate oil was analyzed using FID/GC. H₂ transferred from solvent was calculated from mass balance of naphthalene, decalin for the use of tetralin as the solvent

or tetralin, naphthalene for the use of decalin, before and after the coliquefaction⁴⁾.

3. RESULTS AND DISCUSSION

Coliquefaction of coal with PP, PS or PE using tetralin

In Fig. 1, conversion to THFS, yields of oil, THFS in VR, and gas for coliquefaction of Tanitoharum coal with each of PP, PS or PE using tetralin were plotted against coal concentration in coal/plastics mixture.

Without any coexisting reactant, for each of the coal, PP, PS and PE, conversion of 99.7, 100, 100, 31.9 wt%, oil yield of 37.4, 76.4, 94.0, -1.2 wt%, yield of THFS in VR of 41.1, 13.9, 2.9, 28.8 wt%, and gas yield of 11.9, 10.1, 4.0, 3.9 wt%, respectively were obtained. PE was most difficult to be converted to THFS and oil among the reactants, while PS was almost converted to oil. For PP, conversion was very high, and larger yield of THFS in VR was produced, compared to PS. Gas produced from PP was largest among the plastics. For the coal, oil yield was much lower than those for PP and PS, in spite of very high conversion, and production of THFS in VR was largest among the reactants.

In case of coliquefaction, there existed almost linear relationship of coal concentration with conversion to THFS or oil yield. Oil yield at 75 % of coal concentration for the mixture of coal/PP, coal/PS or coal/PE was higher by 4.9, 4.8, 3.3 wt% respectively than that calculated (arithmetic mean value of results for each reactant). As to THFS in VR, almost linear relationship against coal concentration was obtained for the mixture of coal/PS or coal/PE, but observed values for the coal/PP mixture were higher than those calculated. As to gas yield, observed values for any coal/plastics mixture were lower than those calculated. The difference between the calculated value and the observed value was very large for the coal/PP mixture, compared to the other coal/plastics mixture.

Fig. 2 shows H₂ transferred from gas and solvent in this reaction as a function of coal concentration in coal/plastics mixture.

H₂ transferred from gas or tetralin (mmol/g-daf reactant) was 15.5, 4.6 for the coal, 4.4, 1.9 for PP, 6.6, 3.1 for PS, and 0.94, 0.62 for PE, respectively. H₂ transferred from gas or tetralin for coal was largest among the reactants. It was observed that larger amounts of H₂ from gas or tetralin was transferred for PS than for PP. The amounts of H₂ transferred was small for PE. However, it is thought by considering the difference in conversion between PP and PE that the values for PE would become similar to those for PP when 100 wt% of conversion is obtained for PE.

For the coal/PE mixture, almost linear relationship of H₂ transferred with coal concentration was recognized. For the coal/PS mixture, H₂ transferred from gas were a little larger than those calculated, while H₂ transferred from tetralin were a little lower than those calculated. No difference in total of H₂ transferred between the observed value and the calculated value was observed. For the coal/PP mixture, H₂ transferred from gas or tetralin was lower than that calculated. The results from Figs. 1 and 2 for the coal/PP mixture suggest that radicals from PP cracking would be used for stabilization of radicals from the coal and PP, instead of hydrogen donated from gas and solvent.

Decomposition of PE proceeds as radical chain reaction. In the model experiment of coliquefaction of dibenzyl (DB) as a coal model compound with model plastics using tetralin and the same catalyst, conversion and yield of THFS in VR were higher than those calculated, suggesting that radicals from DB decomposition would secondarily attack PE³⁾. However, the tendency for the coal/PE mixture as seen in Figs. 1 and 2 is different from that in the model experiment. On the other hand, the mixtures of coal/PP and coal/PS showed almost the same tendencies as those from the model experiment.

Coliquefaction of coal with PP, PS or PE using decalin

In Fig. 3, conversion to THFS, yields of oil, THFS in VR, gas, and H₂ transferred for coliquefaction of the coal with each of PP, PS or PE using decalin were plotted against coal concentration in coal/plastics mixture.

Without any coexisting reactant, for each of the coal, PP, PS and PE, conversion of 96.6, 100, 100, 77.3 wt%, oil yield of 42.6, 83.3, 92.5, 15.6 wt%, yield of THFS in VR of 36.4, 3.7, 3.5, 57.8 wt%, gas yield of 12.9, 14.5, 5.0, 3.9 wt%, and total of H₂ transferred from gas and decalin of 18.8, 9.8, 7.7, 2.1 mmol/g-daf reactant, respectively were obtained. Here, (H₂ transferred from gas)/(total H₂ transferred) were 3-7 %. Thus, H₂ transferred from decalin were small, compared to tetralin. The use of decalin instead of tetralin remarkably accelerated PE decomposition. This result indicates that the increase in hydrogen donorability of solvent inhibits PE decomposition, probably due to more rapid stabilization of radicals from PE cracking by hydrogen donation from solvent. For PP, yield of THFS in VR decreased, while yields of oil and gas increased a little. For PS, there was no large difference observed between decalin and tetralin, in respect of conversion, yields of THFS in VR, oil and gas. For the coal, the use of decalin instead of tetralin gave a little lower conversion, while oil yield became a little larger.

In case of decalin, considerably different coliquefaction behavior was obtained for the

coal/PE mixture, compared to tetralin. Conversion, yields of oil and THFS in VR were lower than those calculated, although there existed linear relationship of coal concentration with gas yield and total of H₂ transferred. The differences in conversion, yields of oil and THFS in VR between the observed value and the calculated value were very large at coal concentration of 25 %. The differences were not observed in case of tetralin. Hydrogen donation from hydrogen donor solvent to radicals is much faster than that from hydrogen gas even for catalytic coal liquefaction. For the use of decalin, radicals from cracking of the coal and PE would exist for longer time, compared to tetralin, resulting in larger interaction between radicals to polymerize to give THF-insoluble fraction. On the other hand, in the model experiment of coliquefaction of DB with model plastics using decalin and the same catalyst, PE decomposition proceeded more effectively with coexistence of the coal model compound, giving higher values of conversion and oil yield⁹. Thus, the results in Figs. 1-3 indicate that the coal would interact with PE in a different way, compared to the coal model compound of DB. In case of coliquefaction of the coal with PP, almost linear relationship of coal concentration with conversion or oil yield was obtained. Yield of THFS in VR were higher than those calculated, while gas yield and total of H₂ transferred were lower than those calculated. The tendency for the coal/PP mixture was same, compared to that for the use of tetralin. The differences in total of H₂ transferred between the observed value and the calculated value became larger than those for the use of tetralin. From the results, more effective use of radicals from PP cracking for stabilization of radicals from the coal and PP instead of hydrogen could be expected. For the coal/PS mixture, there existed almost linear relationship of coal concentration with conversion, yield of THFS in VR. Oil yield and total of H₂ transferred were a little higher than those calculated, while gas yield was lower than that calculated. The tendency in respect of conversion, yields of oil, THFS in VR and gas was similar to that for the use of tetralin.

Coliquefaction of coal with mixed plastics of PP, PS and PE

Table 1 shows results of coliquefaction of the coal with mixed plastics of PP, PS and PE using tetralin or decalin and the same catalyst. Coal/mixed plastics was 1/1 and PP/PS/PE was 1/1/1. Two kinds of calculated value (cal¹: arithmetic mean value of results from the coal/PP, the coal/PS and the coal/PE (1/1 mixture), cal²: arithmetic mean value of results for each reactant) are also shown in this table.

Coliquefaction using tetralin gave a little higher gas yield, lower values of conversion and yield of THFS in VR, compared to cal¹. On the other hand, conversion and THFS in VR also became lower, compared to cal² but gas yield was larger. There existed almost no difference in oil yield between the observed value and the calculated value, not depending on the way of calculation. Coliquefaction using decalin gave the same gas yield, higher values of conversion and oil yield, and a little lower yield of THFS in VR, compared to cal¹. On the other hand, almost the same conversion, lower yields of THFS in VR and gas, and higher oil yield were observed, compared to cal². The results indicate that PE decomposition proceeded more effectively with the coexistence of PP and/or PS during coliquefaction of the coal with the mixed plastics, although PE decomposition inhibited by coexistence of the coal in case of coliquefaction of the coal with PE alone. It is also suggested that the results reflected larger interaction between PE and the other plastics (PP, PS) than that between coal and PE. Lower gas yield in case of tetralin or decalin, compared to cal², as seen in Table 1 was probably due to inhibition of gas production by the coexistence of PP, also shown in Figs.1 and 3. Total of H₂ transferred for the use of tetralin or decalin was only a little lower, compared to cal², due to the low concentration of PP in coal/plastics mixture.

As also seen in Table 1, higher values of conversion and oil yield for the use of decalin were obtained, compared to tetralin. The results indicate that a good hydrogen donor solvent would not be necessary in case of the use of catalyst for coliquefaction of coal with waste plastics.

ACKNOWLEDGEMENT

This study was supported by the Original Industrial Technology R&D Promotion Program from NEDO of Japan.

References

1. Cugini, A.V. and Lett, R.G., *Energy and Fuels*, Vol.3, 120 (1989)
2. Rothenberger, K.S. et al., *ACS Div. Fuel Chem. Preprints*, Vol.40, No.1, 38 (1995)
3. Yamaguchi, H. et al., *Proc. of the 1998 Int. Symposium on Advanced Energy Technology*, 163 (1998)
4. Curtis, C.W and Cassell, F.N., *Energy and Fuels*, Vol.2, 1 (1988)

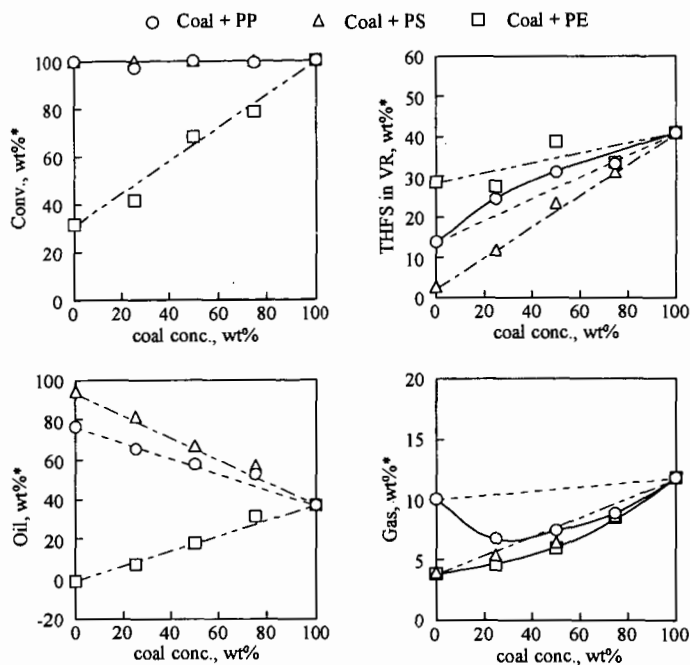


Fig.1 Coliquefaction of Tanitoharum coal with plastics using tetralin as the solvent at 430 °C for 60 min under 7 MPa initial pressure of hydrogen gas
 * based on daf reactant

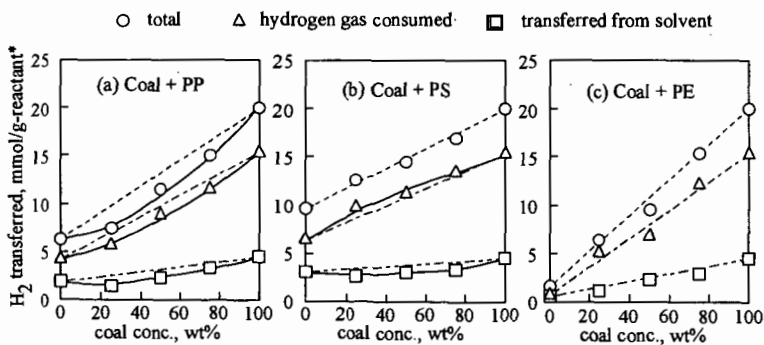


Fig.2 Hydrogen transfer under coliquefaction of Tanitoharum coal with plastics using tetralin as the solvent at 430 °C for 60 min under 7 MPa initial pressure of hydrogen gas

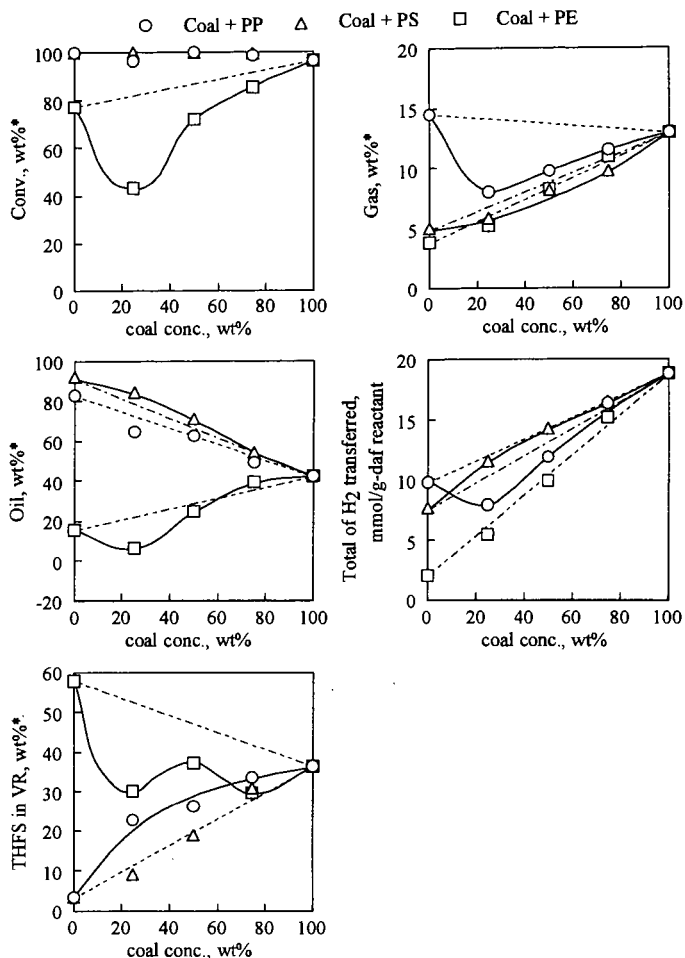


Fig.3 Coliquefaction of Tanitoharum coal with plastics using decalin as the solvent at 430 °C for 60 min under 7 MPa initial pressure of hydrogen gas

* based on daf reactant

Table 1 Coliquefaction of Tanitoharum coal with mixed plastics of PP, PS and PE at 430 °C for 60 min
(coal/mixed plastics = 1/1, PP/PS/PE = 1/1/1 (by weight))

Solvent	Conv. (wt%)	THFS in VR (wt%)	Oil (wt%)	Gas (wt%)	Total of H ₂ transferred (mmol/g-daf reactant)	
Tetralin	85.31	26.65	47.75	7.50	12.41	observed
	89.31	31.38	47.38	6.64	11.80	cal ¹
	88.52	28.17	46.90	8.92	12.95	cal ²
Decalin	93.31	25.39	57.57	8.84	12.04	observed
	90.64	27.43	53.12	8.77	12.08	cal ¹
	94.53	29.02	53.22	10.37	12.70	cal ²

¹ arithmetic mean value of results for the coal/PP, the coal/PS or the coal/PE (1/1 mixture)

² arithmetic mean value of results for each reactant

EFFECT OF VARIOUS ADDITIVES ON COAL EXTRACTION WITH CARBON DISULFIDE / *N*-METHYL-2-PYRROLIDINONE MIXED SOLVENT

Masashi Iino, Hideyuki Kurose, E. Sultan Giray, and Toshimasa Takanohashi
Institute for Chemical Reaction Science, Tohoku University,
Katahira, Aoba-ku, Sendai 980-8577, JAPAN

KEYWORDS: Coal extraction, additive, carbon disulfide / *N*-methyl-2-pyrrolidinone mixed solvent

INTRODUCTION

We have reported (1) that the extraction yield with carbon disulfide / *N*-methyl-2-pyrrolidinone (CS₂ / NMP) mixed solvent (1:1 by volume), which gave very high extraction yields for bituminous coals at room temperature (2), increases by the addition of a small amount of tetracyanoethylene (TCNE) to the solvent. The yield of the room temperature extraction of Upper Freeport coal with the 1:1 CS₂ / NMP mixed solvent increases from 59 wt% (daf) to 85 wt% (daf) by adding only 5% (based on coal) of TCNE to the mixed solvent. *p*-Phenylenediamine(PDA) is also an effective additive for the mixed solvent extraction (3).

We have also found (4) that when the extracts obtained with the CS₂/NMP mixed solvent were fractionated with pyridine to yield pyridine insoluble (PI) and soluble fractions, part of PI became insoluble in the mixed solvent. The addition of a small amount of TCNE, tetracyanoquinodimethane (TCNQ) or *p*-phenylenediamine to the mixed solvent, PI became soluble in the mixed solvent.

While, swelling and viscoelasticity behaviors of coal shows that coal has a kind of macromolecular network structure. The changes of this network structure were often quoted to explain the changes of reactivity and product selectivity of coal by heat or solvent treatment. But the nature of the macromolecular network structure are still unknown. Although covalently connected crosslinking structures are often assumed, the evidences for them are not enough. Recent works, including our results, suggest that for some bituminous coals, large associates of coal molecules i.e., non-covalent (physical) network are a better network model, than the covalent one. Coal extracts and coal-derived liquids are known to readily associate between themselves to form complex associates (5-8).

Solubility limit of coals, i.e., how high extraction yields can be obtained without the breaking of covalent bonds is one of the key points to clarify a kind of network bonds, i.e., covalent or non-covalent (physical) networks. If coal consists of highly developed covalent networks and low molecular weight substances occluded in them, coal extractability is low, as observed in the extraction with conventional solvents such as pyridine. However, 85wt% of the extraction yield obtained for CS₂ / NMP / TCNE solvent system described above suggests that Upper Freeport coal has little covalent networks. The reversibility of the effect of TCNE on the solubility increase for coal extracts (PI) was observed, indicating that no covalent bond breakings occur during this extraction(8).

In this study the effect of electron acceptors and donors on extraction yield of coal, and solubility of the extract component (PI) in the mixed solvent was studied. Formation of charge-transfer complex of TCNE with coal extracts was also investigated. Mechanisms for the enhancement of the extraction yield and the solubility by the additives are discussed.

EXPERIMENTAL

Extraction of coals with CS₂ / NMP mixed solvent

Six Argonne coals were used. The as-received coal samples (2.5 g) were extracted with 60 ml CS₂ / NMP mixed solvent (1:1, volume ratio) and an electron donor under ultrasonic irradiation for 30 min at room temperature (2). PDA, *N,N,N',N'*-tetramethyl-*p*-phenylenediamine (TMPDA), aniline and melamine were used as an electron donor. The quantity of electron donor was 10 - 100 mg/g-coal. For exhaustive extraction the extraction was repeated (usually 3 times) until the color of the extract solution almost disappeared. Extraction yields were determined from the amount of the residue, after the correction for water content in the coals.

Solubility of PI in CS₂ / NMP Mixed Solvent

The extracts obtained by the extraction of Upper Freeport (Argonne Premium coal, 86.2 wt% C(daf)) and Zao Zhuang (Chinese coal, 87.8 wt% C(daf)) coals with the CS₂ / NMP mixed solvent were fractionated to acetone soluble (AS), pyridine soluble/acetone insoluble (PS) and pyridine insoluble (PI) fractions, with acetone and pyridine, respectively (2). The yields of PI are about 30 and 40 wt% (daf coal base), for Upper Freeport and Zao Zhuang coals, respectively.

Solubility of PI in the mixed solvent with or without an electron acceptor was determined using 0.4g of PI and 50ml of the mixed solvent at room temperature under ultrasonic irradiation. The quantity of an electron acceptor added is 8×10^{-5} mol to 0.4g of PI. This quantity corresponds to

2.5wt% (10mg) to 0.4g of PI for TCNE. After the irradiation a centrifugation and filtration of the mixture were carried out, and the amount of the insoluble PI was determined. In the solubility experiments under nitrogen atmosphere all the procedures before a centrifugation were carried out in a glove box filled with nitrogen. The CS₂/NMP mixed solvent were also deaerated by passing nitrogen gas before use. While, solubility of PS and PI in THF or the mixed solvent with and without PDA were examined using 0.2 g of fraction and 50 ml of solvent at room temperature under ultrasonic irradiation. The amount of PDA added is 25 mg/g-PS.

Synthesis of Pyridinium 1,1,2,3,3-pentacyanopropenide (PPCP)

Pyridinium 1,1,2,3,3-pentacyanopropenide (PPCP) was synthesized from TCNE with water in the presence of a base (pyridine) in acetone at -50 °C (9).

RESULTTA AND DISCUSSION

Effect of a Kind of Electron Acceptors on Solubility of PI

Table 1 shows the solubility of PI from Zao Zhuang coal in the mixed solvent when various electron acceptors were added, together with their electron affinities, which are a measure of their electron acceptabilities, i.e., the degree of charge-transfer (donor-acceptor) complex formation with an electron donor. Table 1 shows that only TCNE and TCNQ gave high solubility as expected from their high electron affinities. The three electron acceptors which contain chlorine atom, i.e., DDO, *p*-chloranyl and 2, 6-dichloro-*p*-benzoquinone shows much lower solubilities than those expected from their electron affinities. It could not clarify from this experiment whether charge-transfer interactions are responsible for the solubility enhancement by the addition of TCNE and TCNQ or not.

IR Study on Interaction of PI with TCNE

Figure 1 shows the result of the solubility experiments of PI from Zao Zhuang and Upper Freeport coals in the 1:1 CS₂ / NMP mixed solvent with or without TCNE. For Zao Zhuang coal a part (40.4%) of PI becomes insoluble in the mixed solvent, though PI is a part of the mixed solvent extract, but almost completely (97.6%) soluble in the mixed solvent containing TCNE, as already reported (4). For Upper Freeport coal (the data shown in the parenthesis in Figure 1) a similar result was obtained.

Figure 2 shows that FT-IR spectra of soluble and insoluble fractions of PI from Zao Zhuang coal in the CS₂ / NMP / TCNE solvent indicate the peak at 2200cm⁻¹ due to nitrile group of TCNE. The peak is much greater for the soluble PI than the insoluble PI. We also reported that the peak was almost disappeared by washing with pyridine(1). The removal of TCNE retained in the soluble PI, by washing with pyridine, resulted in the insolubilization in the CS₂ / NMP mixed solvent again i.e., 31.6% of PI became insoluble, but by the addition of TCNE 99.0% of PI became again dissolved in the mixed solvent (8).

The peak at 2200cm⁻¹ is considered to be that due to a charge-transfer complex of TCNE with the aromatic rings of coal (10, 11). Flowers et al. (11) proposed the formation of TCNE (and TCNQ) - coal complex in which TCNE accepts an electron from cooperated delocalized state of structure, not from individual independent aromatic structures of coal, since the shift of the nitrile peak from pure TCNE, about 36cm⁻¹ is unusually large, compared to that for TCNE - model aromatic compounds complex such as phenanthrene.

Figure 3(a) shows IR spectra of the solid obtained by the filtration of the mixture of PS with TCNE in acetone. Figure 3(a) shows the peak at 1500cm⁻¹ in addition to that at 2200cm⁻¹, as indicated in the literature (10). When this sample was washed several times with acetone, acetone soluble component was obtained. Its IR spectrum (Figure 3(b)) shows that the two peaks at 1500cm⁻¹ and 2200cm⁻¹ became predominant, suggesting that they come from some stable compound, which is not a charge transfer complex, since the peaks due to PS appeared in Figure 3(a) drastically decreased in Figure 3(b). Figure 3(c) shows that synthesized pyridinium 1, 1,2,3,3-pentacyanopropenide (PPCP) has a similar spectrum as that of Figure 3(b). According to Middleton et al. (9), the hydrate of free PPCP acid, i.e., 1, 1,2,3,3-pentacyanopropene dihydrate is a strong acid with pKa of 1.9, and has also the peaks at 1500cm⁻¹ and 2200cm⁻¹ like PPCP. Although pyridine and water which need to get PPCP from TCNE are usually present in coal, we can not deny the possibility that other derivatives of PPCP has a similar peaks at 1500cm⁻¹ and 2200cm⁻¹.

PPCP was found to have a similar enhancement effect on the solubility of PI as TCNE, as shown in Figure 4. At present we consider that PPCP or its acid is formed through interaction of TCNE with coal molecules, resulting in the solubility increase of coal molecules.

Effect of Oxygen on Solubility of PI in CS₂ / NMP Mixed Solvent

Figure 4 shows that the removal of oxygen drastically decreases the solubility of PI, regardless of the presence of TCNE. Figure 4 further shows that the addition of PPCP increases the solubility to a similar degree as TCNE, and also decreases it under nitrogen atmosphere. Mechanisms of the enhancement of solubility by oxygen are not clear, but change of association state, i.e., change to smaller associates by the presence of oxygen, like TCNE, is conceivable. In

fact, oxygen is known to have charge transfer interaction with electron donors, and with strong donor oxygen radical anion forms. The occurrence of some chemical reaction such as covalent bond breaking by oxygen is unlikely, since PI was already in enough contact with oxygen during the extraction and subsequent solvent fractionation procedure through which PI was obtained, before this solubility experiment.

Effect of the Addition of Electron Donors on the Extraction Yield.

In Table 2, the yields of the exhaustive extraction of coals studied in the mixed solvent with and without PDA are given. It indicates that the addition of only 25 mg/g-coal of PDA increased extraction yield of Upper Freeport coal from 51.4% to 81.3%. The addition of PDA slightly increased the extraction yield of high-volatile coals. Increasing the amount of PDA to 100mg/g-coal did not increase the extraction yield.

In Table 3, the extraction yields of Upper Freeport coal when an electron donor added into the mixed solvent together with their ionization potentials are given. Table 3 indicates that there is no correlation between the ionization potential of the donors and the extraction yield. According to the ionization potential of TMPDA, it is expected to show higher extraction yield than those of PDA and aniline. However, it doesn't show a significant increase in the extraction yield.

Effect of PDA on the Solubility of Extract Fractions of Upper Freeport Coals.

The solubility of PS fraction of Upper Freeport coal increased 10% in the presence of PDA. PDA is also effective on the solubility of PI fraction of Upper Freeport coal. When we added only 5 mg / 0.2 g-PI of PDA into the mixed solvent, solubility of PI increased from 75.4 to 90.2%.

ACKNOWLEDGMENT

This work was supported by "Research for the Future" project of Japan Society for the Promotion of Science (JSPS).

REFERENCES

1. Liu, H., Ishizuka, T., Takanohashi, T. and Iino, M., *Energy Fuels*, **1993**, 7, 1108-1111.
2. Iino, M., Takanohashi, T., Osuga, H. and Toda, K., *Fuel*, **1988**, 67, 1639-1647.
3. Ishizuka, T., Takanohashi, T., Ito, O. and Iino, M. *Fuel*, **1993**, 72, 579-580.
4. Sanokawa, Y., Takanohashi, T. and Iino, M. *Fuel*, **1990**, 69, 1577-1578.
5. Sternberg, H. W., Raymond, R. and Schweighardt, F. K., *Science*, **1975**, 188, 49-51.
6. Stenberg, V. I., Baltisberger, R. J., Patel, K. M. et al., *Coal Science* (ed Gorbarty, M. L., Larsen, J. W., Wender, I.), Academic Press, New York, **1983**, pp 125-171.
7. Nakamura, K., Takanohashi, T., Iino, M. et al., *Energy Fuels*, **1995**, 9, 1003-1010.
8. Iino, M., Liu, H., Hosaka, N., Kurose, H. and Takanohashi, T., *Prepr. Pap. Am. Chem. Soc., Div. Fuel Chem.* **1997**, 42(1), 248-252.
9. Middleton, W. J., Little, E. L., Coffman, D. D. and Engelhardt, V. A. *J. Amer. Chem. Soc.* **1958**, 80, 2795-2806.
10. Schwager, I., Kwan, J. T., Miller, J. G. and Yen, T. F., *Prepr. Pap. Am. Chem. Soc., Div. Fuel Chem.* **1978**, 23(1), 284-289
11. Flowers, II, R. A., Gebhard, L., Larsen, J. W. et al., *Energy Fuels*, **1994**, 8, 1524-1525.

Table 1. The effect of the addition of electron acceptors on the solubility^{a)} of PI from Zao Zhuang coal in CS₂/NMP mixed solvent at room temperature

Electron acceptor	Solubility of PI (wt%)	Electron affinity ^{b)} (eV)
None	51.0	—
Tetracyanoethylene(TCNE)	99.5	2.2
7,7,8,8-Tetracyanoquinodimethane(TCNQ)	81.0	1.7
2,3-Dichloro-5,6-dicyano- <i>p</i> -benzoquinone(DDQ)	53.8	1.95
1,2,4,5-Tetracyanobenzene	47.7	0.4
<i>p</i> -Benzoquinone	44.1	0.77
2,6-Dichloro- <i>p</i> -benzoquinone	37.0	1.2
<i>p</i> -Chloranil	34.8	1.37

^{a)} Wt% of PI soluble in the mixed solvent when 8×10^{-5} mol of an electron acceptor was added to 0.4g of PI in 50ml of the mixed solvent ^{b)} Electron affinity of the electron acceptors

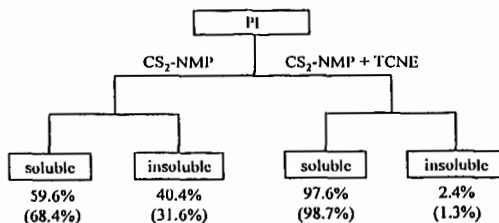


Figure 1. Solubility of PI from Zao Zhuang and Upper Freeport (shown in parenthesis) coals in CS₂/NMP mixed solvent with or without TCNE

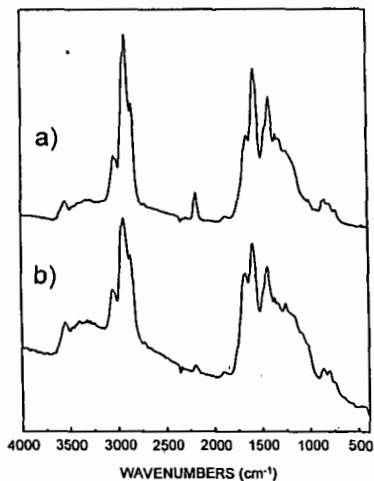


Figure 2. FT-IR spectra of soluble(a) and insoluble(b) fractions of PI from Zao Zhuang coal

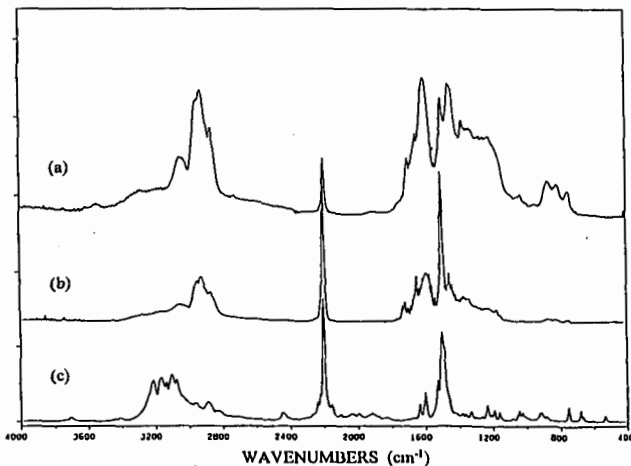


Figure 3. FT-IR spectra of the mixture(a) of PS from Upper Freeport coal with TCNE, its acetone soluble fraction (b), and Pyridinim 1,1,2,3,3-pentacyanopropenide(c)

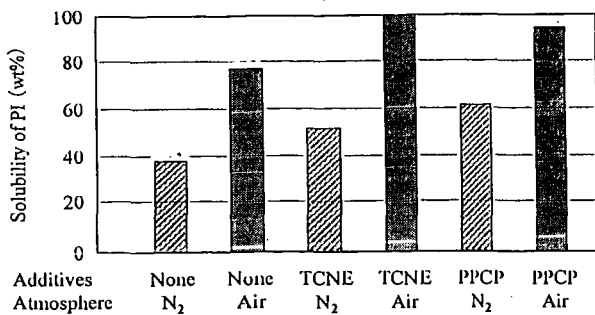


Figure 4. Solubility of PI from Upper Freeport coal in the CS₂/NMP mixed solvent under various conditions

Table 2. Effect of addition of *p*-phenylenediamine(PDA) on exhaustive extraction of Argonne coals with CS₂/NMP mixed solvent

coal ^a	PDA (mg/g-coal)	extraction yield (wt%,daf)
Upper Freeport	none	51.4
	25	81.3
Blind Canyon	none	36.3
	25	40.4
Lewiston- Stockton	none	24.6
	25	29.2
Pittsburgh No.8	none	41.5
	25	44.4
Illinois No.6	none	29.7
	35	34.8
Wyodak- Anderson	none	7.3
	50	11.9

^aas received

Table 3. Effect of addition of electron donors^a on single and exhaustive extraction of Upper Freeport coal with CS₂/NMP mixed Solvent

electron donor	extraction yield (wt%,daf)		ionization potential (eV)
	single	exhaustive	
none	31.5	51.4	
PDA	61.2	81.3	6.87
aniline	32.5	72.3	7.7
TMPDA	42.3	61.4	6.5
melanine	62.6	-	-

^a Amount of electron donors used is 25 mg/g-coal

CHARACTERIZATION OF UNSUPPORTED MoS_2 CATALYSTS BY CONTROLLED-
ATMOSPHERE PROGRAMMED-TEMPERATURE OXIDATION

B. BOCKRATH, R. LaCOUNT*, D. KERN*, D. PARFITT, E. FROMMELL, and
M. KELLER, III

US DEPARTMENT OF ENERGY
FEDERAL ENERGY TECHNOLOGY CENTER
PO BOX 10940
PITTSBURGH, PA 12356

*VIROLAC INDUSTRIES
403 ARBOR COURT
WAYNESBURG, PA 15370

Keywords: MoS_2 catalyst, CAPTO analysis, sulfur forms

INTRODUCTION

Controlled-atmosphere programmed-temperature oxidation, CAPTO, has been used as an effective tool for the quantitative determination and characterization of carbon, hydrogen, and sulfur in coal¹ and related materials.² This technique now has been applied here to provide unique, new information on the oxidation reactivity of sulfur in a variety of unsupported MoS_2 catalysts and of the carbonaceous deposits sometimes associated with them. In this application, the CAPTO analysis provides quantitative determination of three of the key elements in the structure of the working catalysts: sulfur, carbon, and hydrogen. Further, interpretation of the temperature profiles for the evolution of the oxides of these elements provides valuable information on the chemical state of these elements in the particular catalyst under study. This combination of information can shed more light on the structural differences among catalysts prepared by different methods and on the changes that may result from exposure to the processing conditions found under typical hydrotreating applications. To assess the potential of this analytical technique, a series of dispersed catalysts prepared by a variety of widely different methods was analyzed by CAPTO. The results indicate that the method is a useful, new means to characterize these materials.

Molybdenum disulfide has been used for a long time as the basis for many unsupported catalysts used for hydrotreating and related processing applications including direct coal liquefaction.³ Unsupported catalysts of this type have been prepared by various methods using any one of several molybdenum compounds as precursors. Promoted MoS_2 catalysts have been prepared by introducing minor amounts of other metals, primarily cobalt, nickel, or iron. In many cases, the catalyst is prepared *in situ* by the addition of a catalyst precursor just prior to the introduction of the feedstock to the hydrotreating reactor. Typically, this mode of preparation leads to a catalytic material that contains MoS_2 in close contact with a carbonaceous deposit.⁴ Alternatively, the MoS_2 may be generated separately and introduced to the reactor as a pure compound. Both approaches have been used in this work to generate a small set of catalysts of different crystallite sizes and with different degrees of crystallinity. In particular, the exfoliation and restacking technique^{5,6,7,8} has proven to be very valuable as a means to manipulate the structure of MoS_2 . Analysis of these materials by CAPTO provided "fingerprints" of the susceptibility of the sulfur in these catalysts to oxidation. Comparison of the different fingerprints from each sample indicated that the relative prominence of characteristic peaks may be related to the individual history of the catalyst's preparation and use.

EXPERIMENTAL

The CAPTO apparatus has been described previously.¹ Briefly, the sample is mixed with an inert diluent, WO_3 , and packed in a quartz tube. The device heats the sample according to a programmed temperature ramp, typically 3°C min^{-1} . In these analyses, a stream of 100% oxygen was passed through the sample plug. The gas flow was regulated by a mass flow controller. Complete combustion of the gases from the primary reactor was obtained by passage through a secondary catalytic reactor held at 1050°C . An FTIR was used to monitor the exit stream for CO_2 , SO_2 , and H_2O . The detector response was calibrated, allowing the final output to be plotted in terms of the mass of each element evolved as a function of sample temperature. Integration of the area under the curves provided the total mass of each element evolved from a sample, and thus the elemental analysis for carbon, hydrogen, and sulfur. Information

about the chemical forms in which these elements exist in the sample was available from the recorded temperature profiles. The total envelope for each gas was resolved by a peak fitting program into a set of individual peaks, each centered about a characteristic temperature. Experience obtained from the analyses of a wide variety of coals and well-characterized reference materials has made possible the association of the various characteristic temperatures with different chemical forms of the elements. For example, aromatic carbon is readily distinguished from other forms of carbon, and may be quantitatively determined.

CAPTO analysis was carried out on a series of fresh and used catalysts prepared by different methods. Exfoliation techniques were used as one means to manipulate the physical and chemical properties of MoS₂ catalysts. This method has been used to disassemble highly crystalline MoS₂ to form single layers suspended in water, followed by restacking of the layers to regenerate MoS₂ in a less-ordered crystalline form. The experimental procedures used here have been reported in a study of the application of this technique to generate MoS₂ catalysts for use in coal liquefaction and petroleum resid upgrading.^{7,8}

The exfoliated/restacked catalysts used here were prepared by first intercalating a commercial sample of MoS₂ (Alpha) with Li by reduction with 2.5 M n-butyllithium in hexanes (Aldrich) for two or three days in a glove box. The intercalated solid was filtered, dried, then removed from the glove box and added to water agitated by an ultrasonic bath. On addition to water, a suspension developed which is typically associated with the formation of single layer MoS₂. The suspension settled on standing as the restacking of MoS₂ proceeded. The restacked material was filtered, washed, and dried under vacuum.

An *in situ* preparation method was used as another route to MoS₂. A mixture of 4 g dodecane, 2 g pyrene, 0.3 g sulfur, and 0.5 g ammonium molybdate (2.43 mmole Mo) dissolved in 3 g water was added to a 40 mL high-pressure microautoclave. The vessel was pressurized with 500 psig hydrogen, heated to 380 °C over the course of about 1 h, then held at this temperature for another 1 h. Agitation was provided by shaking the reactor. After cooling, the catalyst was recovered by filtration, washed with tetrahydrofuran, and dried under vacuum.

An example of a used catalyst was obtained by recovering it after a standard test for hydrotreating activity.⁸ A mixture of 0.32 g exfoliated/restacked MoS₂, 3.23 g tetralin, and 3.0 g Hondo resid was added to a 40 mL microautoclave. The reactor was charged with 1000 psig hydrogen and heated over the course of about 1 h to 425 °C, then held at this temperature for another 1 h. The reactor was quenched in water, and the product analyzed by determination of heptane solubility using a pressure filtration method. The catalyst was recovered by washing the heptane insoluble portion with tetrahydrofuran, again using the pressure filtration method. The recovered catalyst was dried in a vacuum oven.

The catalysts were also examined by other methods to obtain comparative data, including SEM, X-ray diffraction, BET surface areas, and elemental analyses.

RESULTS AND DISCUSSION

Sulfur Profiles. The same highly crystalline sample of MoS₂ used as the starting material for the exfoliation/restacking method of catalyst preparation was analyzed by CAPTO to provide a reference. The sulfur profile is shown in Fig. 1A. SO₂ evolved producing a broad envelope of peaks beginning about 220 °C and ending by 580 °C. The shape of the whole complex envelope was well simulated by a combination of four peaks. The central temperature and relative area associated with each peak is given in Table 1. The majority of sulfur in this sample lies under the peak at highest temperature, centered around 507 °C. The general appearance and wide breadth of the total sulfur profile reflects considerable variability in sulfur oxidation reactivity. The separation of the total envelope into a series of separate peaks gives evidence that the sulfur contained in the single compound, MoS₂, may be consist of several distinct populations, each associated with a characteristic oxidation temperature.

The sulfur profile for the exfoliated/restacked sample of MoS₂ is given in Fig. 1B. The considerable change in physical structure induced by this treatment is reflected by a profoundly different sulfur profile. The broad envelope of this new profile begins at about 220 °C, just as it does with the highly crystalline starting material. However, the majority of sulfur dioxide from the restacked material evolves at comparatively lower temperatures and the profile already returns to baseline by about 500 °C rather than 580 °C. That means the major oxidative event was complete before

reaching the temperature of the maximum rate of SO_2 evolution observed for the highly crystalline starting material. The large envelope was again very broad and could be resolved into four individual peaks. The pronounced shift to lower oxidation temperatures after exfoliation/restacking implies that the degree of crystallinity of the catalyst is a major factor governing the reactivity of sulfur in MoS_2 toward oxidation. In addition, a small isolated peak centered at 628°C now also appears. Peaks in this area are often associated with metal sulfates.

A third sample was investigated to determine the effect of exposure to hydrotreating conditions on the exfoliated/restacked catalyst. An exfoliated/restacked catalyst sample prepared in the same way as described above was used in hydrotreating Hondo resid⁸ under the conditions summarized in the experimental section. The sulfur profile is given in Fig. 1C. Compared to the fresh catalyst, the center of gravity of the major peak has moved to a higher temperature. However, the endpoint of the major peak still comes at about 500°C , just as with the fresh exfoliated/restacked catalyst. The major envelope of the used catalyst could be resolved using three peaks rather than the four required for fresh catalyst. The three peaks of the used catalyst correspond rather well with three peaks of the fresh catalyst in terms of temperature and width. Comparison of the areas under the peaks reveals that the exposure to hydrotreating conditions for even only a single activity test made the recovered catalyst somewhat more resistant to oxidation. It should be noted that the CAPTO analysis for carbon demonstrated negligible amounts of coke were deposited on this sample. The possibility that sulfur in coke laid down by the Hondo resid contributed to the CAPTO profile for sulfur may be dismissed in this case.

The sulfur evolution profile of the catalyst prepared from ammonium molybdate by the *in situ* method was also obtained (not shown) for comparison to the previous samples. In contrast to both the highly crystalline and the exfoliated/restacked catalysts, the sulfur evolution profile for the MoS_2 catalyst derived from ammonium molybdate is dominated by a low temperature envelope. Again, individual peaks were resolved, five in this case. A difference was found in the atypical breadth of the peak centered at 429°C , which extensively overlapped two neighboring major peaks with widths more typical of the narrow peaks seen in the analyses of other samples of MoS_2 . These four CAPTO analyses demonstrate that there is a wide variation in the reactivity of sulfur in MoS_2 toward oxidation. Furthermore, the fingerprint characteristics obtained by CAPTO are related to the method of catalyst preparation and its history under processing conditions.

Table 1 contains the temperature and the relative amount of sulfur evolved for each peak for all four samples. When the resolved peaks are arranged in this way, it is apparent that there are corresponding peaks among the samples that have similar temperatures for peak maxima and generally similar widths. The CAPTO analyses give evidence that differences in the physical structure of MoS_2 are associated with differences in the distribution of sulfur among several characteristic types. Correlation with X-ray diffraction data, discussed below, shows that the relative amount of sulfur under peaks at higher oxidation temperatures increases with the degree of crystallinity.

Profound differences in crystallinity among the four MoS_2 catalysts became readily evident on comparison of their X-ray diffraction patterns. The highly ordered, three-dimensional structure of the original MoS_2 was apparent from the narrow peaks that compose the diffraction pattern. The 002 line was particularly prominent and narrow. The diffractogram of the exfoliated/restacked material was markedly different. Its broad lines were consistent with a turbostratic structure, indicating that order along the dimension of the stacking plane had been lost. The width of the 002 line at half-height was used to estimate the stacking heights of the crystallites for each sample. The changes in line width indicated that the exfoliation/restacking process reduced the average stacking height from 325 \AA to 185 \AA . An increased degree of crystallinity (loss of turbostratic disorder) was observed for the exfoliated/restacked catalyst recovered after hydrotreatment. However, the changes were modest, and the stacking height remained essentially unchanged at 185 \AA . The catalyst prepared *in situ* presented yet another picture. The 002 peak was the broadest of the four samples, yielding an estimate for average stacking height of 27 \AA . The XRD data thus confirmed that this set of four catalysts exhibits a wide range of crystallinity. When the XRD results are compared with the distributions of sulfur among the various CAPTO peaks, it is evident that the MoS_2 samples of lesser crystallinity and composed of smaller crystallites also have a larger portion of more readily oxidized sulfur.

CONCLUSIONS

The CAPTO technique provides important information about dispersed molybdenum sulfide catalysts. First, the method provided useful basic information in the form of the quantitative determination of the elements sulfur, carbon, and hydrogen, although these data were not discussed here. More importantly, the various patterns for sulfur oxidation with temperature observed for dispersed catalysts prepared by different means and of different crystalline structure indicate the method is quite sensitive to physical characteristics of each catalyst sample. This technique offers the potential for following changes in catalyst structure throughout the course of its preparation and use. Detailed correlation of the shapes of the SO₂ evolution profiles with catalyst activity is not yet possible with the small set of samples investigated so far. However, higher activity has been observed for the exfoliated/restacked catalysts as opposed to the highly crystalline sample¹⁰. The catalyst prepared by the *in situ* method appears to be as active as the exfoliated/restacked example. In general, it appears that higher activity may be associated with a less ordered and more easily oxidized structure.

REFERENCES

- * E-mail: bockrath@fetc.doe.gov
- (1) LaCount, R. B.; Anderson, R. R.; Friedman, S.; Blaustein, B. D. *Fuel* **1987**, *66*, 909-913.
 - (2) LaCount, R. B.; Kern, D. G.; King, W. P.; LaCount, R. B. Jr.; Miltz, D. J.; Stewart, A. L.; Trulli, T. K.; Walker, R. K. *Prepr. Pap.-Am. Chem. Soc., Div. Fuel Chem.* **1991**, *36*, 1217-1224.
 - (3) LaCount, R. B.; Kern, D. G.; King, W. P.; Trulli, T. K.; Walker, D. K. *Prepr. Pap.-Am. Chem. Soc., Div. Fuel Chem.* **1992**, *37*, 1083-1086.
 - (4) Weller, S. W. *Energy Fuels* **1994**, *8*, 415-420.
 - (5) Bearden, R.; Aldridge, C. L. *Energy Prog.* **1981**, *1*, 44-48.
 - (6) Miremadi, B. K.; Morrison, S. R. *J. Catal.* **1987**, *103*, 334-345.
 - (7) Joensen, P.; Frindt, R. F.; Morrison, S. R. *Mat. Res. Bull.* **1986**, *21*, 457-461.
 - (8) Yang, D.; Frindt, R. F. *Prepr. Pap.-Am. Chem. Soc., Div. Petr. Chem.* **1994**, *39*, 612-617.
 - (9) Bockrath, B. C.; Parfitt, D. S. *Catal. Letts.* **1995**, *33*, 210-207.
 - (10) Bockrath, B. C.; Parfitt, D. S. *Proc. Int. Conf. Coal Sci.* **1995**, *2*, 1343-1346.
 - (11) LaCount, R. B.; Kern, D. G.; King, W. P.; LaCount, R. B. Jr.; Miltz, D. J. Jr.; Stewart, A. L.; Trulli, T. K.; Walker, D. K.; Wicker, R. K. *Fuel* **1993**, *72*, 1203-1208.

DISCLAIMER

Reference in this work to any specific commercial product is to facilitate understanding and does not necessarily imply endorsement by the United States Department of Energy.

Table 1. Characteristic Temperatures of Sulfur Evolution for MoS₂ Catalysts.¹

DESCRIPTION	PEAK TEMPERATURES, °C					
	1	2	3	4	5	6
CRYSTALLINE MoS ₂		301 (2.7)	384 (3.0)	440 (28.5)	507 (65.7)	
EXFOLIATED/ RESTACKED	244 (2.1)	299 (2.2)	371 (15.4)	417 (76.6)		628 (3.7)
RECOVERED AFTER HYDROTREATMENT		289 (9.1)	381 (2.0)	425 (86.3)		600 (2.6)
PREPARED IN-SITU FROM AmMo		272 (50.8)	382 (23.9)	429 (10.1) 456 (14.2)		575 (1.0)

1. Central temperature of peaks from curve-fit. Area per cent in parentheses.

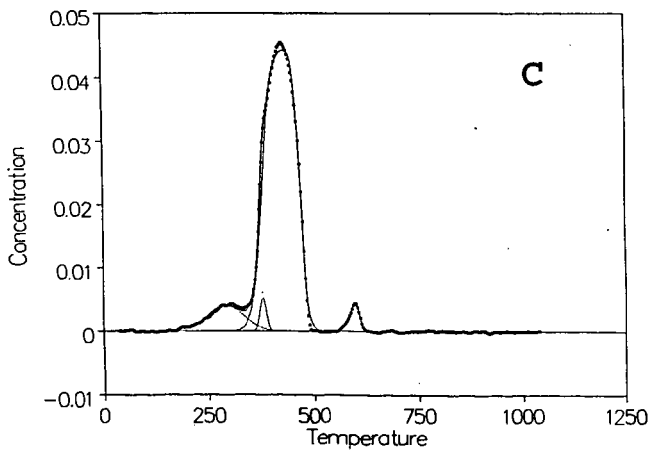
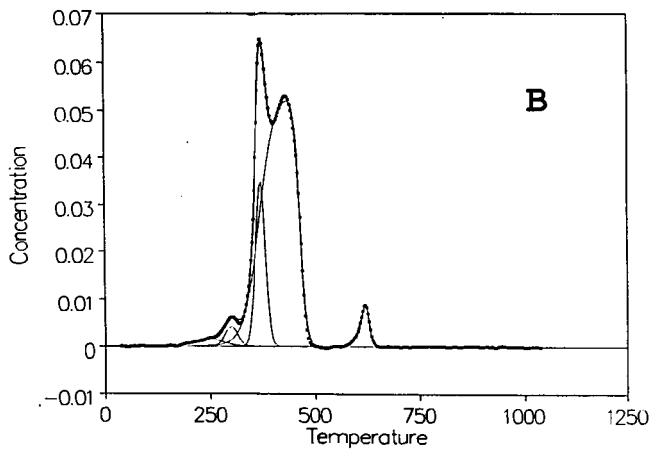
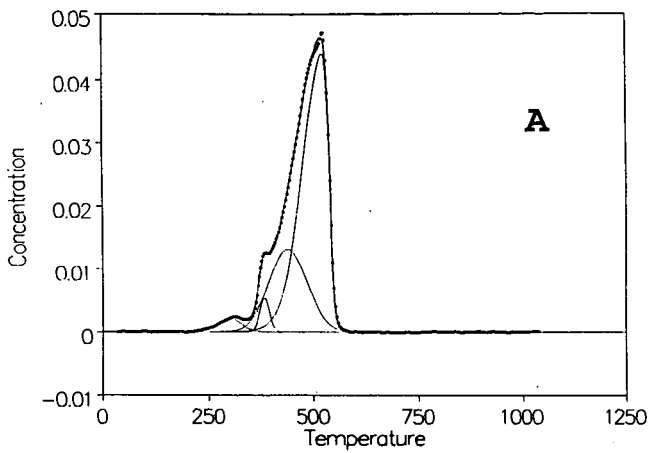


Fig. 1. CAPTO profiles of SO_2 evolution from MoS_2 . **A.** Crystalline MoS_2 . **B.** Exfoliated/restacked catalyst derived from sample A. **C.** Exfoliated/restacked catalyst recovered after use in hydrotreating Hondo resid.

HYDROCARBON SYNTHESIS FROM DIMETHYL ETHER OVER ZSM-5 CATALYST

Abhay Sardesai and Sunggyu Lee
Department of Chemical Engineering
The University of Missouri-Columbia
Columbia, MO 65211

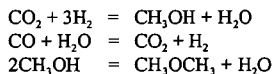
ABSTRACT

The liquid phase synthesis of dimethyl ether from syngas has significant advantages over the liquid phase methanol synthesis in the areas of syngas conversion and reactor productivity. The merits of this dual catalytic process allows dimethyl ether to be utilized as a viable feedstock for petrochemical synthesis. In particular, dimethyl ether can be converted to hydrocarbons using H-ZSM-5 type zeolite catalysts. Appropriate choice of the acidity of the zeolite catalyst as well as the operating parameters such as reaction temperature, partial pressure and space velocity of dimethyl ether dictate the product spectrum, ranging from lower olefins (ethylene and propylene) to gasoline-range hydrocarbons. The focus of this paper is to thoroughly study the aforementioned details of this process and compare its merits with methanol conversion.

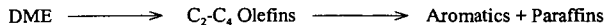
INTRODUCTION

The synthesis of petrochemicals from syngas via methanol has been the focus of research in the chemical industry for several decades. Methanol synthesis from syngas is a well established technology (Lee, 1990). However, the methanol synthesis technology faces a serious impediment because the reaction is severely limited by chemical equilibrium. Due to the reversible nature of the methanol synthesis reaction, the maximum per-pass conversion of syngas is restricted. However, the potential of the reverse reaction and the chemical equilibrium limitation can be alleviated by chemically converting methanol into another chemical species that is not affected by the equilibrium constraint. The in-situ dehydration of methanol to dimethyl ether (DME) is based on this approach.

Of particular interest is the novel process that has been developed by Lee and his co-workers for the co-production of dimethyl ether and methanol from syngas (Lee, 1992). This liquid phase dimethyl ether (LPDME) process consists of a dual-catalytic synthesis in a single reactor stage. Methanol is synthesized over coprecipitated Cu/ZnO/Al₂O₃ catalyst, whereas dimethyl ether synthesis takes place over γ -alumina catalyst. The reactions take place in a liquid phase system involving inert hydrocarbon oil such as Witco-40, Witco-70, Frecczene-100, etc. Various aspects of the methanol synthesis reaction and the co-production of dimethyl ether reaction have been assessed for commercialization of the process (Gogate, 1992). The process merits such as reactor productivities, catalyst life and activity, etc. were significantly higher in the co-production case. For high productivity cases using very high weight hourly space velocities of syngas, the single-stage productivity can be increased by as much as 70%. In terms of catalyst deactivation, the rate of thermal aging of methanol synthesis catalyst becomes slower when it is used in a co-production mode along with γ -alumina. Moreover, the process exhibits excellent control because it is possible to co-produce dimethyl ether and methanol in any desired proportion, from 5% DME to 95% DME, by varying the mass ratios of the methanol synthesis catalyst to the methanol dehydration catalyst. From the economic point of view, dimethyl ether produced from syngas is substantially cheaper than methanol synthesis on a methyl productivity basis. This cost benefit and enhanced effectiveness provides an alternative route to produce a variety of petrochemicals from DME as a starting raw material. The process chemistry is as follows:



Synthesis of lower olefins from methanol over ZSM-5 catalyst has been investigated in detail (Chang, 1983). Lower olefins synthesis from methanol over smaller pore size ZSM-34 catalyst has also been studied (Givens, 1978). Selective conversion of dimethyl ether to lower olefins is a process of growing potential in the chemical industry. Lower olefins are intermediates in the conversion of dimethyl ether to hydrocarbons over ZSM-5 type zeolite catalysts. The reaction pathway can be represented as follows:



Of particular interest is the synthesis of ethylene and propylene from dimethyl ether because of their growing demand as raw materials for a number of petrochemicals. Besides chemicals like ethylene oxide, ethylene glycol, propylene oxide, etc. these olefins are the building blocks for the production of their respective polymers, polyethylene and polypropylene. These polymers are widely used in everyday life applications such as molded plastic items, plastic packaging films, etc. Increasing demand for isobutene is inevitable since isobutene is used as the raw material for MTBE (methyl tert-butyl ether), a high octane gasoline blending oxygenate. Isobutene is also used in the manufacture of methyl methacrylate and isoprene. 1-Butene and 2-Butenes are important ingredients in the synthesis of methyl ethyl ketone. Thus, lower olefins have varied usage in the chemical industry, and so the research devoted toward their production from non-petroleum sources is of economic interest.

EXPERIMENTAL

A schematic of the DME-to-hydrocarbons experimental system is shown in Figure 1. The system can be divided into several sections: feed gas blending section, reaction section, and product separation and analysis section. The feed gas section consists of three mass flow controllers for DME, nitrogen, and carbon dioxide, respectively. A fixed bed reactor 18" in length and 0.5" I.D., manufactured by Autoclave Engineers has been utilized for this study. An axial thermowell runs the entire length of the tube and allows for measurement of the temperature profile in the reactor. The reactor tube is completely filled with 1/16" inert ZrO₂ beads. These beads are highly thermally stable and facilitate heat transfer from the beaded heater to the catalyst. Use of the beads in the reaction zone also helps dilute the reaction exotherm and therefore helps maintain a uniform temperature profile.

The feed gas analysis (DME, nitrogen and in some cases, carbon dioxide and methanol) as well as the analysis of the hydrocarbon product (C₁-C₅ range) was carried out using gas chromatography. The gas samples were withdrawn from the system using a constant rate 50 µl Hamilton syringe, as well as gas sampling bags. The liquid hydrocarbon product (C₅⁺ paraffins and aromatics) was analyzed using gas chromatography/ mass spectrometry.

RESULTS AND DISCUSSION

The assessment of process feasibility of DME conversion to lower olefins, particularly ethylene and propylene, has been carried out over ZSM-5 type zeolite catalysts (Sardesai, 1997). The results obtained from this research have revealed important relevant information about this process. Over the conventional ZSM-5 catalyst (SiO₂/Al₂O₃ ratio of 150), lower olefin (C₂-C₄) selectivity of 70 wt.% of total hydrocarbons was achieved. One of the salient features of this process is that it can be customized to target an individual olefin in the C₂-C₄ range at the expense of the other lower olefins. Process parameters such as operating temperature, partial pressure of DME, contact time, and catalyst acidity were evaluated over a limited range in light of maximizing lower olefin selectivity at optimal conditions. The results indicated that the temperature of the reaction has to be kept high, the partial pressure of DME has to be kept low, and the contact time of the reactants with the catalyst has to be kept low as shown in Figures 2-4. The concentration of strong Bronsted acid sites on the ZSM-5 catalyst has to be kept low by maintaining a lower SiO₂/Al₂O₃ ratio as shown in Figure 5. Also, the pore size of the catalyst has to be small enough to control the product spectrum on the higher end, and has to be large enough not to be a target of rapid deactivation by coking. Optimum results for lower olefin synthesis were obtained using the following parameters: Temperature = 430C, vol% Nitrogen in Feed = 65%, weight hourly space velocity of DME = 30 h⁻¹, SiO₂/Al₂O₃ ratio of ZSM-5 catalyst = 150.

Methanol conversion to hydrocarbons can be represented as follows:



where [CH₂] is the average representation of the hydrocarbon product. The conversion is essentially complete and stoichiometric. The above reaction shows a 44% selectivity by weight toward hydrocarbons, and a 56% selectivity toward water.

Dimethyl ether conversion to hydrocarbons can be represented as follows:



where [CH₂, CH₂] is the average representation of the hydrocarbon product. The conversion is essentially complete and stoichiometric. The above reaction shows a 60.8% selectivity by weight toward hydrocarbons, and a 39.2% selectivity toward water. Thus at nominally identical conditions, the selectivity toward hydrocarbons is 38% higher in the dimethyl ether conversion case as compared to the methanol conversion process (Lee, 1996).

In the methanol to hydrocarbons process, methanol formed from syngas first dehydrates to dimethyl ether in the first, and then an equilibrium mixture of methanol, dimethyl ether, and water is converted in the second reactor to form hydrocarbons. The exothermic of reaction is -398 cal/g methanol converted. The

methanol dehydration step of the reaction liberates 15% of the reaction heat, whereas the rest is given off in the latter step. In the dimethyl ether to hydrocarbons process, the exothermic heat liberated is only 85% of that of the methanol conversion process. This is because dimethyl ether is produced in the syngas reactor, whereas, in the methanol case, dimethyl ether is produced in the dehydration reactor. Thus, the heat management is better in the dimethyl ether conversion process. In addition to this, it obviates the need of a dehydration reactor thereby causing considerable saving in capital investments and working capital.

Dimethyl ether can also be converted to gasoline-range hydrocarbons using ZSM-5 catalysts of very high acidity ($\text{SiO}_2/\text{Al}_2\text{O}_3$ ratio of 30). The experimental and testing results have been very promising from a commercial standpoint. A U.S. patent for the process has been issued (Lee, 1995).

CONCLUSIONS

As a long term commodity chemical, dimethyl ether is proving to be one of the chemical industry's most dynamic product. It can be produced from any fossil fuel source. It finds use as an alternate fuel, as well as a chemical feedstock. Technical and market application efforts are proceeding at a great pace on both its production and uses on an international basis. Dimethyl ether can be easily converted to ethylene and propylene, the building blocks of the chemical industry, using this process which has distinct advantages over methanol conversion. Thus, natural gas-based syngas can be converted to hydrocarbons via dimethyl ether as an intermediate using zeolite catalysts. The merits of this process are very attractive and have been investigated in detail for pre-scale up assessment. The demonstrated process feasibility and excellence are novel and very promising in developing alternative sources for lower olefins.

REFERENCES

- Chang, C. D., "Hydrocarbons from Methanol", Catal. Rev. Sci. Eng., vol. 25, n 1, pp 1-118, 1983.
 Givens, E., U. S. Patent, 4,079,096. 1978.
 Gogate M., "A Novel Single-Step Dimethyl Ether Synthesis from Syngas", Ph.D. Dissertation, The University of Akron, 1992.
 Lee, S., "Methanol Synthesis Technology", CRC Press, Boca Raton, FL, 1990.
 Lee, S., "A Novel DME Synthesis process in a three phase Slurry Reactor from CO-rich Syngas", Chem. Eng. Sci., vol. 47, n 13/14, pp 3769-3776, 1992.
 Lee, S., U.S. Patent, 5,459,166. 1995.
 Lee, S., "Methanol-to-Gasoline vs. DME-to-Gasoline. II. Process Comparison and Analysis", Fuel Science & Technology International, vol. 13, n 8, pp 1039-1058, 1995.
 Sardesai, A., "Catalytic Conversion of Dimethyl Ether to Lower Olefins: Process and Catalyst Deactivation Studies", Ph.D. Dissertation, The University of Akron, 1997.

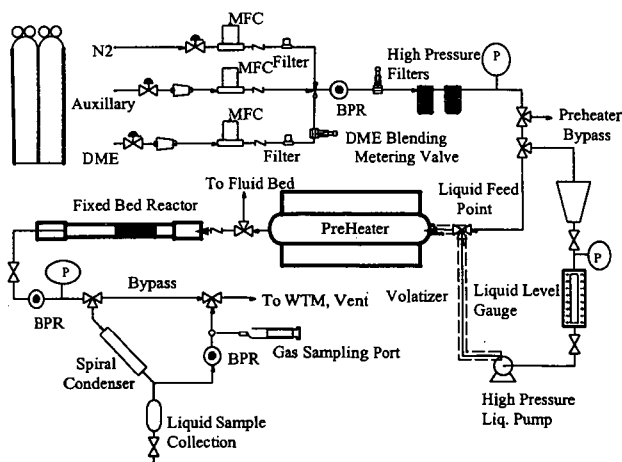


Figure 1. Schematic of the Dimethyl Ether (DME) to Hydrocarbons Experimental Unit.

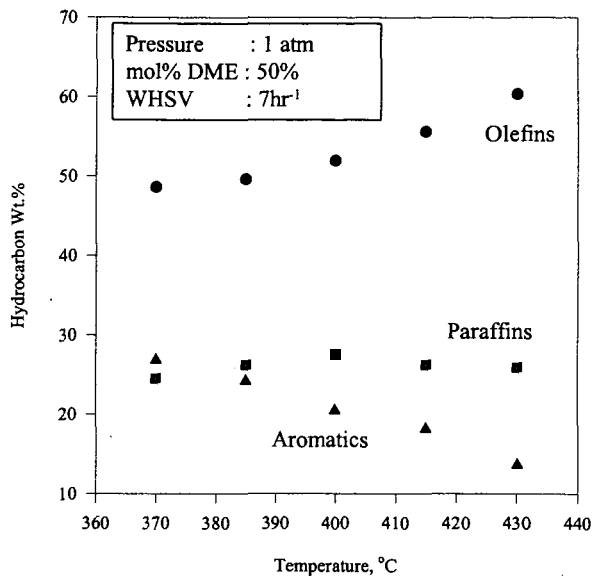


Figure 2. Effect of Reaction Temperature on Hydrocarbon Selectivity

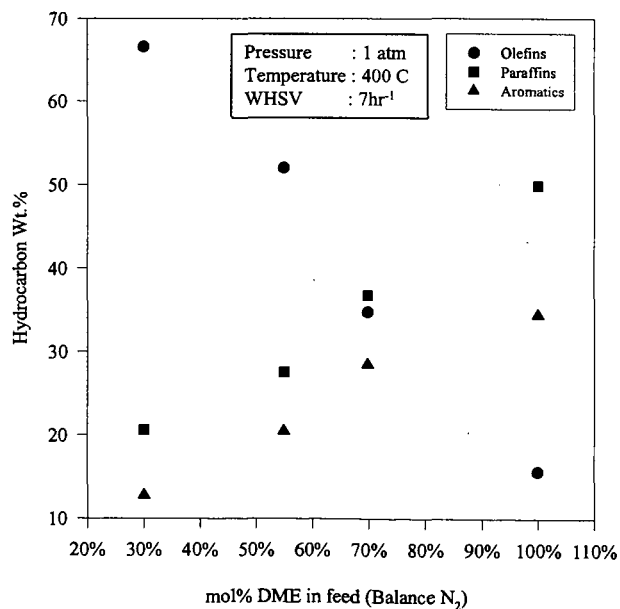


Figure 3. Effect of Feed Dilution on Hydrocarbon Selectivity

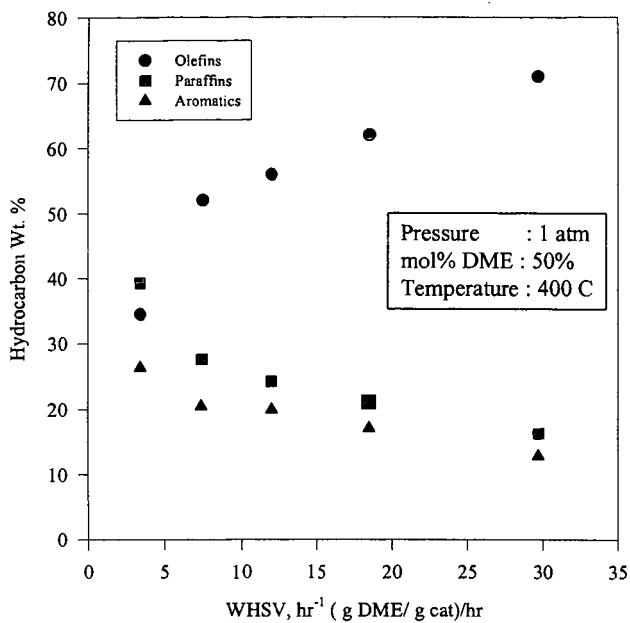


Figure 4. Effect of Space Velocity on Hydrocarbon Selectivity

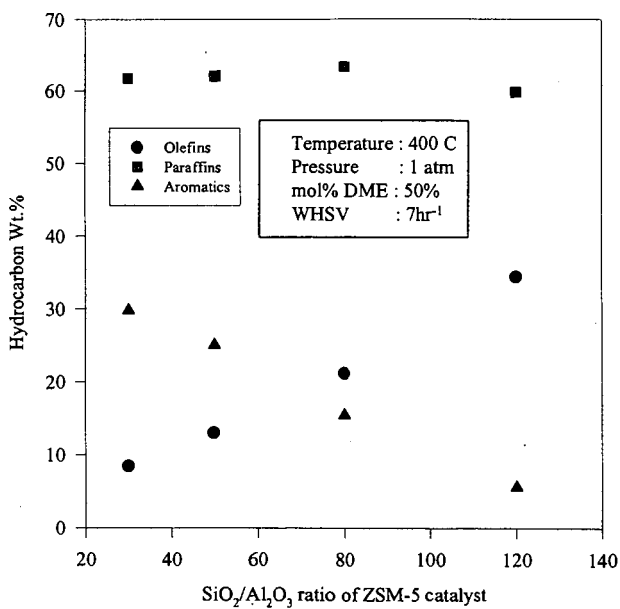


Figure 5. Effect of Zeolite Acidity on Hydrocarbon Selectivity

BIAS TESTING OF MECHANICAL AUTOMATIC SAMPLING SYSTEM INSTALLED AT LAXT FOR LOADING EXPORT COALS AND PETROLEUM COKES

Jun M. Lee, Jeffrey G. Rolle, James J. Baker, Robert Llerena
A. J. Edmond Co., 1530 West 16th Street, Long Beach CA 90813
Jim Holland, Los Angeles Export Terminal, Inc., San Pedro, CA 90731
Robert White, Pacific Carbon Services, Inc., San Pedro, CA 90731
Wendell Cook, Hall-Buck Marine, Inc., San Pedro, CA 90731

Keywords: coal, bias test, mechanical sampling

ABSTRACT

A new modern LAXT (Los Angeles Export Terminal) facility was built in September 1997 and has been operational for export shipment of coals and petroleum cokes. Recently on March 16-18, 1998, bias testing of the mechanical automatic sampling system, which is installed at LAXT for representative sampling, was performed by A. J. Edmond Company to evaluate the performance of the mechanical sampler. The bias test was carried out loading 86600 metric tons of coal in M/V Noshiro Maru. Thirty sets of system (crushed), reference (stopped-belt) and secondary cutter reject (backup) samples were collected for bias analysis. Paired test batch design is employed for sample collection procedure and Walsh averages, non-parametric method is selected for statistical analysis. Test batch size was 2670 metric tons and target coal transfer rate was 4500 metric-tons/hr. Coal characteristics analyzed for the bias test are moisture and dry ash content. In addition size consist analysis will be performed, if necessary to identify sources causing biases. Based on the statistical analysis, bias test results are presented.

INTRODUCTION

The LAXT is a coal and petroleum coke receiving, handling and exporting facility located at the Port of Los Angeles' Pier 300 on Terminal Island. The facility is owned by LAXT, Inc., a consortium of 37 shareholders representing the entire coal chain from the coal mines to power plants and operated by Pacific Carbon Services and Hall-Buck Marine. Throughput capacity is 10 million metric tons of product per year with expansion potential to 18 million metric tons.

Export quality of coals was reported at the ACS Las Vegas Meeting (September 7-11,1997), based on bituminous coal properties determined for M/V ship samples and subbituminous coal properties from western coal round robin samples [1].

Theory involved in non-parametric statistical method for bias analysis can be found in the literature [2,3,4]. Walsh averages, non-parametric method has been practiced in bias analysis of mechanical coal sampling [5,6,7] and methods for mechanical sampling from moving streams of coal are available in American Society for Testing and Materials (ASTM) Standard [8] and International Standard [9].

The objective of this study is to determine the absence or presence of bias of the mechanical automatic sampling system located at the LAXT facility, based on matched-pair experimental designs. Coal sample collection and statistical evaluation procedures must be chosen before the bias test is conducted. The overall bias of the mechanical sampling system is determined. After collection, the test samples (reference, system and backup) are prepared and analyzed using applicable ASTM test methods for coal characteristics such as moisture, dry ash and size consist.

Details of statistical analysis methodology, experimental data obtained from the bias test, and bias test operating conditions are described in the following sections.

SELECTION OF BIAS TEST METHOD

Paired-test batch design is selected for sample collection procedure. The procedure is designed for the overall system test at normal mode of operation. Test batch size was approximately 2670 metric-tons interval. Thirty (30) sets of test samples including stopped-belt reference, mechanically collected system and secondary cutter reject (for backup) were collected for this bias study, loading 86600 metric tons of coal in M/V Noshiro Maru.

The Walsh averages non-parametric method is used for statistical analysis. The median of sorted observed differences is taken as the point estimate of bias. Two-sided confidence limits for multivariate analysis for two variables, moisture and dry ash are obtained based on the Bonferroni

inequality [10]. Interpretation of the results depends on whether or not the confidence interval of any one of the variables encompasses zero for the multivariate case. Ten (10) statistical analyses calculating Walsh averages were performed for this bias test, comparing bias among three collected samples (reference, system and backup). Two (2) statistical calculations for moisture and dry ash content were made comparing mechanical system samples against stopped-belt reference samples; two (2) calculations comparing secondary cutter reject (backup) samples against stopped-belt reference samples; two (2) calculations comparing mechanical system samples against secondary cutter reject samples (as a new reference); and four (4) additional calculations to evaluate outliers arbitrarily defined for this bias test.

GUIDELINE USED IN TEST PREPARATION

The bias test was prepared considering the following guideline and criteria.

- (1) Coal to be tested with consistent quality
- (2) Coal characteristics to be analyzed (ASTM Methods)

Moisture	D 3302
Dry Ash	D 3174
Size Consist	D 4749
- (3) No change in sampler operation mode and coal transfer rate
- (4) Same width of stopped-belt (SB) divider plates ($\geq 6"$)
- (5) Minimum 20 minutes interval between SB reference increments
- (6) Approximately equal amount of laboratory sample prepared from both system and reference samples
- (7) Number of paired data sets, initially 20-40 sets of data
- (8) Approximately same batch size throughout the entire test period

TEST OPERATING CONDITIONS AND PROCEDURE

Each test batch was carefully controlled to meet operating criteria set for the test. Daily operating log was prepared for the test and actual operating data were recorded for test monitoring. Planned target conditions are listed below.

Coal type:	fuel-grade bituminous coal
Feed rate:	4500 metric-tons/hr (4000-6000 range)
Test batch size:	2670 metric-tons/hr (approximately every 36 min operation)
Test lot size:	86600 metric tons
Stopped-belt (SB) interval:	once per batch
SB sampling time:	10-15 min at each stop

As planned thirty (30) sets of samples were collected for the entire test period. SB reference samples were collected within 15 min using a sampling divider as soon as the main conveyor stopped. SB sampling location was about 30 feet downstream after the mechanical automatic sampler. Samples of secondary cutter reject stream (backup) accumulated three times of separate collections for each test batch duration. Mechanical system samples were automatically collected in carousel cans. Each test batch consists of approximately 20-25 lbs of mechanical system, 80-100 lbs of SB reference, and 80-100 lbs secondary cutter reject (backup) sample.

During the bias test coal transfer rate maintained most of time in the range of 3500 to 5500 metric-tons/hr. The test was occasionally interrupted due to unavoidable hold changes and lunch breaks. Other than that the operation was very smooth with exception for one major plugging in the mechanical sampler occurred in Test Batch No. 6 and several minor operational problems experienced for the entire test period. The bias test was successfully complete in five 8-hrs shifts.

During startup of Test Batch No. 6, the mechanical sampler was plugged due to buildup of crushed material from the secondary cutter to crusher and further to carousel can. This buildup was caused by the main conveyor stop at the end of Test Batch No. 5 to collect the stopped-belt reference sample while the mechanical sampler was purging the sampling system. Approximately two (2) hours was spent to clear the plug. In addition the conveyor gate was not properly operational for the test. Test Batch No. 6 aborted and declared as not-for-bias-test (NBT) and sampling was continued for lot analysis only.

In Test Batch No. 19 the first portion of the period loading 1515 metric-tons was not included for the bias test and declared as NBT due to the morning shift break from 0300 to 0800 in the middle

of the test. Sampling was continued for lot analysis only. However, the second portion of the period loading 1316 metric-tons was included for the bias test and officially designated as Test Batch No. 19, which is used for statistical analysis.

Between Test Batch No. 28 and 29 the period loading 331 metric tons was not included for the bias test due to hold change. Sampling was discontinued for this period.

Test Batch No. 31 and 33 were not for bias test (NBT) although test serial numbers were given for convenience identifying samples for lot analysis only. The main conveyor was not stopped during these periods to collect the stopped-belt reference sample. Test Batch No. 32 was official for the bias test.

Operating conditions of the mechanical sampler was set as typical, normally practiced for ship loading at LAXT, at timer settings, 42 sec for primary, 7 sec for secondary and 14 sec for tertiary cutter, respectively. All operating data indicated that ASTM D 2234 ("Standard Test Methods for Collection of a Gross Sample of Coal") minimum increment requirement for individual cutter was met. The ASTM minimum requirements for the consignment lot of 8830 short tons are 104 increments for primary and 624 increments for secondary cutter, respectively.

ANALYTICAL DATA FOR COAL CHARACTERISTICS

Laboratory analysis samples for thirty (30) collected samples, total ninety different samples were prepared following the procedures listed in the ASTM D 2013, "Standard Method of Preparing Coal Samples for Analysis." Analyses of each sample were performed to determine air-dried loss, residual moisture and ash content following the procedures listed in the ASTM D 3302 and D 3174. Then total moisture and dry ash were calculated and reported for statistical analysis. Repeatability and reproducibility checks for ash content was carried out for samples from Test # 27, 28 and 30 (stopped-belt, stopped-belt and secondary cutter reject sample, respectively). For the first raw data with these samples showed significant deviation (difference) of ash content by 2 to 5% compared to 0 to 1.5% normally observed with other samples. Test # 30 sample (secondary cutter reject) was also rechecked and reported although the deviation (difference) of first raw data was smaller (1.3%).

STATISTICAL ANALYSIS DATA (WALSH AVERAGES)

Three different cases were evaluated for statistical bias analysis as described below. Selection of pairs from thirty (30) available pairs was based on 95% confidence interval ($\pm 2\sigma$). This initial screening of the data (reducing # of pairs) was done for the purpose of eliminating outliers. Test for independent differences was performed in each analysis. The sample differences must be independent to correctly draw inference about system bias using this method. So far all cases evaluated for this bias study has passed the test for independent differences.

The Walsh averages non-parametric method is based on creating a super-set of the population of differences by differencing every possible combination of the observed differences and sorting them in ascending order. For instance with a set of thirty ($n=30$) pairs of differences Walsh averages are 465 values [$w = n(n+1)/2$].

Mechanical System Vs. Stopped-Belt Reference Samples

Using raw data screened at a 95% confidence level (29 pairs of moisture and 28 pairs of dry ash values), statistical analysis and bias test results of mechanical system samples against stopped-belt reference samples are summarized below. An example of the Walsh averages method procedure (steps) is shown in Tables 1-4 comparing moisture content.

Table 1:	Observed Data, Difference, Run #, Median
Table 2:	Test for Independence Differences
Table 3:	Sorted Walsh Averages
Table 4:	Point Estimate of Bias (Median) and Confidence Interval (Concluding Statements for Bias Test)

Bias test results with these samples are:

- A) If a chance error with a maximum probability prior to the test of no more than about 1 out of 20, did not occur, biases of mechanically collected samples against stopped-belt reference samples lie within the closed intervals given below:
- Moisture $-0.300 < B(m) < 0.345$

Dry Ash (data under evaluation)

where $B(m)$ and $B(da)$ are point estimates of bias for moisture and dry ash, respectively. $B(m) = 0.005$, $B(da) =$ (data under evaluation).

- B) The confidence interval for moisture includes the value zero. Thus, this test offers insufficient evidence to reject a hypothesis of no bias of system samples against stopped-belt reference samples.

Secondary Cutter Reject (Backup) Vs. Stopped-Belt Reference Samples

Using raw data screened at a 95% confidence level (29 pairs of moisture and 27 pairs of dry ash values), statistical analysis and bias test results of secondary cutter reject (backup) samples against stopped-belt reference samples are:

- A) If a chance error with a maximum probability prior to the test of no more than about 1 out of 20, did not occur, biases of secondary cutter reject (backup) samples against stopped-belt reference samples lie within the closed intervals given below:

Moisture $-0.315 < B(m) < 0.245$
Dry Ash $-0.150 < B(da) < 0.480$

where $B(m)$ and $B(da)$ are point estimates of bias for moisture and dry ash, respectively. $B(m) = -0.030$, $B(da) = 0.1875$.

- B) The confidence interval for each coal characteristic includes the value zero. Thus, this test offers insufficient evidence to reject a hypothesis of no bias of secondary cutter reject (backup) samples against stopped-belt reference samples.

Mechanical System Vs. Secondary Cutter Reject (New) Reference Samples

Using raw data screened at a 95% confidence level (28 pairs of moisture and 29 pairs of dry ash values), statistical analysis and bias test results of mechanical system samples against secondary cutter reject (new) reference samples are:

- A) If a chance error with a maximum probability prior to the test of no more than about 1 out of 20, did not occur, biases of mechanical system samples against secondary cutter reject (new) reference samples lie within the closed intervals given below:

Moisture $-0.215 < B(m) < 0.165$
Dry Ash $-0.050 < B(da) < 0.520$

where $B(m)$ and $B(da)$ are point estimates of bias for moisture and dry ash, respectively. $B(m) = -0.0025$, $B(da) = 0.238$.

- B) The confidence interval for each coal characteristic includes the value zero. Thus, this test offers insufficient evidence to reject a hypothesis of no bias of mechanical system samples against secondary cutter reject (new) reference samples.

EVALUATION OF OUTLIERS

Two different statistical analyses were additionally performed to evaluate outliers arbitrarily defined for this bias test (95% confidence level). Sources of variability are coal quality, loading rate and operating conditions, analysis sample preparation, analytical methods, sample handling and storage, etc.

Using revised data from repeated ash values for Test # 27, 28, 30 and 32 (30 pairs of dry ash values), outliers for dry ash content were evaluated with secondary cutter reject samples and mechanical system samples against stopped-belt reference samples, respectively. The evaluation was designed to sensitivity affected by reducing laboratory analytical errors and increasing # of pairs. Additional outlier evaluation was performed with mechanical system samples against stopped-belt reference samples, using raw data screened with difference less than 1% (25 pairs of moisture and 24 pairs of dry ash values). The additional evaluation was designed to sensitivity affected by reducing # of pairs using majority of data, 80 to 85%, with smaller differences. Implication is to see sensitivity affected by reducing combined process operational and laboratory analytical errors.

The outlier evaluation shows a significant band reduction in the bias confidence interval by 0.045 to 0.135% absolute (about 10-20% of magnitude). Improvement in accuracy and precision can be achieved by eliminating or minimizing process operational and/or laboratory analytical errors.

SUMMARY OF TEST RESULTS

The following is a summary of major findings obtained from the bias test:

- Five out of six statistical analysis results include no bias in the confidence interval calculated.
- Bias analysis result with moisture content includes no bias when compared mechanical system samples against stopped-belt reference samples.
- Both bias analysis results with moisture and dry ash content include no bias when compared secondary cutter reject samples against stopped-belt reference samples.
- Both bias analysis results with moisture and dry ash content include no bias when compared mechanical system samples against secondary cutter reject (new) reference samples.
- Evaluation of outliers indicates that a significant band reduction in the bias confidence interval can be achieved by eliminating or minimizing process operational and/or laboratory analytical errors. This results in better accuracy and precision of bias test. The observed reduction of confidence interval varies in the range of 0.045 to 0.135% absolute (by about 10-20% of magnitude).

Based on the above findings, the following is recommended for future additional bias test.

- To perform dynamic (improved) bias test around secondary cutter and crusher components using paired increment design. This test will not require stopping the main conveyor; thus no interruptions will occur in loading. Specifically ash content will be analyzed for bias test. If necessary, size consist analysis will be performed additionally to pinpoint biases.
- To calculate biases for comparison using different statistical analysis methods such as ISO 9411, parametric methods, etc.

ACKNOWLEDGMENT

A. J. Edmond Company and Hall-Buck Marine staff, who participated in this bias test, are acknowledged.

REFERENCES

1. J. M. Lee, J. J. Baker, R. Llerena, J. G. Rolle, 214th American Chemical Society National Meeting, Las Vegas, Preprints of Symposia, Division of Fuel Chemistry, Vol. 42, No. 3, 844-853 (1997).
2. R. H. Randles, Encyclopedia of Statistical Sciences, Vol. 9, Wiley, New York, NY, 124-129 (1988).
3. N. L. Johnson and F. C. Leone, Statistics and Experimental Design, Vol. I, 2nd Ed., New York, NY, Chapter 9 (1977).
4. M. Holland and D. A. Wolfe, Non-parametric Statistical Methods, Wiley, New York, NY, 35-38 (1973).
5. A. M. Long, J. B. Long Company, private communication.
6. P. Reagan, Sampling Associates International, private communication.
7. C. D. Rose, The Journal of Coal Quality, Vol. 9, No. 4, 124-129 (1990).
8. ASTM D 2234.
9. International Standard, ISO 9411-1:1994(E).
10. F. B. Alt, Encyclopedia of Statistical Sciences, Vol. 1, Wiley, New York, NY, 294-300 (1982).

Table 1. Observed Moisture Values

SB Ref	Mech System	Sys. Ref	Above + Below -		Ordered Sample Difference	Run #
			Median	Run #		
1	9.81	10.45	0.64	+	-1.62	1
2	10.47	10.13	-0.34	-	-1.14	2
3	10.66	10.06	-0.60	-	-0.68	2
4	11.97	11.04	-0.93	-	-0.63	2
5	11.95	11.63	0.48	+	-0.59	3
6	11.95	11.16	0.10	+	-0.58	3
7	10.76	10.81	-0.14	-	-0.57	4
8	10.93	10.72	-0.21	-	-0.53	4
9	10.16	10.63	0.47	+	-0.35	5
10	10.61	10.66	-0.35	-	-0.34	6
11	10.24	10.80	0.56	+	-0.21	7
12	11.95	10.81	-1.14	-	-0.20	8
13	10.30	10.68	0.28	+	-0.14	8
14	10.31	10.16	-0.13	-	-0.13	10
15	12.99	11.37	-1.62	-	0.10	10
16	11.20	12.70	1.50	+	0.18	11
17	12.80	11.92	-0.88	-	0.28	12
18	11.27	10.89	-0.68	-	0.38	12
19	11.16	10.63	-0.53	-	0.43	12
20	10.11	10.64	0.43	+	0.47	13
21	11.00	10.90	-0.20	-	0.47	14
22	11.01	10.44	-0.67	-	0.48	14
23	11.00	11.53	0.53	+	0.53	15
24	10.81	11.22	0.81	+	0.54	15
25	10.76	11.31	0.66	+	0.56	15
26	11.33	11.49	0.16	+	0.56	15
27	10.79	11.80	1.01	+	0.51	15
28	11.14	11.62	0.36	+	1.01	15
29	11.37	11.84	0.47	+	1.50	15

Median	11.000	10.800	0.100
Average	10.986	11.001	0.005
STDEV	0.706	0.616	0.073

Table 2. Test for Independent Differences

Test criteria are:
 If $r < -u$, passed and the sample differences are independent.
 If $r < -l$ or $r > u$, failed and the process is viewed as inconclusive.

r	\bar{D}_1	\bar{D}_2	B	l	u	P of F
15	14	14	2	10	20	passed

Legend: r = number of runs
 p = number of coal characteristics tested
 n_1 = number of lowest like signs
 n_2 = number of most like signs
 l = lower significance value
 u = upper significance value

Table 4. Point Estimate of Bias (Median) and Confidence Interval

Point estimate of bias = 0.005
 median = 218th ordered value
 Confidence interval
 d = counting value
 L_d = the d th smallest value = 114th ordered value = -0.300
 U_d = the d th largest value = 322th ordered value = 0.345

n	p	d	L_d	U_d	Closed Confidence Interval [L_d, U_d]
28	2	114	-0.300	0.345	[-0.300, 0.345]

Table 3. Sorted Walsh Averages for Moisture

Order	W								
1	-1.620	54	-0.570	107	-0.335	160	-0.130	213	-0.010
2	-1.380	55	-0.480	108	-0.335	161	-0.125	214	-0.010
3	-1.250	56	-0.355	109	-0.330	162	-0.125	215	-0.010
4	-1.140	57	-0.350	110	-0.330	163	-0.120	216	-0.005
5	-1.125	58	-0.545	111	-0.310	164	-0.105	217	0.000
6	-1.105	59	-0.545	112	-0.305	165	-0.100	218	0.005
7	-1.100	60	-0.540	113	-0.305	166	-0.100	219	0.010
8	-1.095	61	-0.540	114	-0.300	167	-0.095	220	0.010
9	-1.075	62	-0.535	115	-0.295	168	-0.095	221	0.010
10	-1.010	63	-0.530	116	-0.290	169	-0.090	222	0.015
11	-0.985	64	-0.530	117	-0.280	170	-0.080	223	0.015
12	-0.980	65	-0.520	118	-0.275	171	-0.080	224	0.015
13	-0.915	66	-0.510	119	-0.275	172	-0.080	225	0.015
14	-0.910	67	-0.505	120	-0.270	173	-0.075	226	0.020
15	-0.885	68	-0.505	121	-0.265	174	-0.075	227	0.020
16	-0.880	69	-0.490	122	-0.265	175	-0.075	228	0.025
17	-0.880	70	-0.490	123	-0.265	176	-0.070	229	0.030
18	-0.875	71	-0.485	124	-0.250	177	-0.065	230	0.040
19	-0.865	72	-0.470	125	-0.245	178	-0.060	231	0.040
20	-0.860	73	-0.485	126	-0.245	179	-0.060	232	0.045
21	-0.855	74	-0.485	127	-0.240	180	-0.060	233	0.060
22	-0.835	75	-0.480	128	-0.240	181	-0.055	234	0.080
23	-0.780	76	-0.480	129	-0.240	182	-0.055	235	0.060
24	-0.755	77	-0.455	130	-0.235	183	-0.055	236	0.065
25	-0.745	78	-0.440	131	-0.235	184	-0.055	237	0.065
26	-0.740	79	-0.440	132	-0.235	185	-0.050	238	0.065
27	-0.735	80	-0.435	133	-0.215	186	-0.050	239	0.065
28	-0.730	81	-0.420	134	-0.215	187	-0.050	240	0.065
29	-0.730	82	-0.415	135	-0.210	188	-0.050	241	0.070
30	-0.725	83	-0.400	136	-0.210	189	-0.050	242	0.085
31	-0.705	84	-0.395	137	-0.205	190	-0.050	243	0.090
32	-0.680	85	-0.395	138	-0.205	191	-0.045	244	0.090
33	-0.675	86	-0.390	139	-0.205	192	-0.045	245	0.095
34	-0.670	87	-0.390	140	-0.205	193	-0.045	246	0.095
35	-0.640	88	-0.390	141	-0.200	194	-0.040	247	0.100
36	-0.635	89	-0.385	142	-0.200	195	-0.040	248	0.100
37	-0.630	90	-0.385	143	-0.185	196	-0.035	249	0.100
38	-0.620	91	-0.380	144	-0.186	197	-0.030	250	0.105
39	-0.615	92	-0.380	145	-0.175	198	-0.030	251	0.105
40	-0.610	93	-0.370	146	-0.175	199	-0.030	252	0.110
41	-0.610	94	-0.365	147	-0.170	200	-0.025	253	0.110
42	-0.605	95	-0.365	148	-0.170	201	-0.025	254	0.115
43	-0.600	96	-0.360	149	-0.170	202	-0.025	255	0.120
44	-0.595	97	-0.360	150	-0.165	203	-0.025	256	0.125
45	-0.590	98	-0.360	151	-0.185	204	-0.020	257	0.130
46	-0.585	99	-0.355	152	-0.185	205	-0.020	258	0.130
47	-0.580	100	-0.355	153	-0.180	206	-0.020	259	0.130
48	-0.580	101	-0.355	154	-0.180	207	-0.020	260	0.130
49	-0.580	102	-0.350	155	-0.155	208	-0.020	261	0.135
50	-0.575	103	-0.350	156	-0.140	209	-0.015	262	0.135
51	-0.575	104	-0.345	157	-0.135	210	-0.015	263	0.135
52	-0.575	105	-0.340	158	-0.135	211	-0.015	264	0.135
53	-0.570	106	-0.335	159	-0.135	212	-0.015	265	0.140

Table 3. Sorted Walsh Averages for Moisture (continued)

<u>Order</u>	<u>W</u>	<u>Order</u>	<u>W</u>	<u>Order</u>	<u>W</u>	<u>Order</u>	<u>W</u>
266	0.145	319	0.330	372	0.505	425	0.985
267	0.150	320	0.330	373	0.505	426	0.985
268	0.160	321	0.335	374	0.505	427	0.990
269	0.160	322	0.345	375	0.510	428	1.010
270	0.165	323	0.345	376	0.510	429	1.015
271	0.165	324	0.360	377	0.510	430	1.020
272	0.165	325	0.355	378	0.515	431	1.025
273	0.165	326	0.355	379	0.515	432	1.030
274	0.170	327	0.360	380	0.515	433	1.055
275	0.170	328	0.365	381	0.520	434	1.255
276	0.170	329	0.365	382	0.520	435	1.500
277	0.170	330	0.370	383	0.530		
278	0.170	331	0.380	384	0.535		
279	0.175	332	0.385	385	0.540		
280	0.175	333	0.395	386	0.540		
281	0.175	334	0.400	387	0.540		
282	0.180	335	0.400	388	0.540		
283	0.180	336	0.405	389	0.545		
284	0.180	337	0.405	390	0.545		
285	0.190	338	0.405	391	0.545		
286	0.195	339	0.410	392	0.550		
287	0.200	340	0.425	393	0.550		
288	0.200	341	0.425	394	0.555		
289	0.200	342	0.430	395	0.555		
290	0.205	343	0.430	396	0.560		
291	0.205	344	0.435	397	0.570		
292	0.205	345	0.435	398	0.575		
293	0.210	346	0.435	399	0.575		
294	0.210	347	0.440	400	0.580		
295	0.210	348	0.450	401	0.580		
296	0.210	349	0.450	402	0.585		
297	0.215	350	0.455	403	0.585		
298	0.215	351	0.455	404	0.610		
299	0.220	352	0.455	405	0.635		
300	0.235	353	0.460	406	0.645		
301	0.240	354	0.460	407	0.650		
302	0.240	355	0.465	408	0.680		
303	0.240	356	0.465	409	0.685		
304	0.260	357	0.470	410	0.695		
305	0.265	358	0.470	411	0.720		
306	0.270	359	0.470	412	0.740		
307	0.285	360	0.470	413	0.740		
308	0.285	361	0.475	414	0.745		
309	0.290	362	0.475	415	0.770		
310	0.295	363	0.480	416	0.775		
311	0.310	364	0.480	417	0.760		
312	0.315	365	0.485	418	0.765		
313	0.315	366	0.485	419	0.800		
314	0.315	367	0.490	420	0.810		
315	0.320	368	0.495	421	0.830		
316	0.320	369	0.495	422	0.860		
317	0.320	370	0.500	423	0.940		
318	0.325	371	0.500	424	0.965		

STRUCTURAL ANALYSIS OF ASPHALTENES IN PETROLEUM HEAVY OILS BY LASER DESORPTION MASS SPECTROMETRY

M. Fujii, Y. Sanada and T. Yoneda,
Advanced Catalysts Research Laboratory, Petroleum Energy Center
KSP D-1237, 3-2-1, Sakato, Takatsu-ku, Kawasaki, Kanagawa 213-0012, Japan

M. Sato
Center for Advanced Research of Energy Technology
Hokkaido University, Kita-13, Nishi-8, Kita-ku
Sapporo, 060-8628, Japan

Key words: laser desorption mass spectrometry, asphaltenes, type analysis

INTRODUCTION

Asphaltenes are obtained as the precipitates when adding alkane to heavy oil such as vacuum residue, which are defined as n-heptane insoluble-toluene soluble, for example. For the reason of their heavy characteristics, they are a major component that occurs the deactivation of catalyst under the hydrotreating reaction, and make troubles such as the pipe plugging by forming sludges at the transportation. A number of analyses have been made by using many kinds of measurements, and many structure models have been proposed(1,2). In spite of these efforts, there have not been well-defined structures yet. Having the strong interaction of molecules for its chemical structure, they aggregate to form micelles as high-dimension structure in oil(3). Therefore, this would make difficult to measure the molecular weight of a unit molecule.

In this study, we have attempted to measure the molecular mass and the distribution for asphaltenes in Arabian heavy vacuum residue (AH-VR), Sumatra light vacuum residue (SL-VR) and hydrotreated oil of Arabian heavy atmospheric residue (AH-AR) by laser desorption time of flight mass spectrometry (LDMS). LDMS techniques have been applied to many kinds of heavy oils by the capability of larger mass range, but there are few observations of molecular mass above 2000 Da, especially for asphaltenes(4,5). We found that useful mass spectra were obtained from the selected measuring conditions, and compared the average molecular weight with those measured by vapor pressure osmometry (VPO) and gel permeation chromatography (GPC). Then, we made the structure analysis of asphaltenes which were fractionated by solvent or GPC separation. Furthermore, the type analysis of the homologous peaks observed at increasing the laser power was provided the difference of aromatic skeleton structures in asphaltenes.

EXPERIMENTAL

Asphaltenes were prepared from AH-VR and SL-VR by precipitation with n-heptane according to the procedure of Japan Petroleum Institute Standard (JPI-5S-22). Maltene (n-heptane soluble) was separated to 3 fractions (saturate, aromatic and resin) by column-chromatography. LDMS were measured with Thermoquest Co., Ltd. Vision 2000 Spectrometer, using angiotensin as a calibration standard. Samples were dissolved in solution of toluene(1 or 0.1 mg/ml), and 1 μ l of the solution was dropped on the laser target, then dried in air. Laser beams were shot on the sample surface with changing the place as every shot. Spectra were

gained by averaging about 20 shots. VPO measurements were made using UIC Inc. Osmomat 070-SA with toluene as the solvent at 333K and with nitrobenzene at 373K, calibrating by benzil. GPC measurements were made using Sensyu Scientific Co., Ltd. SSC-7100 (column : Shodex K-802.5 and K-805L, 8mmI.D.300mml.) in nitrobenzene for the eluent at 373K, calibrating by polystyrene.

AH-VR asphaltene was fractionated into 4 parts (S-1~S-4) by solvent separation using mixtures of methanol / toluene. The toluene solution of asphaltene of 1/30 wt/vol% was precipitated by addition of methanol, ratio of 30/70 vol/vol. The precipitant was settled for 5 hr at 283 K, and separated by centrifugation. The soluble, then, was separated stepwise by addition of methanol / toluene mixtures of 40/60 and 45/55, respectively. GPC separation was made using Toso Co., Ltd. Model SC-8020 (column : TSKgel G 3000H, 55 mmI.D.600 mmL) in chloroform for the eluent at room temperature, and 4 fractions (G-1~G-4) were obtained.

Hydrotreating was performed in a bench-scale fixed-bed continuous flow reactor system, using the demetallization catalyst. Five reactors having 18 mmI.D.560 mmL each were connected in series. The reaction conditions were: temperature at 653 K; pressure of 12 MPa; LHSV of 0.5 hr⁻¹, and H₂/oil ratio of 800 vol/vol. The feedstock was Arabian heavy atmospheric residue (AH-AR) (b.p. of 616°K). The product oil samples were obtained from the bypass line of each reactor outlet by 2% of the flow rate. These oils were distilled, and asphaltenes were prepared from the distillation residue.

RESULTS AND DISCUSSION

LDMS spectra of asphaltenes

The LDMS spectra of AH-VR and SL-VR asphaltenes are shown in Figure 1, where broad distribution profiles were observed up to m/z 6000. Some peaks below 200 might be assigned to metals, such as Na, K and Fe. Peak intensities grew up with the laser power increasing, and many fragments appeared in lower mass range. The addition of matrix, for example, 2,5-dihydroxybenzoic acid showed no effects to suppress the fragmentation. We extracted the spectrum with stronger intensity and less fragment to calculate the weight average molecular weight (M_w) and number average molecular weight (M_n). It showed a broad peak in the range from m/z 200 to 6000 with a maximum near 1500 and a shoulder peak near 400. The spectral shape was almost the similar for AH and SL. M_w and M_n for AH and SL with those by GPC and VPO are summarized in Table 1. It was noted that M_w or M_n obtained by LDMS was the smallest in value. It was reported that the polar solvent such as nitrobenzene was preferable to minimize the aggregation of asphaltene in measuring molecular weight, except for the calibration standard problem(6). However, the LDMS results indicated that asphaltene was measured at the stage of less aggregation. It means the values of almost an unit molecule, assuming that the whole molecules could be desorped or ionized without cracking. Again, it was noted that the average molecular weight of AH-VR asphaltene was almost the same as that of SL-VR, though the difference between AH-VR and SL-VR were appeared by means of GPC and VPO. This implies that the substantial molecules consisting of asphaltenes are not dependent upon kinds of crude oil.

Figure 2 shows the LDMS spectra of AH-VR saturate, aromatic and resin compared with the asphaltene. The saturate showed many sharp peaks below m/z 200 and a broad one from 200 to 1000, the aromatic had a broad peak from 200 to 2000, and the resin had a bimodal peak from 200 to 6000. The shoulder peak near 400 appeared in the asphaltene seems to coincide with that of aromatic or resin. It would be caused by the drawing of the partial components of aromatic or resin due to the structure similarity at the precipitation. Asphaltenes were further separated into 4 fractions by solvent and GPC. The LDMS spectra of solvent separated fractions (S-1~S-4) are shown in Figure 3. The fraction, S-1, behaves bimodal peaks having 2 tops near m/z 400 and 1500. The peak near 400 decreased and the peak near 1500 increased for the heavy fractions, S-2 and S-3. As for S-4, a peak near 1500 was observed only. The fraction is thought to be heavier or more polar in order from S-1 to S-4 standing upon the solvent separation mechanism(7). Therefore, the major part of S-1 is found to be aromatic or resin which might be drawn at the precipitation. There was no change in these profiles in the vicinity of 1500. This suggests that the asphaltene becomes separated as a function of solubility of micelles except for the drawn fraction, S-1 as contaminants. Figure 4 shows the LDMS spectra of GPC fractions. Their molecular weight distributions were shifted to larger in order from G-1 to G-4. While G-1 showed a bimodal spectrum in the range from m/z 200 to 6000, the others were almost the same of the broad one from 200 to 6000. The profile of G-1 seems to coincide with aromatic or resin. So, it can say again that the drawn component of asphaltene would be aromatic or resin. As asphaltenes are thought to be aggregated in solvent as described earlier, they would be separated by the solubility difference of micelles, not that of molecular structure due to no differences in the LDMS spectra. This suggests that they might have the other properties related to forming micelles.

Next, we tried to analyze the asphaltenes in the hydrotreated oils to make sure the structural changes by the reaction. Figure 5 shows the LDMS spectra of those asphaltenes (Rx-1, Rx-3 and Rx-5), prepared from the product oils of the first, the third and fifth reactor, respectively. It was observed that the profiles became flat and the peak of m/z 1500 in the profiles shifted to smaller mass near 600 with increasing the reaction pass. As there occurred the transfer from asphaltenes to maltenes, and the decrease of asphaltene contents under hydrotreating, it is hard to estimate the structural changes from analyzing the residual oil. But, we could insist that the molecular weight lowering of asphaltenes molecules would occur under hydrotreating.

Type analysis of homologous LDMS peaks

When increasing the laser power for the sample prepared by the solution of 0.1 mg/ml, many sharp homologous peaks appeared in the range from 200 to 5000, together with a lot of fragment peaks. The spectra of AH-VR asphaltene are shown in Figure 6. This phenomenon implies that the cracking of side chains attached to aromatic cluster and skeleton in asphaltenes was caused by the laser abrasion resulting the homologous compounds series with cracked fragments. The prominent series with a Δm of 24 interval is assigned to cata-type aromatic compounds. The ring number increases with one by two carbons. The proposed structural change of condensed aromatic rings is shown in Figure 7. The appearance of homologous peaks was also

observed in SL-VR as well as hydrotreated oils. We make sure the type analysis for these series of an interval of m/z 24 for AH-VR and SL-VR. The analysis is that (1) general formula of hydrocarbons is expressed as C_nH_{2n+z} , and (2) separation of hydrocarbons belonging to a given group with the definite z -value from the spectrum having lots of sharp peaks in LDMS. Calculation was computed by a personal computer system. The plots of the various types in the sample shown in Figure 8 provide "finger printing" of asphaltene. The notations mean that each series are classified by the component of the initial mass. It is clear that the type distribution in the asphaltene is dependent upon the kind of crude oils, while the average molecular weight and its distribution are the almost same. That is, the type analysis provides one of characterization of mixture of hydrocarbon and asphaltenes. LDMS is a useful tool for the structure analysis of asphaltenes with complexity and will be applied to obtaining deep insight of structure such as shape and size of aromatic skeleton.

CONCLUSIONS

The structures of the asphaltene in petroleum heavy oils were investigated from molecular weight distribution by LDMS. It was observed that the mass spectrum of asphaltene in AH-VR was in the range from m/z 200 to 6000 having two peaks, and that the former was small near 400 and the latter was large and broad near 1500. This distribution was almost the same for that in SL-VR, but not for that in the hydrotreated oil, which showed the shifting of the peak to the lower mass. From the results of fractions by solvent fractionation and GPC for AH-VR asphaltenes, it is found that the peak near 400 is assigned to aromatic or resin fraction drawn at the separation and that asphaltenes in micelles are comprised from the same molecular weight distribution.

Type analysis was made for the homologous peaks of a Δm of 24 in the range from 200 to 5000, which appeared by increasing the laser power. The appearance of these peaks might be suggested the number of aromatic cata-condensed ring system, that is, asphaltene would be association of compounds with the similar aromatic ring structures.

ACKNOWLEDGMENTS

This work has been carried out as a research project of the Petroleum Energy Center with the subsidy of the Ministry of International Trade and Industry.

LITERATURE CITED

- (1) Speight, J. G., *The Chemistry and Technology of Petroleum*, Marcel Dekker Inc.
- (2) Yen, T. F. and Chilingarian, G. V., *asphaltenes and asphalts, I*, Elsevier Science
- (3) Moschopedis, S. E., Fryer, J. F. and Speight, J. G., *Fuel*, **55**, 227(1976)
- (4) Parker, J. E., et al., *Fuel*, **72**, 1381(1993)
- (5) Hunt, J. E., Lykke, K. R. and Winans, R. E., *Pre. Pap. ACS. Div. Fuel Chem.*, **36**, 1325(1991)
- (6) Nali, M. and Manclossi, A., *Fuel Scie. and Tech. Int'l*, **13**, 1251(1995)
- (7) Andersen, S. I., Keul, A. and Stenby, E., *Petr. Scie. and Tech.*, **15**, 611(1997)

Table 1. Properties of asphaltenes

Sample	LDMS		GPC		VPO	(Mn)	density	fa	H/C
	Mw	Mn	Mw	Mn	nitrobenzene 373K	toluene 333K	g/cm ³	III-NMR	-
AH-VR	2040	1560	2280	1840	2870	12710	1.165	0.52	1.05
SL-VR	1980	1490	-	-	3170	12870	1.115	-	1.03

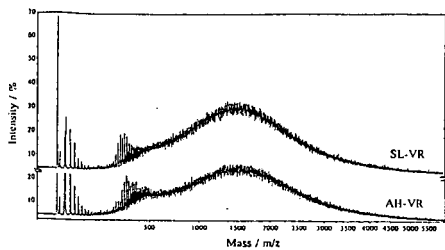


Figure 1. LDMS spectra of asphaltenes

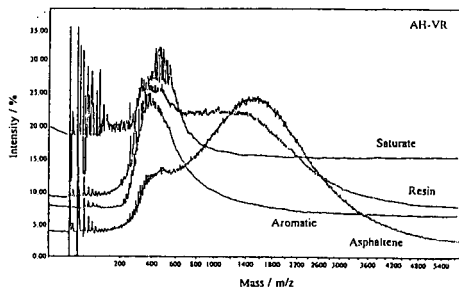


Figure 2. LDMS spectra of fractions by column chromatography

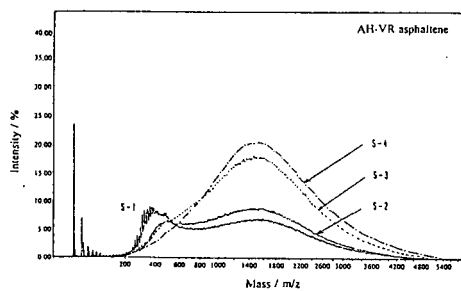


Figure 3. LDMS spectra of fractions by solvent separation

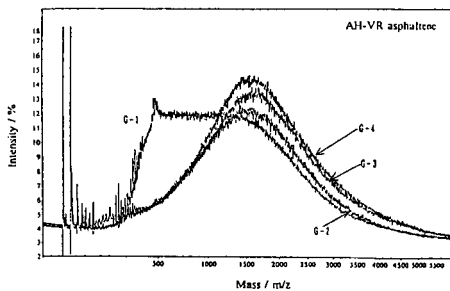


Figure 4. LDMS spectra of GPC fractions

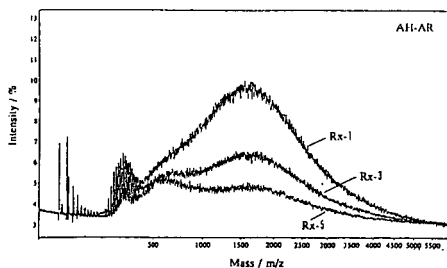


Figure 5. LDMS spectra of asphaltenes in the hydrotreated oils

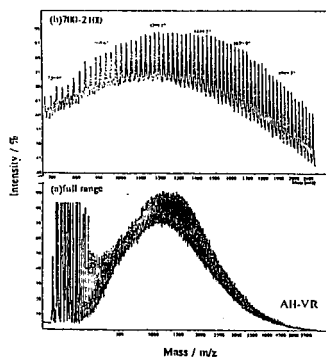


Figure 6. Homologous peaks of LDMS spectrum

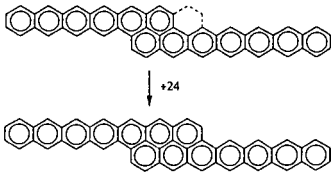


Figure 7. A model of structural changes with a Δm of 24

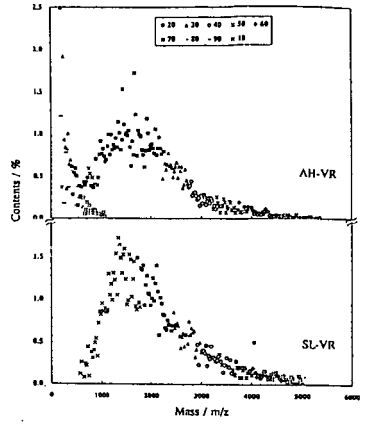


Figure 8. Type analyses of homologous peaks

UPGRADING OF BITUMEN WITH SUPERCRITICAL WATER FOR A SYSTEM COMBINED WITH SAGD.

H. Kamimura*, S. Takahashi†, A. Kishita*, T. Moriya†, C.X. Hong*, and H. Enomoto*

* Tohoku University, Dept. of Geoscience and Technology, Sendai 980-8579 Japan

† Japan National Oil Corp., Technology Research Center, 1-2-2 Hamada, Mihama-Ku, Chiba-Shi, 261-0025 Japan

‡ Tohoku Electric Power Co., Research and Development Center, 7-2-1 Nakayama, Aoba-Ku, Sendai, 981-0952 Japan

Key words: Upgrading, Bitumen, Supercritical Water

INTRODUCTION

Recent development of Steam Assisted Gravity Drainage (SAGD), which is believed to be an economically feasible recovery method of bitumen from oil sand deposits, is now asking for a new upgrading technology. In the operation of SAGD, mixture of bitumen and hot water at the temperature above 500 K is continuously recovered, so that the mixture recovered can be fed into a ground reactor. Then, the on-site upgrading by hydrothermal reaction could be a new technology as a combined system with SAGD.

Functions of water in hydrothermal reactions have been studied, and it was found by NMR analysis that hetero-atoms contained in low molecular compounds were easily substituted by hydrolysis and polymers were easily cracked to useful low molecular compounds with the supply of hydrogen from water [1].

On the basis of these fundamental studies, studies on the upgrading of bitumen in supercritical water were carried out.

EXPERIMENTAL

Batch-type autoclaves of 45 cm³ in volume were used. The autoclave and the induction furnace used for heating are shown in Fig.1. Experimental conditions of hydrothermal treatment are shown in Table 1. The sample oil was prepared by extraction from athabasca oil sands with toluene and subsequent evaporation of toluene. The viscosity of original oil (bitumen) is over 10⁵ mPa·s at 303 K.

In each experiment, 5 g of the bitumen was put into an autoclave with a certain amount of alkali aqueous solution and a stirring ball made of the same alloy as that of inner vessel of the autoclaves (Inconel 600). The autoclave was inserted horizontally at the center of the furnace and was heated up to a reaction temperature at the heating rate of 40°C/min. The content of autoclave was stirred with the stirring ball by rocking the furnace. After keeping the temperature for a certain time, the autoclave was taken out of the furnace and was cooled down to the room temperature at the similar cooling rate to the heating rate. Then the oil product was separated from water with separation funnel, but when the fractions of product were measured, toluene was used to wash the inner wall of the autoclave to ensure the recovery.

A rotational viscometer was used for measuring the viscosity of oil products at 303 K. Molecular weight distribution of oils was obtained with HPLC, which was calibrated with standard polystyrenes. Sulfur content was analyzed by CNS analyzer. Light oil components were analyzed with GC/MS and GC/AED (Atomic Emission Detector).

RESULTS AND DISCUSSION

Products

In all cases of hydrothermal treatment, bitumen was converted to much lighter oil. Fig.2 shows that the viscosity of oil products decreases with increasing temperature, and the reaction condition of 703 K for reaction temperature and 15min for reaction time is enough to produce sufficiently light oils for pipeline transportation.

Figure 3 shows the viscosity reduction with the reaction time as well as the water loading which is the ratio of the volume of water loaded into the reaction chamber to that of the reaction chamber. Drastic reduction was achieved in first 5 min. And the effect of water loading, that is water density, is also seen.

Figure 4 shows the influence of KOH concentration. As the KOH concentration increased, the viscosity of oil product slightly decreased, but when the KOH concentration is more than 5 mol/dm³ (M), the viscosity reduction is less. The viscosity

of oil product in case of without alkali is slightly lower than those with around 1 M alkali. In kinds of alkali, KOH was most effective.

Figure 5 shows normalized molecular weight distributions of oil products and original oil. Because of the characteristics of the separation column used, the distribution in the region of molecular weight less than 100 ($\text{LogMw}=2$) is not accurate. But, it is seen that the heavy components are diminished as the reaction proceeds.

Figure 6 shows the fraction of products by weight at different temperatures. Fractions of coke (toluene-insoluble), and gas and water-soluble organic compounds are increased with increasing temperature. But, the fraction of gas and water-soluble organic compounds is obtained as difference, and about a half of it is estimated to be lighter oil components which are evacuated in evaporating toluene used as the extractant. Therefore, it can be said that the fraction of asphaltene (n-pentane-insoluble but toluene-soluble) for the original oil is roughly equal to the sum of those of others than malten (n-pentane-soluble), that is to say, the fraction of malten does not change much.

Fraction of coke produced at 703 K is ca. 5%, which is much less than that in the thermal cracking. This may imply that hydrogen is supplied from water and/or the water prevents polymerization. The original vanadium content of 160 ppm was reduced to 12 ppm by the 15 min reaction at 703 K.

As to the gas composition, H_2 and CH_4 were produced, but CO_2 and H_2S gases did not exist when alkali solution was used. However, when pure water was used instead of alkali solution, CO_2 and H_2S as well as H_2 and CH_4 were produced.

Desulfurization

Figure 7 shows the desulfurization at various temperatures. The sulfur content of oil product at 703 K decreased to 2.0% from 4.5% (original). Fig.8 shows the variation of sulfur content with the reaction time. The sulfur content decreased to a half of the original value in first 5 min in all cases of water loading. After first 5 min, influence of water loading appears, but 30% of sulfur still remains even in the case of 40% water loading. In the case of thermal cracking without water, sulfur removal was less.

Figure 9 shows the GC/MS total ion chromatogram of oil product after 100 min reaction. The parent peaks of a series of paraffin and low molecular aromatic compounds were mainly detected. Fig.10(A) shows a S atom chromatogram of the oil product obtained with GC/AED. These peaks are grouped as C_1 to C_3 alkyl benzothiophenes and dibenzothiophenes with the help of GC/MS selected ion chromatograms. As examples, selected m/e number chromatograms corresponding to the parent peaks of C_1 to C_3 alkyl dibenzothiophenes are shown in Fig.10(B) to (D). The parent peaks of benzothiophene and dibenzothiophene were not detected.

As shown in Fig.8, it was difficult to decrease the sulfur content of oil products further by increasing the reaction time. Table 2 shows results of GC/MS and GC/AED analysis of oil products in long time reactions. It is seen that the concentrations of benzothiophenes (BTs) and dibenzothiophenes (DBTs) increased with reaction time and/or reaction temperature, though the total sulfur content changes little. This means that these BTs and DBTs are produced by breaking aliphatic C-C bonds in high molecular aromatic sulfur compounds and these aromatic compounds are hardly decomposed. Table 2 also shows the effect of water loading, which implies more breakage of C-S bonds with high water loading, probably in aromatic structures.

Decomposition of benzothiophenes and dibenzothiophenes

Figures 11 and 12 show results of hydrothermal decomposition of BT and DBT. BT was easily decomposed in the region of subcritical water. 5-Methyl BT is less reactive than BT but it was decomposed in the subcritical region. DBT was hardly decomposed in the near-critical region of water but was decomposed in the supercritical region of water as shown in Fig.12. However, only 50% of 2,8-dimethyl DBT was decomposed at the reaction condition of 703 K, 120 min, 40% water loading and 5 M KOH, at which 96% of DBT was decomposed.

These results show that low molecular aromatic sulfur compounds themselves, at least BTs, can be decomposed by hydrothermal reaction in the supercritical region of water, but they are hardly decomposed when mixed with other oil products.

DISCUSSION ON THE HYDROTHERMAL CRACKING

From the results so far described, it may be summarized that the viscosity reduction occurs simultaneously with desulfurization, but the dominant mechanisms in the first 5 min and subsequent reactions are different each other. In the first 5 min reaction, the thermal cracking may be dominant and the breakage of C-S bonds in aliphatic structures may occur. In this process, increase of water loading may cause hindering the thermal cracking, which proceeds by radical reactions, because of the enhancement of ionic character of water. At the next stage of cracking, the slow thermal cracking of C-C bonds and the hydrothermal cracking of C-S bonds probably in aromatic structures may lead to the reduction of viscosity and sulfur content. Through the whole process of cracking, water acts to suppress the production of coke. Data are not shown here, but experimental results of hydrothermal cracking of polymers show that hydrogen is supplied from water, which may prevent coking, where oxygen goes mostly into water-soluble compounds and some form CO_2 . Similar mechanisms may act in the hydrothermal cracking of bitumen, but it does not accelerate the reaction.

CONCLUSIONS

Fundamental studies on the hydrothermal cracking of oil sands in the region of supercritical water were carried out to clarify the reaction condition for developing a new on-site upgrading method. Reaction conditions of temperature of 700K reaction time of 5-15min, water loading of 20% (pressure \approx 3.1MPa) and 0.1-1 M KOH give us upgraded oils of viscosity of 10-20 mPa·s, sulfur content of less than a half and vanadium content of less than 10%, with less coke. It should be also emphasized that neither hydrogen gas nor catalyst was used, and neither CO_2 nor H_2S was issued. A combined system with SAGD can utilize the waste water to generate steam for injection.

ACKNOWLEDGMENT

The authors are grateful to Japan Petroleum Exploration Co., Ltd. (JAPEX) for financial support of a part of this work.

REFERENCE

[1] Nakahara, M., Tenuh, T., Wakai, C., Fujita, E., and Enomoto, H., ^{13}C -NMR Evidence for Hydrogen Supply by Water for Polymer Cracking in Supercritical Water. *Chemistry Letters* 1997, 163-164.

Table 1 Experimental Conditions.

water loading (%)	20-40
temperature (K)	673-723
time (min)	0-30
KOH (M)	1-10

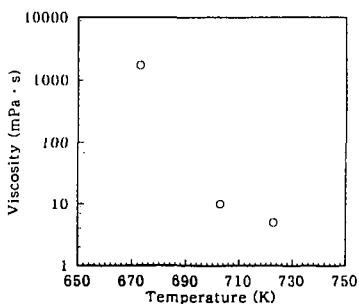


Fig. 2 Viscosity of oil products. (1M KOH, 20% water loading)

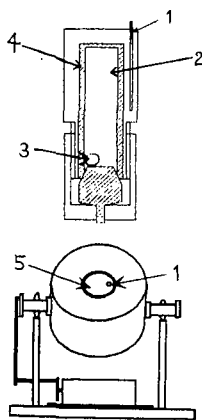


Fig. 1 A batch type autoclave (top) and the induction furnace (bottom).
1: thermocouple, 2: chamber
3: stirring ball, 4: inner vessel,
5: autoclave

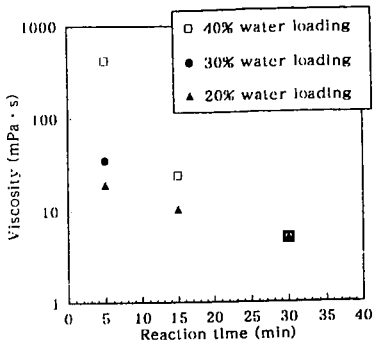


Fig.3 Viscosity of oil products with reaction time.

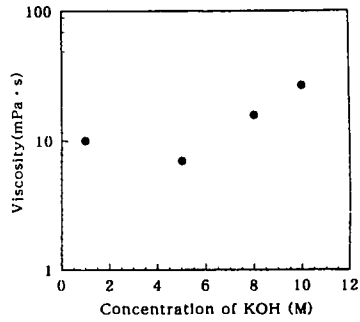


Fig.4 Influence of KOH concentration on the Viscosity of oil products. (Reaction temperature: 703K, Reaction time:15min, 20% water loading,)

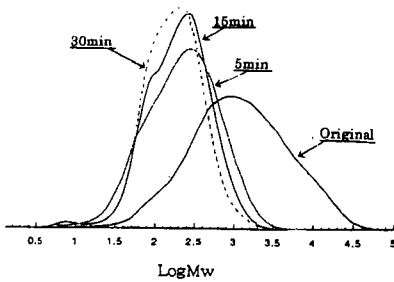


Fig.5 Comparison of molecular weight distribution. (Reaction temperature: 703K, 1M KOH, 20% water loading)

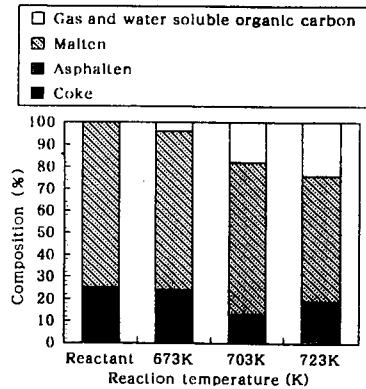


Fig.6 Fraction of products. (Reaction time: 15min, 1M KOH)

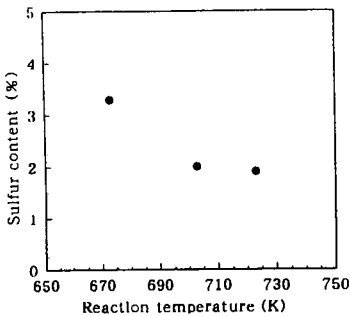


Fig.7 Sulfur content of oil products. (Reaction time:15min, 1M KOH 20% water loading)

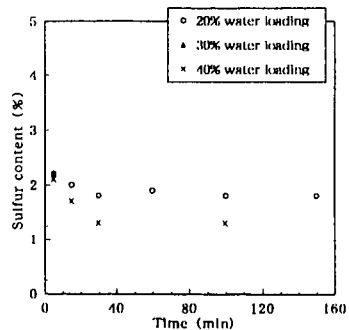


Fig.8 Influence of reaction time on sulfur contents of oil products. (1M KOH)

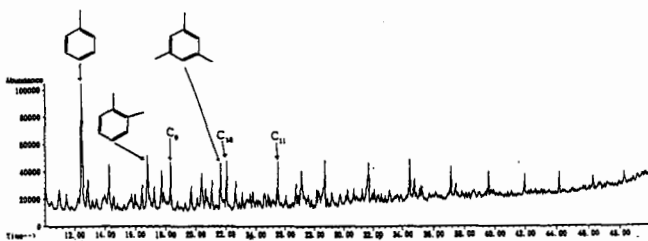


Fig.9 GC/MS chromatogram of n-hexane soluble oil products.
(Reaction temperature: 703K, Reaction time: 100min,
1M KOH, 20% water loading)

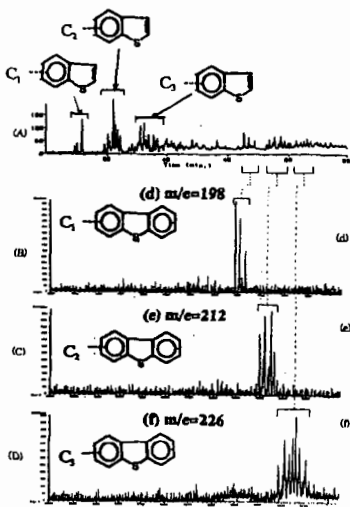


Table 2 Concentration of sulfur compounds.

No.	1	2	3	4	5	6
Temperature(K)	430	430	430	450	430	430
Time(min)	60	100	150	100	100	100
KOH (M)	1	1	1	1	1	5
Water Loading(%)	20	20	20	20	40	20
Sulfur content(%)	1.9	1.8	1.8	1.7	1.3	1.5
C ₁ -BT(wt%)	0.03	0.05	0.06	0.10	0.02	0.02
C ₂ -BT	0.06	0.10	0.12	0.17	0.06	0.07
C ₃ -BT	0.07	0.11	0.12	0.15	0.08	0.11
C ₁ -DBT	0.02	0.03	0.04	0.06	0.02	0.02
C ₂ -DBT	0.04	0.07	0.08	0.10	0.03	0.04
C ₃ -DBT	0.03	0.07	0.08	0.10	0.03	0.02
SUM	0.25	0.43	0.50	0.68	0.24	0.28

Fig.10 Chromatograms of low molecular sulfur compounds.

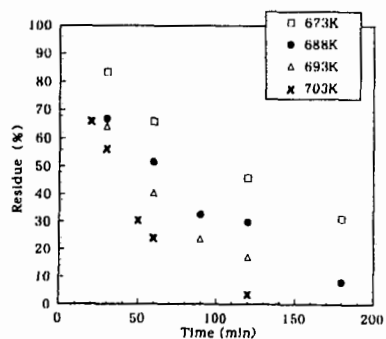


Fig.12 Decomposition of Dibenzothophene by hydrothermal reaction.
(5M KOH)

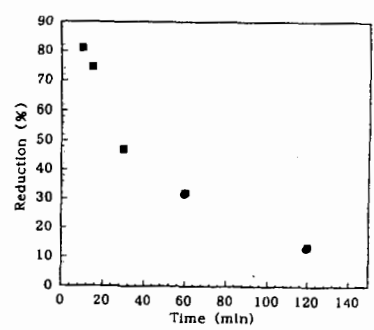


Fig.11 Decomposition of Benzothophene by hydrothermal reaction.
(Reaction Temperature:573K,5M NaOH)

HYDROCONVERSION CHARACTERISTICS ON NARROW FRACTIONS OF RESIDUA

Chaohe Yang¹, Jianfang Zhang, Chunming Xu, Shixiong Lin
State Key Laboratory of Heavy Oil Processing, University of Petroleum
Dongying city, Shandong province, China, 257062

ABSTRACT

An atmospheric residuum from Dagang crude of China(DGAR) and two vacuum residua from Arabian Light crude and Arabian Medium crude(SQVR and SZVR) were fractionated into 7-8 cuts by supercritical fluid extraction fractionation (SFEF) technique developed by State Key Laboratory of Heavy Oil Processing. The major properties of these fractions were measured, and each fraction was catalytically hydroprocessed in a 100 mL autoclave with crushed commercial Ni-Mo catalyst at the same reaction conditions. Removal of sulfur and nitrogen decreases with increase of the average molecular weight(AMW) of the feedstock, but the total conversion of heavy portion greater than 500 for every fraction is similar. The yield of coke increases with increasing AMW of feed, especially for the several heavier fractions, and the SFEF residue inhibits the HDS and HDN of other SFEF fractions to a certain extent.

INTRODUCTION

Due to increasing use of heavy oils and bitumen as refinery feedstock and the growing demand of light distillate oils, catalytic hydroprocessing of heavy oil plays an increasingly important role in modern petroleum deeply processing. Considerable effort has been focused worldwide on characterizing oils from the points of view of feedstock properties and the resultant kinetic properties. Much of this effort, however, has been directed at characterizing the reaction kinetics of whole oils, and the investigations about the hydroconversion features of narrow fractions of heavy oils are scarce. Hoog(1950)^[1] upgraded two narrow-boiling fractions and a whole gas oil, all at 375°C with a Co/Mo catalyst. The rate of desulfurization decreased with increasing boiling point. Yitzhaki and Aharoni(1988)^[2] processed a whole gas oil and fractionated the feed and products into narrow-boiling cuts. The desulfurization kinetics were estimated for each fraction based on the assumption that no sulfur compounds migrated between fractions. Their modeled kinetics showed that the HDS rate decreases with the increase of average boiling point of the feed. Constantine Philippopoulos and Nickos Papayannakos(1988)^[3] investigated the hydrocracking reaction of asphaltene from an atmospheric residuum and the HDS kinetics and diffusion properties of asphaltene and deasphaltene oil(DAO) of the atmospheric residuum in a small trickle-bed reactor. The hydrocracking of asphaltene and the HDS of DAO were elucidated very well with second order kinetic equations, the HDS reaction of asphaltene was represented by third order kinetics. The effective diffusivity of DAO is 5.85 times as big as that of asphaltene and the HDS rate of DAO is obviously faster than that of asphaltene. Trytten and Gray(1990)^[4] fractionated a heavy gas oil, produced by thermal cracking of Athabasca bitumen, into six narrow boiling cuts of nominal 50° width and a high boiling residue, and catalytically hydroprocessed them in a 150 mL CSTR with a commercial Ni/Mo catalyst. The AMW of the fractions range from 197 for the lightest one to 653 for high-boiling residue. The reaction conditions were $P_{H_2}=13.9\text{MPa}$ $V_{H_2}=1.05\text{L}/\text{min}$ $H\text{SV}=12.5\text{ml}/(\text{hg})$. Reaction results were treated by first order kinetics. The removal of sulfur and nitrogen as well as conversion of aromatic carbon decrease with the increase of feed AMW. The intrinsic activation energies of HDN and HDS do not change significantly with increasing feed AMW, but the apparent activation energies increase gradually. The estimated effectiveness factors increase with the increase of feed AMW for both reactions and pass through a maximum at a molecular weight of 362 for the feed. The reactivity decreasing of the sulfur and nitrogen with increasing feed AMW due to the steric effects or inhibition by components in the mixture plays a dominant role on the decrease of effectiveness factors for lighter fractions, although the estimated diffusivity decreases gradually.

Dai^[5] fractionated the Shengli Vacuum residuum into 14 cuts by the SFEF technique and separated each fraction into saturate, aromatics and resin by SARA method. Every resin in different fraction was catalytically cracked in a small reactor designed oneself. When the total yield of extract oil in SFEF is not greater than 78%, the resin in each fraction can be

cracked easily with a liquid yield of 65-75%. The reactivity of resin is greatly affected by its AMW, the greater the AMW of resin is, the poorer its cracking reactivity.

As a whole, the reaction features of feed vary with the AMW, or molecular size. Now there are not investigations about the hydroconversion characteristics of narrow fractions of residuum reported for lack of proper separation method. The SFEF technique developed by State Key Laboratory of Heavy Oil Processing affords the possibility to do such a work. In this paper, three residua were fractionated into narrow fractions by the SFEF method and all fractions were catalytically hydroprocessed at the same conditions.

EXPERIMENTAL

Feedstocks. Two vacuum residua of Arabian Light crude and Arabian medium crude were provided by Fushun Research Institute of Petroleum Processing, and Dagang atmospheric residuum came from Dagang refinery. Such three residua were separated respectively into 8 fractions by the SFEF method. The main properties of each fraction were measured and summarized in table 1.

Table-1 SFEF fraction properties of residua

DGAR, iso-butane as solvent in SFEF									
Fraction No.	1	2	3	4	5	6	7	8	residue
Fraction, m%	10.26	11.10	10.30	10.65	9.98	10.27	10.07	10.54	16.83
Sum, m%	10.26	21.36	31.66	42.31	52.29	62.56	72.63	83.17	100.0
20° density, g/cm ³	0.8721	0.8793	0.8855	0.8905	0.8960	0.9027	0.9103	0.9267	1.0616
Molecular weight	353	379	407	420	443	467	505	582	1473
S m%	0.101	0.112	0.149	0.152	0.176	0.197	0.234	0.315	0.780
N µg/g	436	1119	1430	1770	2066	2398	2940	3841	12979
H/C, mol/mol	1.81	1.80	1.78	1.77	1.75	1.73	1.71	1.66	1.39
SQVR, normal pentane as solvent in SFEF									
Fraction No.	1	2	3	4	5	6	7	8	residue
Fraction, m%	9.9	10.2	10.1	10.0	10.1	10.1	10.0	12.0	18.3
Sum, m%	9.9	20.1	30.2	40.2	50.3	60.4	70.4	80.4	98.7
20° density, g/cm ³	0.9432	0.9559	0.9634	0.9714	0.9789	0.9947	1.0232	1.0606	
Molecular weight	558	610	644	653	690	744	900	1128	3047
Carbon residue m%	2.2	6.1	6.2	6.5	8.4	12.6	15.4	26.8	33.1
S m%	2.55	2.60	2.94	3.20	3.48	4.11	4.74	5.56	5.89
N µg/g	1845	2088	2550	2823	3000	3863	5356	6100	8100
H/C, mol/mol	1.67	1.62	1.63	1.63	1.59	1.55	1.46	1.38	1.14
SZVR, normal pentane as solvent in SFEF									
Fraction No.	1	2	3	4	5	6	7	8	residue
Fraction, m%	10.2	10.2	10.2	10.0	10.2	10.0	9.9	5.0	24.6
Sum, m%	10.2	20.4	30.6	40.6	50.8	60.8	70.7	75.7	100.3
20° density, g/cm ³	0.9369	0.9484	0.9610	0.9740	0.9937	1.0056	1.0320	1.0533	1.1405
Molecular weight	498	611	657	711	802	826	1079	1124	3394
Carbon residue m%	3.0	4.0	4.8	6.8	10.3	14.5	21.3	27.0	44.8
S m%	2.70	2.71	2.92	3.54	4.18	4.41	4.83		6.40
N µg/g	2169	2490	3280	3950	4600	5803	7132		9700
H/C, mol/mol	1.69	1.66	1.64	1.63	1.56	1.51	1.47		1.19

Catalyst. A key catalyst used in Chevron VRDS process (CAT1) and another catalyst (CAT2) produced in China were chosen in this research, their major properties were listed in table 2. The average pore diameter of both catalysts is 30Å - 40Å, pore volume is 0.39 - 0.45 mL/g, and specific surface area is 203 - 275 m²/g. The main metal active components are molybdenum and nickel. Catalyst was crushed and sieved into 60/80 mesh particles (average diameter of 0.35mm), and the catalyst particles were presulfurized before use in reaction.

table-2 Major properties of catalysts

	CAT1	CAT2
Particle size/ mm	0.79	0.84
Particle density/ g/cm ³	1.52	1.50
Bulk density/ g/cm ³	0.89	0.88
Specific area/ m ² /g ⁻¹	275	203
Pore volume/ mL/g ⁻¹	0.45	0.39
Pore radius/ Å	33	38
Active components	Mo, Ni, Fe, Co	Mo, Ni, Fe,
support	γ-Al ₂ O ₃	γ-Al ₂ O ₃

Hydroconversion and Separation.

The flowsheet of heavy oil hydroconversion and separation was shown in figure 1. The crushed catalyst was presulfurized firstly, washed with solvent and dried in a vacuum drying oven. The presulfurized catalyst and sample were charged into the autoclave with the ratio of 1 to 10. After loading the catalyst and sample, the system was purged with hydrogen three times, then the temperature was increased gradually and the agitator was switch on when the temperature reached from 100°C - 150°C. Standard reaction conditions include a temperature of 400°C, initial hydrogen pressure(IHP) of 8.5Mpa at ambient temperature, and stirring rate of about 850rpm. After reaction, the autoclave was taken out from the heating furnace and put it into cooling water. When the temperature reaches to about 200°C, the reactor was placed into an isothermal water bath of 60°C in order to assure the consistency of sampling conditions and avoid or reduce the evaporation of light components in liquid product. While the autoclave comes to about 60°C, reactor was connected to a gas ration and sampling system for collecting gas product. The in-situ temperature, atmospheric pressure and the collected gas volume were recorded. Then the gas product was transferred into a gas sample bag for composition analysis. After sampling gas, the reactor was cooled down to ambient temperature, opening the reactor and taking immediately a little liquid product into a centrifugal test tube. The catalyst contained in the liquid product was deposited on the bottom of the test tube by centrifugation separation in a centrifugal machine at 5000rpm for 5 minutes. The upper oil in test tube was transferred to a sealed vial for simulated distillation analysis.

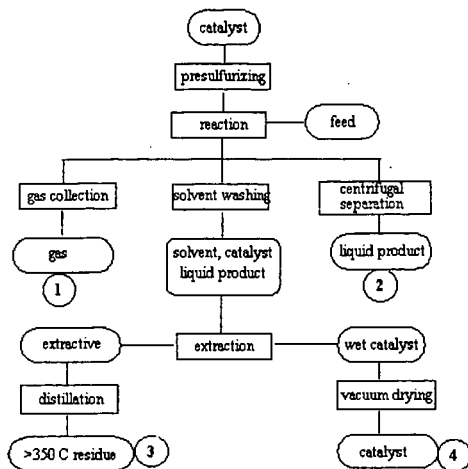


Fig.1 Hydroconversion and separation flowsheet

The remaining liquid product and catalyst in reactor was diluted with solvent and transferred into a Soxhlet apparatus, then extracted with dichloro-ethane for one hour, finally the extracted liquid should be not color. The wet catalyst in the extractor was taken out and placed into a vacuum drying oven to dry for coke content and other properties analysis. The extractive was distilled at atmospheric pressure to recover the solvent, then the liquid product was transferred into a small distillation flask of 150mL and subjected to vacuum distillation to obtain the high boiling residue of >350°C for analyzing the sulfur and nitrogen contents, molecular weight, and hydrocarbon group composition.

In the present study, the loss in experiment could be ignorable and sum of yields of gas, coke and liquid product accounted as 100%. Once the gas and coke yields are determined, the yield of any distillate can be calculated according to the simulated distillation data of liquid product.

RESULTS AND DISCUSSION

Hydroconversion of DGAR fractions. It is shown in table 3 that the removal of sulfur and nitrogen are similar for both catalysts. The HDS conversions are very high for No.1 to No. 8 fractions, all greater than 90%. The HDN conversion is greater than 75% for fraction lighter than No.7 fraction. HDS and HDN conversions decrease obviously with the increase of AMW of feed, and the declining rate for HDN is greater than that for HDS. The removal of sulfur and nitrogen in the SFEF residue is more difficult than other fractions, the conversion of HDS and HDN are only 44.3% and 16.4% respectively.

From the distribution of cracked product, the gas yield of each fraction do not change obviously except for the SFEF residue. In the latter case, the short side chains may be directly cracked into gas product, which results in the high gas yield. The yields of gasoline and diesel distillates lower with increasing the AMW of SFEF fractions. The distribution of product trends towards two ends for the SFEF residue, that is, gas and coke are produced greatly, which is same as the

features of polyaromatics cracking. It also can be seen that the coke yield increases gradually with the fraction becoming heavier. The coke yield of SFEF residue is about 4 times larger than that of No.8 fraction and 13 times as big as that of No.1 fraction.

Hydroconversion of SZVR and SQVR fractions. It is shown from the data in table 3 that the reactivity of HDS and HDN for SFEF fractions of SZVR and SQVR is obviously poorer than that of DGVR. Most of HDS conversions is less than 70%, and the HDN conversion is less than 60% for all fractions. This could be ascribed to the higher boiling point, larger molecular weight and stronger aromaticity of SZVR and SQVR compared with DGAR and most of sulfur and nitrogen atoms existing in the heterocyclic structures, which results in the difficulty of HDS and HDN reactions.

In general, the gas and coke yields increase with the fraction becoming heavier, although some experimental points fluctuate due to experiment and analysis errors. There is not coincident trend for the distribution of liquid product. The gas and coke yields increase seriously compared with other fractions.

Table-3 Hydroconversion results (400°C, 240 min, IHP of 8.5MPa)

SFEF fractions of DGAR									
feed	DGAR-1	DGAR-3	DGAR-5	DGAR-7	DGAR-2	DGAR-4	DGAR-6	DGAR-8	residue
catalyst	CAT1	CAT1	CAT1	CAT1	CAT2	CAT2	CAT2	CAT2	CAT1
S removal, %	96.3	95.0	94.7	91.6	95.8	94.4	93.4	90.7	44.3
N removal, %	95.2	87.6	79.1	60.9	94.9	84.8	76.1	48.3	16.4
Material balance, %									
gas	1.13	0.87	1.18	0.71	1.18	1.07	0.96	0.96	1.58
<200°C	7.76	6.94	5.37	3.96	5.37	4.93	3.65	3.89	7.21
200-350°C	37.81	24.86	19.76	14.49	22.94	18.92	14.28	12.76	10.47
350-500°C	53.10	60.65	59.66	49.14	61.89	58.51	52.51	39.27	27.01
>500°C	0.00	6.41	13.75	31.36	8.35	16.23	28.23	42.58	51.12
coke	0.20	0.27	0.29	0.33	0.27	0.36	0.38	0.56	2.60
SFEF fractions of SZVR									
feed	SZVR-1	SZVR-3	SZVR-5	SZVR-7	SZVR-2	SZVR-4	SZVR-6	residue	DGAR
catalyst	CAT1	CAT1	CAT1	CAT1	CAT2	CAT2	CAT2	CAT1	CAT1
S removal, %	92.5	70.9	51.1	31.0	85.9	75.7	54.0	27.4	78.1
N removal, %	59.8	42.2	20.2	13.3	53.7	38.0	19.7	7.4	41.9
Coke on Cat, %	4.56	5.59	10.74	15.69	6.06	8.19	11.78	23.74	
Coke amount, g	0.22	0.27	0.54	0.84	0.29	0.40	0.60	1.40	
Coke yield, %	0.49	0.60	1.22	1.87	0.64	0.89	1.33	3.11	
Material balance, %									
gas	1.22	1.18	2.24	3.13	0.49	0.93	2.07	3.16	
<200°C	8.70	7.14	11.24	12.32	7.83	8.61	9.60	2.95	
200-350°C	22.69	17.46	22.34	20.43	18.62	18.87	17.96	12.90	
350-500°C	42.72	31.02	29.18	21.32	32.92	29.54	24.65	15.90	
>500°C	24.18	42.60	33.79	40.92	39.50	41.16	44.38	61.98	
coke	0.49	0.60	1.20	1.87	0.64	0.89	1.33	3.11	
SFEF fractions of SQVR									
feed	SQVR-2	SQVR-4	SQVR-6	SQVR-8	residue	SQVR	SQVR		
catalyst	CAT1	CAT1	CAT1	CAT1	CAT1	CAT1	CAT2		
S removal, %	78.3	70.8	61.0	48.2	23.8	48.1	52.3		
N removal, %	31.2	24.8	15.3	5.5					
Coke on Cat, %	8.01	7.34	9.94	13.84	28.75	18.45	14.77		
Coke amount, g	0.44	0.40	0.55	0.80	1.81	1.02	0.78		
Coke yield, %	0.88	0.80	1.10	1.60	4.02	2.27	1.73		
Material balance, %									
gas	1.02	0.98	1.34	2.04	2.89	1.29	1.47		
<200°C	9.04	8.32	6.57	11.00	2.81	6.28	5.14		
200-350°C	16.88	16.00	16.79	14.57	11.46	14.43	12.91		
350-500°C	31.35	29.43	28.17	19.47	12.33	25.73	22.21		
>500°C	40.83	44.47	46.03	51.32	66.49	50.01	56.54		
coke	0.88	0.80	1.10	1.60	4.02	2.27	1.73		

Relation of coke yield and feed properties. Coking trend is an important factor of feed processing characteristics, it affects not only the activity and selectivity of catalyst and the distribution of product, but also the increase of bed pressure drop of reactor, energy consumption and the operation period. Coke yield increases with the increase of aromatic carbon fraction, f_a , in the average molecule, and is directly proportional to the content of resin and asphaltene in

feed, x_{RA} . The fitting equations are as follows,

$$y_{\text{coke}} = 8.076 \cdot f_a^{1.495} \quad (1)$$

$$y_{\text{coke}} = 0.05049 \cdot x_{RA} + 0.1776 \quad (2)$$

Where y_{coke} is the coke yield, wt%. The coking characteristics can also be represented by the heavy oil characteristic parameter, K_H , which is defined as,^[6]

$$K_H = 10 \cdot \frac{H/C}{AMW^{0.1236} \cdot d_4^{20}} \quad (3)$$

Where H/C is the atomic ratio of hydrogen to carbon, d_4^{20} is the relative density. With the decrease of feed K_H , coke yield increases slowly when $K_H=6.0-8.0$, the increasing rate of coke yield rises gradually with decreasing the feed K_H value, and grows seriously for $K_H < 6.0$. Such a relationship can be represented by the following equation,

$$y_{\text{coke}} = 444.5 \cdot K_H^{-3.23} \quad (4)$$

Relations of HDS & HDN reactivity and feed properties. The HDS and HDN conversions decrease quickly with the increase of the content of resin and asphaltene, and the decrease of atomic ratio of hydrogen to carbon. This suggests that it is more difficult to remove the sulfur and nitrogen atom in the heavier component. Figure 2 shows the relationships between the percentages of sulfur and nitrogen removal and the heavy oil characteristic parameter. With decreasing the K_H value, the removal of nitrogen decreases quickly when the K_H is bigger, and gradually tends towards a constant level which approximates the conversion for thermal cracking reaction. While $K_H > 8.0$, the declining rate of HDN reaction is faster than that of HDS reaction. This relationship behaves as S-type curve for HDS and as an ice stick for HDN. The HDS conversion is always greater than that of HDN for any fraction at the same reaction conditions. This implies that the reactivity of HDS and HDN lowers obviously with the increase of fraction AMW, and the removal of nitrogen is more difficult than that of sulfur.

The solid circle and bold plus sign are the data points of whole DGAR HDN and HDS. The K_H value of DGAR is 9.1, the responding HDS and HDN conversions predicted from the curves in figure 2 are 94% and 77% respectively, but the real HDS and HDN conversion are 71.0% and 41.9% respectively. This shows that the heavy components in residuum may inhibit the HDS and HDN reaction of lighter components to a certain extent. Due to the strong adsorptivity and high coking trend, these heavy components would affect the activity of catalyst and then decrease the catalytic reaction rate.

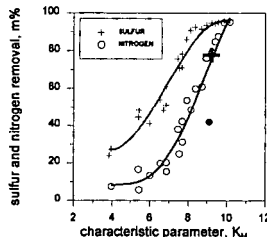


Fig.2 sulfur and nitrogen removal versus K_H

Comparing the HDS and HDN results for CAT1 catalyst with those for CAT2 catalyst shown in table 3, it is found that CAT1 has a similar HDS and HDN activity with CAT2 for lighter SFEF fractions, but for heavier fractions the latter has stronger catalytic activity than the former. This phenomenon may be attributed to the larger pore size of the CAT2 catalyst.

REFERENCE

1. Hoog H. J Inst Petro. 1950,36:738
2. Yitzhaki D, Aharoni C. AIChE J. 1988,23:342
3. Philippopoulos C, Papayannkos N. IEC Res. 1988,27(3):415
4. Trytten L C, Gray M R. IEC Res. 1990,29(5):725
5. Dai wenguo. The catalytic cracking characteristics of resins of narrower fractions of Shengli vacuum residuum. Master thesis, University of Petroleum, China. March 1993
6. Si Tiepan, Hu Yunxiang, et al. Acta Petrolei Sinica(Petroleum Processing Section).1997, 13(2):1

CHARACTERISTICS ON HDS AND HDN KINETICS OF NARROW FRACTIONS FROM RESIDUA

Chaohu Yang, Feng Du, Chunming Xu
State Key Laboratory of Heavy Oil Processing, University of Petroleum
Dongying city, Shandong province, 257062 China

ABSTRACT

An atmospheric residuum from Dagang crude of China (DGAR) and two vacuum residua from Arabian Light crude and Arabian Medium crude (SQVR and SZVR) were fractionated into 7-8 cuts by supercritical fluid extraction fractionation (SFEF) technique developed by State Key Laboratory of Heavy Oil Processing. These SFEF fractions were catalytically hydroprocessed in a 100 mL autoclave with crushed commercial Ni-Mo catalyst. The HDS and HDN diffusion-reaction model of residue in autoclave reactor was established. The diffusion and HDS and HDN characteristics of these fractions were discussed.

KEYWORDS: heavy oil, diffusion, HDS and HDN

INTRODUCTION

Because of the increase of heavy oils and bitumen as refinery feedstock and the growing demand of amount and quality for light distillate oils, catalytic hydroprocessing of heavy oil plays a growingly important role in modern petroleum deeply processing. Considerable effort has been focused worldwide on characterizing oils from the points of view of feedstock properties and the resultant kinetic properties. Much of this effort, however, has been directed at characterizing the reaction kinetics of whole oils, and the investigations about the hydroconversion features of narrow fractions of heavy oils are scarce. Hoog(1950)^[1], Yitzhaki and Aharoni(1988)^[2], Papayannakos(1988)^[3], and Trytten & Gray(1990)^[4] studied the hydroconversion of narrow fractions from distillates. The removal of sulfur and nitrogen as well as conversion of aromatic carbon decreases with the increase of average molecular weight (AMW) of feed. Although the hydroconversion is affected by its intrinsic reactivity and diffusion property, the intrinsic reactivity is the controlling factor of reaction rate, especially for the heavier fractions. In a small reactor designed oneself, Dai^[5] investigated the resin catalytic cracking of each SFEF fraction from Shengli Vacuum residuum. When the total yield of extract oil in SFEF is not greater than 78%, the resin in each fraction can be cracked easily with a liquid yield of 65-75%. The reactivity of resin is greatly affected by its AMW, the greater the AMW of resin is, the poorer the cracking reactivity.

As a whole, the reaction feature of feed varies with the AMW, or molecular size. Now there is not investigation about the hydroconversion characteristics of narrow fractions of residuum reported for lack of proper separation method. The SFEF technique developed by State Key Laboratory of Heavy Oil Processing affords the possibility to do such a work. In this paper, three residua were fractionated into narrow fractions by the SFEF method and the hydroconversion characteristics of every fraction were studied at the same conditions.

EXPERIMENTAL

Feedstocks Two vacuum residua of Arabian Light crude and Arabian medium crude were provided by Fushun Research Institute of Petroleum Processing, and Dagang atmospheric residuum came from Dagang refinery. Such three residua were separated respectively into 8 fractions by the SFEF method. The main properties of each fraction were measured, density at 20°C is of 0.8721 to 1.1405g/cm³, AMW of 353-3394, sulfur of 0.101-6.40 m%, nitrogen of 436-9700 µg/g, H/C atomic ratio of 1.40-1.81.

Catalyst A key catalyst used in Chevron VRDS process (CAT1) and another catalyst (CAT2) produced in China were chosen in this research. The average pore diameter of both catalysts is 33Å and 38Å, pore volume is 0.45 and 0.39mL/g, and specific surface area is 275 and 203m²/g. The main metal active components are molybdenum and nickel. Catalyst was crushed and sieved into 60/80 mesh particles (average diameter of 0.35mm), and the catalyst particles were presulfurized before use in reaction.

Hydroconversion and Separation The crushed catalyst was presulfurized firstly, washed with solvent and dried in a vacuum drying oven. The presulfurized catalyst and sample were charged into the autoclave with the ratio of 1 to 10. Reaction conditions were set as follows: 400°C 8.5Mpa of initial hydrogen pressure, 4 hours and 850rpm of agitation rate. After loading the catalyst and sample, the system was purged with hydrogen three times, then the temperature was increased gradually and the agitator was switched on when the temperature reached from 100° - 150°C. After reaction, the autoclave was taken out from the heating furnace and put it into cooling water. When the temperature reaches to about 200°C, the reactor was placed into an isothermal water bath of 60°C in order to assure the consistency of sampling conditions and avoid or reduce the evaporation of light components in liquid product. While the autoclave comes to about 60°C, reactor was connected to a gas ration and sampling system for collecting gas product. The in-situ temperature, atmospheric pressure and the collected gas volume were recorded. Then the gas product was transferred into a gas sample bag for composition analysis. After sampling gas, the reactor was cooled down to ambient temperature, opening the reactor and taking immediately a little liquid product into a centrifugal test tube. The catalyst contained in the liquid product was deposited on the bottom of the test tube by centrifugation separation in a centrifugal machine at 5000rpm for 5 minutes. The upper oil in test tube was transferred to a sealed vial for simulated distillation analysis.

The remaining liquid product and catalyst in reactor was diluted with solvent and transferred into a Soxhlet apparatus, then extracted with dichloro-ethane for one hour, finally the extracted liquid should be not color. The wet catalyst in the extractor was taken out and placed into a vacuum drying oven to dry for coke content and other properties analysis. The extractive was distilled at atmospheric pressure to recover the solvent, then the liquid product was transferred into a small distillation flask of 150mL and subjected to vacuum distillation to obtain the high boiling residue of >350°C for analyzing the sulfur and nitrogen contents, molecular weight, and hydrocarbon group composition.

In the present study, the loss in experiment could be ignorable, and sum of yields of gas, coke and liquid product accounted as 100%. Once the gas and coke yields are determined, the yield of any distillate can be calculated according to the simulated distillation data of liquid product.

DIFFUSION-REACTION MODEL

Reaction Kinetic Model The non-homogenous catalytic reaction with order of n can be described generally as follows:

$$r = -\frac{dN}{dt} \cdot \frac{1}{w_c s_g} = k_s c_m^n \quad (1)$$

Where, r--amount consumed on unit surface area of catalyst in unit time, mol/(m²·s);

N--amount of reactant, mol

t--reaction time, s;

w_c--catalyst weight, g;

s_g--specific surface area of catalyst, m²/g

c_m--concentration of reactant, mol/m³;

k_s--apparent rate constant for first-order reaction based on the surface area of catalyst, m³ⁿ/(mol⁽ⁿ⁻¹⁾·m²·s)

If the volume of reaction mixture is thought changeless in reaction process, the right end of equation above can be written as,

$$\frac{dN}{dt} \cdot \frac{1}{w_c s_g} = \frac{d(c_m \cdot v_r)}{dt} \cdot \frac{1}{w_c s_g} = \frac{v_r dc_m}{w_c s_g \cdot dt}$$

That is,

$$-\frac{dc_m}{dt} = \frac{w_c \cdot s_g}{v_r} \cdot k_s \cdot c_m^n \quad (2)$$

When v_r is the volume of reaction mixture(m³). The molar concentration of reactant is converted

into mass fraction, $c = \frac{c_m \cdot M}{\rho_r}$

Where, c--the mass fraction of reactant ;

M--molecular weight of reactant/g mol⁻¹;

ρ_r--density of reaction mixture at reaction temperature/gm³.

Substitution of the above relation in equation (2) gives,

$$-\frac{dc}{dt} = \frac{w_c \cdot S_g}{V_r} \cdot \left(\frac{\rho_r}{M}\right)^{n-1} \cdot k_i \cdot c^n \quad (3)$$

In the special case of $n=1$, equation (3) reduces to

$$-\frac{dc}{dt} = \frac{w_c \cdot S_g}{V_r} \cdot k_s \cdot c \quad (4)$$

Integrating equation (4), we get,

$$\ln \frac{c_0}{c} = \frac{w_c \cdot S_g}{V_r} \cdot k_s \cdot t \quad (5a)$$

or

$$-\ln(1-x) = \frac{w_c \cdot S_g}{V_r} \cdot k_s \cdot t \quad (5b)$$

Where x is the conversion of reactant $x = (c_0 - c) / c_0$. Solving the k_s From equation (5b) gives

$$k_s = -\frac{V_r \cdot \ln(1-x)}{w_c \cdot S_g \cdot t} \quad (6)$$

Many investigators^[6] have correlated their experimental data with first-order kinetics for the HDS and HDN reactions of residua. In general, the conversions of HDS and HDN are not greater than 90% in this study, and the feed with narrow range has similar reactivity for all compounds contained in it. For simplicity, HDS and HDN are treated as first-order irreversibly reactions, so the apparent rate constants can be calculated by equation (6).

Diffusion Effect The external diffusion effect on reaction rate is ignorable in the stirred autoclave with high agitation speed^[7]. The effect of reactant migration through catalyst micropores on reaction rate can be described by the effectiveness factor,

$$\eta = \frac{\text{actual reaction rate within pore}}{\text{rate of not slowed by pore diffusion}} \quad (7)$$

For first-order reaction, the relationships between effectiveness factor and Thiele modulus have been proposed for different catalyst shape.

$$\text{Single cylindrical pore}^{[8]} \quad \eta = \frac{\tanh(\phi)}{\phi} \quad (8)$$

$$\text{Long cylinder particle}^{[9]} \quad \eta = \frac{1}{\phi} \frac{I_1(2\phi)}{I_2(2\phi)} \quad (9)$$

$$\text{Sphere particle}^{[10]} \quad \eta = \frac{1}{\phi} \left[\frac{1}{\tanh(3\phi)} - \frac{1}{3\phi} \right] \quad (10)$$

$$\phi = \frac{V_p}{A_p} \cdot \left(\frac{\rho_p \cdot S_g \cdot k_i}{D_e} \right)^{1/2} \quad (11)$$

Where, ϕ —Thiele modulus, dimensionless

V_p —volume of catalyst particle, m^3

A_p —external surface area of catalyst particle, m^2

ρ_p —particle density of catalyst, g/m^3

k_i —intrinsic rate constant based on the surface area of catalyst, m/s

D_e —effective diffusion coefficient of reactant, m^2/s .

Although the forms of three equations above for different shape of catalyst particle are different, the predicted values of η at the same ϕ are similar, especially for the case of $\phi < 4$. In the present study, equation(10) for sphere particle was selected to describe the relationship of effectiveness factor of HDS and HDN reactions and Thiele modulus.

Assuming no temperature gradient exists between the external surface and the center of catalyst particle, for first-order irreversible reaction we have,

$$\eta = \frac{k_s}{k_i} \quad (12)$$

$$\text{for sphere catalyst particle} \quad \frac{V_p}{A_p} = \frac{d_p}{6} \quad (13)$$

where d_p is the equivalent sphere diameter(m). Substitution of equation (11), (12) and (13) in

equation (10) gives,

$$\frac{k_s}{k_i} = \frac{3}{A k_i^{0.5}} \left[\frac{1}{\tanh(A k_i^{0.5})} - \frac{1}{A k_i^{0.5}} \right] \quad (14)$$

where,

$$A = \frac{d_p}{2} \left(\frac{\rho_p \cdot s_g}{D_e} \right)^{1/2} \quad (15)$$

If the parameter d_p , ρ_p , s_g , v_r , w_c , t and x in equation (6), (14), (15) are obtained, the apparent rate constant k_3 can be calculated by equation (6), parameter A can be determined once the effective diffusivity is given. Instituting k_s and A into equation (14), the intrinsic rate constant, k_i , can be calculated by Newton iteration, and the effectiveness factor, η , will be determined by equation (12).

Estimation of Effective Diffusivity For heavy oil hydroconversion, three phases of gas, liquid and solid exist simultaneously, the reactant must firstly migrate through the micropores filled with liquid to the internal surface of catalyst, and then the catalytic reactions take place there. The transport in liquid-filled pores is usually described by a Fickian diffusion relation with a effective diffusion coefficient^[11] ($D_e = \frac{\epsilon}{\tau} D_b$). When the size of diffusion molecules and the pores are of the same order of magnitude, the interaction between the walls and coefficient tends to decrease the effective diffusivity. It belongs to the configuration diffusion and the effective diffusivity can be computed by the equation,

$$D_e = \frac{\epsilon}{\tau} D_b \cdot F(\lambda) \quad (16)$$

Where D_e —effective diffusion coefficient, m^2/s ;
 D_b —bulk diffusion coefficient, m^2/s ;
 ϵ —catalyst porosity, $\epsilon = V_g \cdot \rho_p$;
 V_g —pore volume of catalyst, m^3/g
 τ —catalyst tortuosity which have a value of 1-6, For catalysts in this study, τ was set to be equal to 4 according to the reference^[10].

$F(\lambda)$ is named as restricted diffusion Factor, $F(\lambda) = k_p \cdot k_r$ ^[12]. k_p is the ratio between the concentration of diffusion molecules inside and outside the pore and depends on λ , the ratio of pore to molecule diameter. For small solvent molecules, k_p satisfies the relation: $k_p = (1 - \lambda)^2$. When either the solute or the solvent absorb on the surface of pore, there is a resistance caused by drag exerted on the moving molecules by the walls. This influence is expressed through the drag coefficient, k_r .

Some relation of $F(\lambda)$ and λ were summarized in chapter I of reference [13], which are illustrated schematically in figure 1. Figure 1 shows that the theoretical model proposed by Renkin is very close to the experimental model developed by Lee through the kinetic experiment. Here the Renkin's relation was chosen to computer the restricted diffusion factor.

$$F(\lambda) = (1 - \lambda)^2 \cdot (1 - 2.104\lambda + 2.09\lambda^3 - 0.95\lambda^5), \quad \lambda < 0.5 \quad (17)$$

Bulk diffusion coefficient is calculated by Stokes-Einstein equation^[14],

$$D_b = \frac{kT}{3\pi \cdot \mu \cdot d_r} \quad (18)$$

Where, k —Boltzmann constant, $1.38 \times 10^{-23} J / K$;
 T —absolute temperature, K ;
 d_r —diameter of spherical solute, m ;
 μ —viscosity of solvent, $Pa \cdot s$.

The empirical relation between the equivalent spherical diameter and the molecular weight was selected to estimate the size of reactant^[13],

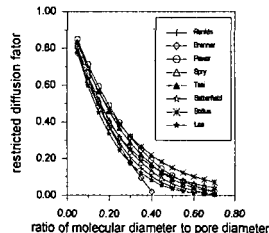


Fig.1 $F(\lambda)$ versus λ

$$d_r = 0.403 \cdot M^{0.537}$$

(19)

In industrial process, all molecules with different size exist in one system with the same viscosity of solvent. The viscosity of reactant mixture was estimated to be $1.24 \times 10^{-4} \text{ Pa} \cdot \text{s}$ under 390°C , 7.6 MPa in the study of residuum hydroprocessing. In the present study, every SEFE fraction was subject to hydroconversion, then the viscosity of reaction system may be different for different fraction. The viscosity of feed and product at reaction conditions was calculated using ASPEN software, and the viscosity in equation (18) was taken as an average of calculated viscosity of feed and product. The deviation of the viscosity for heaviest fractions may be larger for lack of distillation data of feed.

Now, the effective diffusivity can be determined through equations (19), (18), (17) and (16).

RESULTS AND DISCUSSION

The reaction product was classified into two lumps, the heavy lump of $>350^\circ\text{C}$ and the light lump of $<350^\circ\text{C}$. The sulfur and nitrogen in light lump migrated from heavy lump were thought removal by hydrogenation. Therefore, the conversion of HDS and HDN can be calculated according to the distillation data and the element analysis results.

The equivalent spherical diameter, bulk diffusion coefficient, effective diffusivity, effectiveness factor, apparent and intrinsic rate constant of HDS and HDN were obtained for every SEFE fraction in terms of the diffusion-reaction model mentioned above. The result was summarized in table 1.

Table 1A HDS diffusivities and kinetic parameters of SFEF fractions

feed	$d_r/\text{\AA}$	$F(\lambda)$	$D_b/10^{-10} \text{ m}^2 \cdot \text{s}^{-1}$	$D_e/10^{-10} \text{ m}^2 \cdot \text{s}^{-1}$	$k/10^{-4} \text{ m}^3 \cdot \text{s}^{-1}$	$k_p/10^{-4} \text{ m}^3 \cdot \text{s}^{-1}$	η
DGAR-1	9.34	0.522	112.2	10.01	9.250	9.323	0.992
DGAR-2	9.71	0.507	93.53	8.109	8.894	8.978	0.990
DGAR-3	10.1	0.492	85.27	7.175	8.405	8.490	0.990
DGAR-4	10.3	0.483	76.00	6.274	8.087	8.177	0.989
DGAR-5	10.6	0.474	72.30	5.858	8.242	8.341	0.988
DGAR-6	10.8	0.462	63.83	5.046	7.626	7.725	0.987
DGAR-7	11.3	0.445	51.71	3.936	6.949	7.055	0.985
DGAR-8	12.2	0.413	27.55	1.946	6.664	6.862	0.971
DGAR residue	20.2	0.198	2.116	0.072	1.641	1.997	0.821
DGAR	11.0	0.456	62.23	4.856	4.261	4.293	0.992
SZVR-1	11.2	0.448	38.48	2.949	7.267	7.422	0.979
SZVR-2	12.5	0.402	7.207	0.495	5.496	6.045	0.909
SZVR-3	13.1	0.385	6.894	0.454	3.463	3.697	0.936
SZVR-4	13.6	0.367	5.141	0.322	3.969	4.411	0.899
SZVR-5	14.5	0.339	3.415	0.197	2.007	2.189	0.916
SZVR-6	14.8	0.332	2.582	0.146	2.178	2.475	0.880
SZVR-7	17.1	0.269	1.761	0.081	1.475	1.725	0.855
SZVR residue	31.7	0.053	0.772	0.0069	0.785	1.839	0.426
SQVR-2	12.6	0.402	7.213	0.496	4.286	4.616	0.928
SQVR-4	13.0	0.386	5.383	0.356	3.454	3.753	0.920
SQVR-6	13.9	0.356	3.295	0.201	2.642	2.957	0.893
SQVR-8	17.5	0.258	1.413	0.062	1.845	2.375	0.776
SQVR residue	30.0	0.066	0.723	0.0082	0.762	1.584	0.481
SQVR	14.7	0.335	3.134	0.179	1.840	2.009	0.915
SQVR	14.7	0.334	3.134	0.179	2.077	2.293	0.905

Table 1B HDN diffusivities and kinetic parameters of SFEF fractions

feed	$d_r/\text{\AA}$	$F(\lambda)$	$D_b/10^{-10} \text{ m}^2 \cdot \text{s}^{-1}$	$D_e/10^{-10} \text{ m}^2 \cdot \text{s}^{-1}$	$k/10^{-4} \text{ m}^3 \cdot \text{s}^{-1}$	$k_p/10^{-4} \text{ m}^3 \cdot \text{s}^{-1}$	η
DGAR-1	9.34	0.522	112.2	10.01	8.520	8.582	0.992
DGAR-2	9.71	0.507	93.53	8.109	8.350	8.423	0.991
DGAR-3	10.1	0.492	85.27	7.175	5.857	5.898	0.993
DGAR-4	10.3	0.483	76.00	6.274	5.285	5.324	0.992
DGAR-5	10.6	0.474	72.30	5.858	4.392	4.420	0.993
DGAR-6	10.8	0.462	63.83	5.046	4.016	4.043	0.993
DGAR-7	11.3	0.445	51.71	3.936	2.634	2.650	0.994
DGAR-8	12.2	0.413	27.55	1.946	1.851	1.866	0.991
DGAR residue	20.2	0.198	2.116	0.072	0.502	0.533	0.941
DGAR	11.0	0.456	62.23	4.856	1.523	1.527	0.997
SZVR-1	11.2	0.448	38.48	2.949	2.357	2.376	0.992
SZVR-2	12.5	0.402	7.207	0.495	2.160	2.217	0.974
SZVR-3	13.1	0.385	6.894	0.454	1.338	1.383	0.971
SZVR-4	13.6	0.367	5.141	0.322	1.341	1.402	0.956
SZVR-5	14.5	0.339	3.415	0.197	0.833	0.650	0.973
SZVR-6	14.8	0.332	2.582	0.146	0.615	0.638	0.964
SZVR-7	17.1	0.269	1.761	0.081	0.400	0.417	0.958
SZVR residue	31.7	0.053	0.772	0.0069	0.215	0.281	0.766
SQVR-2	12.6	0.402	7.213	0.496	1.049	1.068	0.982
SQVR-4	13.0	0.386	5.383	0.356	0.799	0.815	0.980
SQVR-6	13.9	0.356	3.295	0.201	0.465	0.475	0.980
SQVR-8	17.5	0.258	1.413	0.062	0.158	0.162	0.978

The molecular size of SEFE fractions is 10-20Å and 20-30Å for the SEFE residue. The largest ratio of diffusion molecule diameter to pore diameter is 0.48, which is less than 0.5. In the present study conditions, bulk diffusivity is $0.7 \sim 112 \times 10^{-10} \text{ m}^2/\text{s}$, and the effective diffusivity is $0.006 \sim 10 \times 10^{-10} \text{ m}^2/\text{s}$. The bulk diffusivity varies within the range of liquid diffusivity for less viscous system. The effective diffusivity belongs to the range of configuration [16]. For less viscous system the diffusivity agrees with that in reference very well [17], but for more viscous system, no published data can be used to compare.

The apparent and intrinsic rate constants are $0.76 \sim 9.25 \times 10^{-12} \text{ m/s}$ and $1.58 \sim 9.32 \times 10^{-12} \text{ m/s}$ for HDS, and $0.15 \sim 8.52 \times 10^{-12} \text{ m/s}$ and $0.16 \sim 8.58 \times 10^{-12} \text{ m/s}$ for HDN. For the same feed, HDS reaction rate is always greater than HDN. Which means that the removal of nitrogen is more difficult than that of sulfur in heavy oil.

The differences of rate constants between HDS and HDN for different feeds are shown in figure 2. Such differences are obviously greater for medium fractions than for lighter and heavier fractions. It may be ascribed to the difficulty for lighter fraction reaching to high conversion of HDS reaction and for the removal of sulfur and nitrogen of heavier fraction with high aromaticity. Therefore, the deeply HDS of lighter fraction is very difficult as the HDS and HDN of heavier fraction.

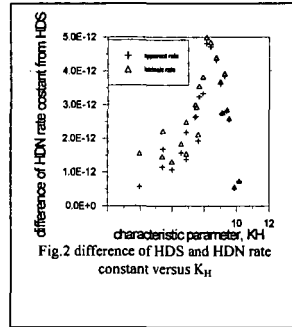


Fig.2 difference of HDS and HDN rate constant versus K_H

Figure 3 and 4 shows the relationships of apparent and intrinsic rate constant of HDS and HDN and the heavy oil characteristic parameter^[18], K_H , and the molecular weight of feed. The apparent and intrinsic rate constants decrease quickly with the increase of AMW, and reach to a stable value. Rate constants vary with the decrease of K_H with the similar mode mentioned above, and the minimum value in close to the level of thermal cracking. It is better to describe the HDS and HDN reactivity of SEFE fractions with the heavy oil characteristic parameter than AMW. The intrinsic reactivity decreases most quickly at $K_H=8.0$ for HDS reaction, and quickly at the startup of $K_H=9.5$. This phenomenon agrees with the common views that the HDS reactivity is obvious greater than that of HDN for lighter distillate.

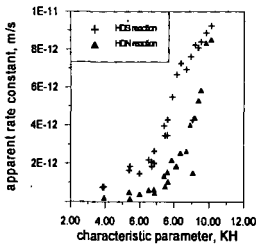


Fig.3A k_a versus K_H

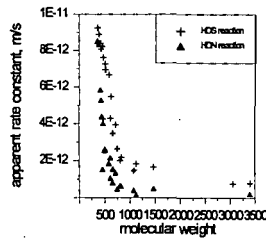


Fig.3B k_a versus AMW

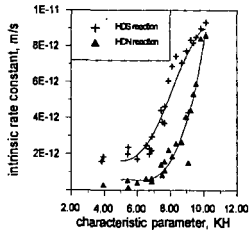


Fig.4A k_i versus K_H

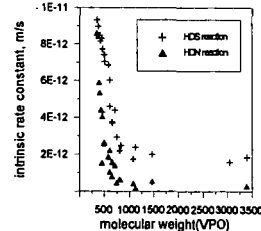


Fig.4B k_i versus AMW

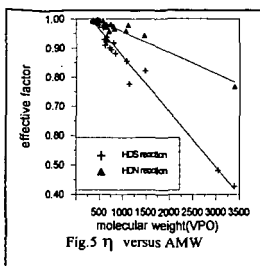


Figure 5 is the plots of relationships of effectiveness factors of HDS and HDN and the molecular weight of feed. The effectiveness factors decrease proportionally with the increase of AMW. This means that diffusion effect exists in the present reaction conditions, and the heavier the fraction is, the larger the molecular size, and the severer the diffusion effect.

With the increase of fraction AMW, the decrease of intrinsic rate constant for HDN is faster than for HDS, but the decrease of effectiveness factor for HDN is slower than for HDS. Therefore, the poorer HDS and HDN reactivity for heavier fractions can be explained by the lower intrinsic reactivity as

well as stronger diffusion resistance, and the decrease of intrinsic reactivity is the controlling factor for HDN reaction.

CONCLUSION

Through the catalytical hydroconversion of SFEF fractions which properties change in a large range, some conclusions were emerged. The diffusion of macromolecule in catalyst micropore filled with liquid belongs to configuration diffusion. The HDS and HDN diffusion-reaction model of residue in autoclave reactor was established. The intrinsic and apparent rate constants of HDS and HDN reaction obtained in terms of the kinetic model decrease quickly and reach to stable values with the increase of average molecular weight. HDN rate constant declines faster than that of HDS, but the effective factor of HDS decreases more quickly than that of HDN. It means that the low conversion of HDS and HDN reaction for heavier SFEF fractions could be ascribed to the poorer reactivity and the stronger diffusion resistance. The heavier the SFEF fraction, the larger the molecular size, and the severer the effect of diffusion on the reaction.

REFERENCES

1. Hoog H. *J Inst Petro.* 1950,36:738
2. Yitzhaki D, Aharoni C. *AIChE J.* 1988,23:342
3. Philippopoulos C, Papayannkos N. *IEC Res.* 1988,27(3):415
4. Trytten L C, Gray M R. *IEC Res.* 1990,29(5):725
5. Dai wenguo. The catalytic cracking characteristics of resins in different narrow fractions of Shengli vacuum residuum. Master thesis, University of Petroleum, China. March 1993
6. Chang Jie, Kinetics and Catalyst Deactivity Model of Residua. Doctoral thesis, Beijing Research Institute of Petroleum Processing, China, August 1997
7. Shah Y T, Paraskas J A. *ICE Press Des.Dev.* 1975, 14(4):368
8. Levenspiel O. *Chemical Reaction Engineering(second edition).* JohnWiley & Sons, Inc. 1972, P474
9. Ruckenstein E, Tsai M C. *AIChE J.* 1981, 27(4):697
10. Chen Gantong, *Chemical Reaction Engineering(Chinese).* Chemical Industry Press, July 1981, P182
11. Carberry J J, *Chemical Reaction and Reactor Engineering.* Marcel Dekker, Inc. 1987, P251
12. Renkin E M. *Journal of General Physiology.* 1954, 38:225
13. Yang Chaohe. Characteristics and kinetics of heavy oil Hydroconversion. Doctoral Thesis, University of petroleum, Beijing, China, 1997
14. Shi Jun. *Handbook of Chemical Engineering(section 10)Mass Transfer.* Chemical Industry Press, October 1989, P10-80
15. Chen Y W, Thasi M C. *IEC Res.* 1995, 34:898
16. Weisy P B. *Chem. Techn.* 1973:504
17. Baltus R E. *Fuel Sci & Techn.Intl.* 1993, 11(5&6):52
18. Si Tiepan, Hu Yunxiang, et al. *Acta Petrolei Sinica(Petroleum Processing Section).* 1997, 13(2):1

COKE FORMATION AND CHARACTERIZATION DURING THERMAL TREATMENT AND HYDROCRACKING OF LIAOHE VACUUM RESIDUUM

Zong-xian Wang, Ai-Jun Guo, Guo-he Que
National Heavy Oil Processing Laboratory, University of Petroleum
Dongying, Shandong 257062, P. R. China

The physical and chemical properties and structural compositions of Liaohe residuum were studied. The coke formation in the processes of thermal conversion and slurry catalytic hydrocracking reaction of the residuum was subsequently investigated. Then, the relationship between coke formation tendency and physicochemical compositions of the residuum was studied. The effect of initial coke formation on the propagation of coke formation was also studied. Using high-precision microscope and FTIR, the formed coke was characterized. With increasing processing severity, the coke formed in the bulk of reaction fluid system is changing from fine particulate form to coke cluster form. Initially formed coke seems to promote coke formation and growth of coke clusters during thermal treatment under low pressure. The on-set of coke formation is quite closely related to the ability of reaction system to peptize coke precursors.

KEY WORDS: coke formation, thermal treatment, hydrocracking, vacuum residue.

INTRODUCTION

Coke formation has long been a concern of petroleum refiners and researchers because petroleum residue processing is often limited by coke formation. This limitation is very severe in the cases of visbreaking, catalytic hydrotreating and catalytic hydrocracking, in which no appreciable amount of coke can be tolerated because of the need to flow freely through coils or catalyst-bed and the need to keep catalysts active. In the FCC or RFCC and slurry-bed catalytic hydrocracking (SBCH) processes, coke formation may deactivate catalysts and decrease the depth of upgrading. Even the delayed-coking process would be limited by coke formation in heating coils. Hence, the coke formation is one of key factors influencing petroleum residue upgrading.

In addition to processing conditions, the physical and chemical properties and structural composition of petroleum residues dictate the action of coke formation (1-4). A vacuum residue (VR) with low H/C atomic ratio and high carbon residue may be of high propensity to produce large amount of coke, to which much attention has been paid by RFCC, Coking and SBCH processes. The inducing period of coke formation is not only related to carbon residue value but to the miscibility of residue sub-fractions and particularly to the ability for vacuum residue system to peptize its asphaltene and coke precursors (5-7). Evidently, the long inducing period of coke formation is relevant to visbreaking and hydrotreating processes. Therefore, the study on coke formation is of significance in searching for coke inhibition procedures.

This work is intended to take Liaohe vacuum residue as a specimen to study, in detail, its physical and chemical properties and structural composition, and to investigate coke formation during its thermal, hydrothermal conversion and slurry-bed catalytic hydrocracking.

EXPERIMENTAL

Sample

Liaohe vacuum residue was collected from Liaohe Petrochemical Plant in March 1996; Gudao VR was collected from Shengli Oil Refinery. Their general properties are listed in Table 1.

Analytical Procedures

Isolation of Six Sub-fractions

Liaohe and Gudao vacuum residues were chromatographically separated into six fractions, i.e. light oil (F1), heavy aromatic fraction (F2), light resin (F3), middle resin (F4), heavy resin (F5) and n-pentane asphaltene (F6) by using a procedure described in reference (8)

Ultimate Analysis and Molecular Weight Measurement

Carlo Erba 1160 elemental analyzer was used for C, H, N analysis; atomic absorption method was used to determine Ni, V, Fe and Ca contents. Average molecular weight was measured by using VPO method (benzene as solvent, 45 °C) with Knauer molecular weight analyzer.

FTIR and Microscopic Characterization of Petroleum Coke

FTIR analysis of coke was conducted at Nicolet Magna 750 IR analyzer, a mold flat of coke and KBr mixture as sampling. An OLYMPAS HS-2 microscope was used to visualize the coke formed in the bulk of reaction system.

Liaoh VR Thermal and Hydrothermal Conversion and Catalytic Hydrocracking

The experiments were carried in a 100ml FDW-01 autoclave reactor with an up-and-down stirrer at 120 times of reciprocation per minute. Initial pressure was 5.0Mpa N₂ for thermal conversion and 7.0Mpa H₂ for hydrothermal conversion and catalytic hydrocracking. Catalyst used in hydrocracking reaction was Mo based oil soluble additive (ca.200 PPM Mo in reaction feed), and was pre-sulfided by elemental sulfur at 320°C for 30minute after mixing with Liaoh VR (S/Mo atomic ratio=3/1). Reaction temperature (430°C) was reached within 25minute from room temperature. After 1 hr. reaction time, the reactor was quenched (cooled) to room temperature, the reactor gas was vented, and toluene slurry was prepared from the reactor contents. Any solids adhering to the reactor walls or internals was carefully scraped off. The slurry was centrifuged into the toluene insoluble (TI or coke) and the toluene soluble; the toluene insoluble was then washed (extracted) with boiling toluene and separated by using quantitative filter paper, and then dried and weighed. The toluene soluble was distilled into several fractions. The data are listed in table 4.

RESULTS AND DISCUSSION

Relation Between Feed Properties and Coke Formation

The data in table I show that Liaoh VR, in contrast to Gudao VR, is high in viscosity, CCR, heavy metals, nitrogen content, aromaticity (f_a) and the ratio of aromatic ring number to naphthenic ring number (R_a/R_n). This indicates that Liaoh VR will generates more coke than Gudao VR under high processing severity (e.g. delayed coking and RFCC).

However, the SARA analysis (group composition) is similar for these two VR, for example, the oil fractions (saturates+aromatics) are 47.7% and 49.3% for Liaoh VR and Gudao VR respectively. Even the n-heptane asphaltene (nC7-At) content of Liaoh VR is less than that of Gudao VR. Even the oil fraction of Liaoh VR has lower density, viscosity, pour point, CCR, sulfur, nitrogen and metal contents, contrast to the oil fraction of Gudao VR.

Therefore, it can be inferred that the qualities of resin and asphaltene fractions of Liaoh VR must be much inferior to those of Gudao VR. It is verified by further analysis of six sub-fractions of these two VR, as seen in table 3. The nitrogen, nickel and CCR in heavy resin and asphaltene account for 69.1%, 78.6% and 74.1% respectively of total N, Ni and CCR in Liaoh VR, while the corresponding values are only 61.0%, 61.0% and 63.0% for Gudao VR. The aromaticity and R_a/R_n ratio of Liaoh resin and asphaltene are much higher than those of Gudao resin and asphaltene, indicating that the cracking performance of Liaoh resin and asphaltene must be quite poor.

Besides, there exists a great difference in molecular weight distribution in Liaoh VR six sub-fractions. The ratio of asphaltene molecular weight to oil molecular weight for Liaoh VR is about 9.5, while that for Gudao is only about 4.6. The gap between properties of oil fraction and resin-asphaltene fraction of Liaoh VR is much wider than that of Gudao VR, which implies that the system of Liaoh VR is not harmonious, and its colloidal stability must be very low. All those above show that Liaoh VR is kind of inferior heavy oil; the propensity to coke formation is much higher than Gudao VR during processing. A preliminary thermal treatment test has shown that the inducing period of coke formation of Liaoh VR is shorter than that of Gudao VR.

Distribution of Products in Thermal Treatment and Hydrocracking of Liaoh VR

Table 4 lists 450°C⁻ fraction, 450°C⁺ cracked residue, coke content in reaction products and

pentane asphaltene content in cracked residue. With reaction temperature being increased, 450°C fraction yields increases for all three series of reactions, and the increment is the highest for thermal reaction and the least for catalytic hydrocracking with Mo based catalyst. But the conversion to light products is the highest for the latter process under unit coke formation condition. Under the reaction condition of 430°C and reaction time 1 hr, the coke formation is less than 1% and conversion reaches up to 50% for the latter process; while coke formation is much greater than 1% as conversion reaches 50% for other two series of reactions of Liaohe VR. The coke formation increases rapidly with temperature for thermal treatment of Liaohe VR, but quite slowly for catalytic hydrocracking. The asphaltene contents in three reaction systems are changed in the similar tendency with cracked residue proportions. The molecular weight of asphaltene decreases with increasing reaction temperature for all these three reaction systems. The decrease of asphaltene molecular weight for thermal treatment is most eminent.

Characterization of Coke Formation by Microscopic Analysis

Reacted materials were sampled from the bulk of reaction system with thin glass plate as the samplers and then visualized by using an OLYMPAS HS-2 microscope. Three series of microphotographs (10×40×3.3) were taken of reacted materials from three series of reaction systems of Liaohe VR thermal treatment, hydro-thermal treatment and catalytic hydrocracking. The microscopic analysis showed that there was yet little coke at 420°C for hydrocracking system. With temperature increasing, the coke formed in the bulk of reaction system was changing from fine dispersed particle forms to small clusters(about 0.1-0.2% coke contents), corresponding temperatures being at 425, 415 and 400°C for thermal treatment, hydro-thermal treatment and catalytic hydrocracking respectively; and further to coke clusters corresponding temperatures being at 430, 420, 415°C respectively.

Characterization of Coke by FTIR

Fourier Transition Infrared spectrometry (FTIR) is a useful technique for characterizing organic functional groups of organic substances. Naturally it can be used to characterize the coke formed in reaction system and to describe the changes of different organic function groups, such as aromatic carbon, paraffinic carbon and substitution extent of aromatic ring periphery, of coke with increasing reaction severity.

Aromatic C=C double bond vibrates at 1600 cm^{-1} aromatic C-H bond vibrates at 3030 cm^{-1} , and 750 cm^{-1} , 810 cm^{-1} , 870 cm^{-1} . Paraffinic C-H vibrates at 2920 cm^{-1} , 2860 cm^{-1} , 1460 cm^{-1} and 1380 cm^{-1} . Here, the relative vibrating strength (A_x), i.e., the ratio of vibrating strength (A_x) of function groups to C=C vibrating strength (A_{1600}), was used to describe the relative changes of coke function groups and to reveal the way in which chemical structures change. The relative vibrating strengths of several organic function groups of coke formed at different severity in Liaohe VR reaction systems were tabulated in table 5. With temperature increasing, A_{2920} and A_{2860} seemed gradually decreasing, showing the paraffinic portion of coke decreasing and aromaticity relatively increasing. A_{870} , A_{810} and A_{750} increased with temperature increasing, showing that constitution extent of aromatic ring was decreasing and side chain cracking occurred. Therefore, FTIR is an effective means for characterization of coke formation during VR processing.

Mechanism of Initial Coke Formation and Its Effect

Vacuum residue is a colloidal system with asphaltene and heavy resin as dispersed phase and oil fraction and light resin as media. If physical and chemical properties of dispersed phase were much different from those of media constituents, the media would not properly peptize the asphaltene, and the colloidal system would not be stable. For example, asphaltene can be precipitated by n-pentane because pentane dilutes the colloidal system and makes the media less aromaticity, low average molecular weight and low polarity. When heating disturbs vacuum residue system, the molecules move fast, the micelle made up of asphaltene and media would become loser, some of asphaltene molecules may bump off the micelle cages to coalesce. The vacuum residue colloidal system can also be disturbed by some fine solid polar particles due to the adsorption of asphaltene molecules to these particles. At high heating severity, some weak bonds in asphaltene molecules may crack. Asphaltene micelles may break apart; some asphaltene molecules may physically coalesce or chemically interact to form large molecules. At the same time, the ability for media to peptize asphaltene molecules becomes lower due to light fractions

increasing, thus causing asphaltene molecules to coalesce and to be precipitated.

All these factors can account for the initial coke formation of vacuum residue reaction system. In fact, the initial coke is the physical-chemically-coalescent phase of asphaltene molecules, whose properties are very similar to those of asphaltene-coke precursor. Hence initial coke may have high an affinity for asphaltene molecules and promote coalescence of asphaltene molecules and coke formation.

In order to testify the effect of the initial coke on reaction system, Liaohe VR with some pre-added coke powders was subjected to thermal treatment and hydrocracking tests. The thermal treatment under atmospheric nitrogen gas was conducted in a quartz tube reactor (30 ml) heated by an electric tin bath, other tests were carried out in an autoclave of 100 ml under 7MPa hydrogen gas. The results were tabulated in table 6.

Coke formation was about 0.73% for Liaohe VR thermal treatment under conditions of 406°C 2hr and nitrogen atmosphere. When 0.5% coke was pre-added in the thermal treatment system, total coke was about 1.93%, net coke formation was 1.20%, net coke increment was about 0.47% contrast to blank test without pre-added coke; 1% pre-added coke promoted 1.22% net coke formation compared with the blank thermal treatment. It was obvious that initial coke could considerably promote coke formation during thermal treatment of vacuum residue under low pressure (a relatively open system). In hydrothermal treatment of VR, it seemed, superficially, that pre-added coke was of little influence on coke formation. In fact, the Ni, Fe in pre-added coke might act as hydrocracking catalysts, the catalytically active hydrogen could saturate the coke precursor free radicals and chemically inhibit condensation of these free radicals, thus inhibit the coke formation. The counteraction between the coke promotion by initial coke and the coke inhibition by heavy metals in the coke makes total coke formation similar to the coke formation in virgin hydrothermal treatment. In the catalytic hydrocracking process, pre-added coke could markedly inhibit net coke formation. In addition to activating hydrogen, the pre-added coke and Mo sulfide solid particles were of high affinity for asphaltene free radicals, and made these coke precursor radicals adsorbed around them. Thus, the active hydrogen on catalysts could instantly terminate coke precursor radicals; thus the coke inhibition efficiency was enhanced. The performance for catalyst particles to enrich asphaltene-coke precursors around them and to promote the utilization of active hydrogen may be the important factors for slurry-bed catalytic hydrocracking of heavy oils to effectively inhibit coke formation.

CONCLUSION

The SARA group composition of Liaohe VR is similar to that of Gudao VR, the nature of its oil fraction is even better than that of the Gudao VR counterpart, but its resin and asphaltene fractions are much inferior to those of Gudao VR. The uniformity of Liaohe VR system is lower than that of Gudao VR, its colloidal system is not stable, and the coke formation tendency is high during further processing.

With processing severity increasing, coke formation in VR reaction system is developed from dispersed fine particles to coke clusters. FTIR technique can effectively characterize the evolution of aromatic part and paraffinic part of the coke formed at different severity.

The initial coke could promote coke formation during low-pressure thermal treatment of VR. During hydrothermal and hydrocracking treatments, pre-added coke seems to promote catalysis.

LITERATURE CITED

1. Weihe, I. A., *Ind. Eng. Chem. Res.*, **31**: 530(1992)
2. Weihe, I. A., *Ind. Eng. Chem. Res.*, **32**: 530(1993)
3. Xu, Y.-M., *Acta Petrolei Sinica (Petroleum Processing Section)*, **1**(3): 13(1985)
4. Que, G.-h. *Fuel*, **71**:1483(1992)
5. Weihe, I. A., *PREPRINTS, Div. Petol. Chem., ACS*, **38**: 428(1993)
6. Li, S.-h., Liu, C.-G., Que, G.-H., Liang, W.-J., *Fuel*, **75**:1025(1996)
7. Deng, W.-A., Que, G.-H., *Acta Petrolei Sinica (Petroleum Processing Section)*, **13**(1): 1(1997)
8. Wang, Z.-X., Que, G.-H., Liang, W.-J., *PREPRINTS, Div. Petol. Chem., ACS*, **43**(1): 155(1998)

Table 1 Properties of Liaohe vacuum residue (VR)

Property	Liaohe VR	Gudao VR
Density(20°C), g/cm ³	0.9976	0.9998
Viscosity(100°C)/mm ² .s ⁻¹	3375	1710
Pour point, °C	42	41
Flash point, °C	312	327
Carbon residue, %	19.0	15.6
Elemental composition		
C, %	87.0	85.4
H, %	11.4	11.4
S, %	0.43	2.52
N, %	1.08	0.80
H/C(Atomic ratio)	1.50	1.60
Total Metal/PPM		
Ni, PPM	122.6	48.0
V, PPM	2.9	2.2
Fe, PPM	37.5	13.8
Ca, PPM	95.6	33.8
Ash, %	0.056	0.026
SARA fractions:		
Saturates, %	17.1	14.5
Aromatics, %	30.3	34.8
Resins, %	50.2	47.2
nC7-Asphaltene, %	2.1	3.5
Structural Parameters		
F _A	0.267	0.181
F _N	0.258	0.330
R _A /R _N	0.93	0.47

Table 2 Properties of oil fraction of Liaohe VR

Properties	Oil fraction of Liaohe VR	oil Fraction of Gudao VR
Density(20°C), g/cm ³	0.9392	0.9558
Viscosity(100°C), mm ² .s ⁻¹	84.1	103.0
Pour point, °C	36.0	39.0
Carbon residue, %	3.5	5.8
MW	630	860
Elemental composition		
C, %	87.2	85.0
H, %	12.3	11.9
S, %	0.34	2.0
N, %	0.33	0.45
H/C(Atomic ratio)	1.68	1.67
Metals		
Ni, PPM	1.3	6.0
V, PPM	2.4	/
Ca, PPM	1.1	19.8

Table 3 Properties and composition of six fractions of Liaohe VR

Property	F1	F2	F3	F4	F5	nC ₅ -At
<i>Liaohe VR:</i>						
Yield, %	36.1	11.6	16.8	9.0	12.3	14.2
MW	590	810	1050	1380	2240	5970
f _A	/	/	0.329	0.357	0.371	0.509
f _N	/	/	0.201	0.153	0.151	0.082
R _A /R _N	/	/	1.5	2.2	2.4	6.2
H/C	1.75	1.48	1.44	1.41	1.38	1.19
N, %	0.16	0.85	1.42	1.70	1.78	1.96
N _f /N _T , %	2.1	10.8	18.0	21.6	22.6	24.9
Ni, ppm		1.3	197.3		225.2	502.3
Ni _f /Ni _T , %		0.2	21.3		24.3	54.3
CCR, %		3.5	23.2		31.1	45.3
CCR _f /CCR _T , %		3.4	22.5		30.2	43.9
<i>Gudao VR:</i>						
Yield, %	34.9	14.2	15.6	7.9	8.8	15.9
MW	800	1000	1370	1760	2430	3920
f _A	/	/	0.285	0.290	0.297	0.437
f _N	/	/	0.149	0.182	0.166	0.128
R _A /R _N	/	/	1.8	1.5	1.7	3.3
H/C	1.83	1.50	1.51	1.49	1.48	1.29
N, %	0.10	0.75	1.17	1.37	1.43	1.48
N _f /N _T , %	4.2	12.9	21.9	13.0	19.7	28.3
Ni, ppm	0.6	9.7	109.1	43.7	49.6	127.3
Ni _f /Ni _T , %	0.4	2.9	35.7	7.2	12.0	41.8
CCR, %	2.4	15.9	21.7	23.6	21.7	41.8
CCR _f /CCR _T , %	4.8	12.9	19.3	10.6	14.5	37.9

MW- molecular weigh t. N_f/N_T-the ratio of nitrogen in fraction to total nitrogen in VR

Ni_f/Ni_T-the ratio of nickel in fraction to total nickel in VR

CCR_f/CCR_T-the ratio of carbon residue of fraction to total carbon residue in VR

Table 4 Yields of conversion products under three series of reaction conditions
(Reaction time 1hr)

Reaction condition			<450°C product, %	>450°C cracked residue, %	Coke, %	nC ₅ -At in cracked residue	
						%	MW
N2 5MPa	400		37.7	62.2	0.1	/	/
	410		44.4	54.2	1.4	24.6	3349
	420		67.1	32.9	10.9	15.8	2829
	430		62.8	17.7	19.5	9.2	1499
H2 7MPa	400		28.27	71.68	0.05	/	/
	410		40.90	59.00	0.10	23.1	3837
	420		50.20	46.60	3.20	17.9	2989
	430		61.40	30.78	7.92	13.3	1979
H2 7MPa Mo 200ppm	400		18.95	81.00	0.05	/	/
	410		25.60	74.31	0.09	/	/
	420		35.54	64.24	0.22	15.8	3477
	430		50.19	49.13	0.68	14.8	2932
	440		53.79	42.0	4.21	12.2	2063

Table 5 Relations between coke FTIR Data and reaction conditions

Coke samples	A ₂₉₂₀	A ₂₈₆₀	A ₃₀₃₀	A ₈₇₀	A ₈₁₀	A ₇₅₀
N ₂						
410°C	0.780	0.493	0.060	0.271	0.206	0.185
420°C	0.650	0.426	0.095	0.283	0.243	0.241
430°C	0.273	0.210	0.098	0.349	0.312	0.294
H ₂ , Mo200ppm						
425°C	0.574	0.385	0.068	0.280	0.152	0.149
430°C	0.375	0.256	0.058	0.278	0.210	0.184
435°C	0.265	0.176	0.060	0.214	0.215	0.196
440°C	0.183	0.155	0.030	0.390	0.422	0.406

Table 6 Effect of initial coke on coke formation of reaction system

Reaction condition	sample	<450°C product, %	>450°C cracked residue, %	** coke, %	*** coke increment, %
* N ₂ (blowing), 2hr					
406°	LHVR	/	/	0.73	
406°	LHVR+0.5%coke	/	/	1.20	0.47
406°	LHVR+1.0%coke	/	/	1.95	1.22
H ₂ , 7MPa, 2hr					
412°	LHVR	53.37	43.70	2.93	
412°	LHVR+0.5%coke	54.06	42.50	2.94	0.01
H ₂ , 7Mpa, 2hr Mo, 200ppm					
425°	LHVR	56.87	41.50	1.63	
425°	LHVR0.5%coke	52.96	45.40	1.14	-0.49

* conducted by using a quartz tube reactor with N₂ as a blowing gas ;

** net coke formation, i.e., total coke minus added coke.

*** coke increment on the base of blank test.

AUTHOR INDEX, VOLUME 43, (ISSUE NUMBER) PAGE NUMBER

Aceves, S. M.	(3) 570	Chang, C. H.	(3) 580
Ahmed, S.	(3) 543	Chang, R.	(4) 871
Ali, M. F.	(4)1063	Chavadej, S.	(3) 490
Ali, S. A.	(3) 543	Chen, S.	(3) 596
Allardice, D. J.	(3) 407	Chen, S.	(4) 871
Allen, M.	(3) 575	Cheng, H.	(4) 990
Amadeo, N. E.	(3) 689	Chinn, M. J.	(4) 885
Amouroux, J.	(4) 890	Chippes, J. F.	(4)1057
Anderson, D. A.	(4)1069	Chocrón, M.	(3) 689
Andriollo, A.	(3) 563	Chollar, B.	(4)1031
Antal, M. J.	(3) 363	Chollar, B. H.	(4)1083
Antal, M. J.	(4) 825	Chollar, B. H.	(4)1090
Arenillas, A.	(4)1120	Chollar, B. H.	(4)1096
Arenillas, A.	(4)1133	Chu, I.	(3) 451
Armour, S. J.	(4)1115	Chung, K.	(4) 929
Atha, T.	(4)1045	Clarkson, R. B.	(4) 955
Aulich, T.	(3) 383	Comolli, A. G.	(3) 441
Aurilio, V.	(4)1031	Contescu, A.	(4) 833
Badger, M. W.	(3) 461	Contescu, C. I.	(4) 833
Bahia, H. U.	(4)1041	Cook, W.	(3) 727
Baker, J. J.	(3) 727	Cotte, E.	(3) 678
Baleo, J. N.	(4) 875	Coulibaly, K.	(4) 890
Ban, H.	(4)1010	Crelling, J. C.	(4) 924
Banfield, T. L.	(4) 995	Cyr, T.	(3) 496
Barnakov, Ch. N.	(4)1107	Dai, X.	(4) 825
Barnes, P. A.	(4) 885	Daly, W. H.	(4)1075
Bates, D. R.	(3) 575	Davini, P.	(4)1129
Beisel, A. J.	(4) 995	Davison, R. R.	(4)1057
Belford, R. L.	(4) 955	Dawson, E. A.	(4) 885
Benedetti, M. F.	(4) 829	Demirel, B.	(3) 466
Benham, M.	(4) 770	Demirel, B.	(3) 501
Bermejo, J.	(4) 941	Dente, M.	(3) 653
Berry, G. D.	(3) 570	Desai, S.	(4) 814
Beznisko, S. I.	(4) 838	Dieterle, M.	(3) 501
Bi, J.	(3) 703	Dongré, R.	(4)1019
Bi, J.	(3) 707	Du, F.	(3) 668
Billiter, T. C.	(4)1057	Du, F.	(3) 673
Biswas, M. E.	(3) 543	Du, F.	(3) 751
Blackwell, A. G.	(3) 645	Dubois, A. M.	(3) 640
Bockrath, B.	(3) 694	DuBose, S. B.	(4) 796
Bockrath, B.	(3) 717	Dunham, G. E.	(4) 867
Borole, A. P.	(3) 506	Dutta, R.	(3) 538
Boudou, J-P.	(4) 829	Economy, J.	(4) 880
Bozzano, G.	(3) 653	Embaid, B. P.	(3) 521
Brackman-Danheux, C.	(4) 857	Enomoto, H.	(3) 741
Branthaver, J.	(4)1037	Enqvist, J.	(3) 400
Brasquet, A.	(4) 970	Enqvist, M.	(3) 400
Bridges, J. L.	(4) 796	Erdmann, K.	(4) 905
Britt, P. F.	(3) 630	Eser, S.	(3) 471
Buchanan, A. C.	(3) 630	Eser, S.	(3) 611
Caldwell, T. A.	(3) 490	Espino, R. L.	(3) 388
Carrillo Guarin, J. A.	(3) 431	Fairbridge, C.	(3) 476
Casal, E.	(4) 941	Fedorak, P. M.	(3) 515
Ceroke, P.	(4) 955	Fernandes, F. A. N.	(3) 621
Cerqueira, H. S.	(3) 626	Ferrance, J. P.	(3) 694

AUTHOR INDEX, VOLUME 43, (ISSUE NUMBER) PAGE NUMBER

Filgueiras, E.	(3) 521	Holland, J.	(3) 727
Finseth, D.	(4)1010	Hong, C. X.	(3) 741
Foght, J. M.	(3) 515	Howard, B. H.	(4) 862
Fontana, A.	(4) 857	Hower, J. C.	(4) 975
Frommell, E.	(3) 717	Hower, J. C.	(4)1014
Fuentes, A.	(3) 563	Huang, B. Y.	(3) 606
Fujii, M.	(3) 735	Hudgins, R. R.	(4) 844
Fuller, E. L.	(4) 770	Hurt, R.	(4) 965
Fuller, E. L.	(4) 775	Hurt, R. H.	(4) 980
Furutsuka, T.	(4)1125	Iino, M.	(3) 712
Galiasso, R. E.	(3) 563	Iglesias, M. J.	(4) 820
Gamble, V.	(4) 913	Ingram, J. P.	(3) 575
Gao, Y.-M.	(4) 980	Ishihara, S.	(4)1125
García, A.	(4) 820	Itoh, Y.	(4) 852
Gentzis, T.	(4) 929	Iwamatsu, E.	(3) 543
Gentzis, T.	(4) 933	James, B. D.	(3) 568
Gerlach, T.	(3) 383	Jaroniec, M.	(4) 780
Gibbins, J. R.	(4)1000	Joaquim de Souza, E. J.	(3) 640
Gibbins, J. R.	(4)1138	Johns, M. M.	(4) 805
Giles, K. A.	(4) 995	Johns, M. M.	(4) 810
Giray, E. S.	(3) 712	Judd, R. W.	(3) 575
Givens, E. N.	(3) 466	Kamimura, H.	(3) 741
Givens, E. N.	(3) 501	Kamo, T.	(3) 658
Gladding, D. T. M.	(3) 575	Kamo, T.	(3) 703
Glover, C. J.	(4)1057	Kamo, T.	(3) 707
Gonzalez-Gimenez, F.	(3) 521	Kaufman, E. N.	(3) 506
Graham, U. M.	(4) 985	Kawano, S.	(4) 848
Granda, M.	(4) 941	Kawashima, H.	(3) 699
Gray, M. R.	(3) 515	Keller, M.	(3) 717
Gray, R. J.	(4) 924	Kern, D.	(3) 717
Gregoire Padró, C. E.	(3) 353	Kern, D. G.	(4) 995
Grosso, J. G.	(4) 985	King, W. P.	(4) 995
Guisnet, M.	(3) 626	Kishita, A.	(3) 741
Gülder, Ö. L.	(3) 435	Kodera, Y.	(3) 658
Guo, A.-J.	(3) 486	Kodera, Y.	(3) 703
Guo, A.-J.	(3) 530	Kodera, Y.	(3) 707
Guo, A.-J.	(3) 758	Kondo, T.	(4)1125
Guran, S.	(4) 990	Korai, Y.	(4) 848
Hada, T.	(4) 848	Kornievich, M. V.	(4) 838
Hagaman, E. W.	(4) 951	Kosbab, S.	(4) 796
Hamid, H.	(3) 543	Kozlov, A. P.	(4)1107
Hamilton, J. R.	(3) 407	Krivohlavek, D. D.	(4)1102
Harke, F. W.	(3) 645	Kroo, E.	(4)1005
Harrigan, E.	(4)1031	Kruk, M.	(4) 780
Hatcher, P. G.	(3) 611	Külaots, I.	(4) 980
Hattori, H.	(3) 426	Kurose, H.	(3) 712
Hawkins, R. W. T.	(3) 496	Kuvshinov, D. G.	(4) 946
Hequet, V.	(4) 875	Kuvshinov, G. G.	(4) 895
Herrmann, J.-M.	(4)1112	Kuvshinov, G. G.	(4) 946
Hidalgo, R.	(3) 368	Kyotani, T.	(4) 960
Hill, R. L.	(4) 975	Lablanchy, P.	(4) 829
Ho, K.	(4) 801	Laborde, M. A.	(3) 689
Ho, S.	(4)1026	LaCount, R.	(3) 717
Hodrien, R. C.	(3) 575	LaCount, R. B.	(4) 995
Hogan, E. N.	(3) 416	Ladner, E. P.	(3) 645

AUTHOR INDEX, VOLUME 43, (ISSUE NUMBER) PAGE NUMBER

Laine, J.	(4)1112	McGreavy, C.	(3) 684
Le Cloirec, P.	(4) 875	Memom, G. M.	(4)1045
Le Cloirec, P.	(4) 970	Memom, G. M.	(4)1083
Lebedev, M. Yu.	(4) 895	Memom, G. M.	(4)1090
Lee, J. M.	(3) 727	Memom, G. M.	(4)1096
Lee, S.	(3) 722	Memom, M.	(4)1019
Lee, T. L. K.	(3) 441	Menéndez, E. M.	(4) 820
Lemberton, J. L.	(3) 547	Menéndez, J. A.	(4) 820
Lewandowski, M.	(4) 909	Menéndez, R.	(4) 941
Li, P.-P.	(3) 558	Mercer, M.	(4) 770
Li, T. X.	(4)1010	Michaud, P.	(3) 547
Li, X.	(3) 435	Mikuni, M.	(3) 426
Liang, S. H. C.	(4)1115	Mill, T.	(4)1053
Lin, S.	(3) 673	Miller, S. J.	(4) 867
Lin, S.	(3) 746	Miyamoto, S.	(4) 848
Linkous, C. A.	(3) 358	Mochida, I.	(4) 848
Linkous, C. A.	(3) 378	Mogilnykh, Yu. I.	(4) 895
Liu, C.	(3) 481	Mogilnykh, Yu. I.	(4) 946
Lizzio, A. A.	(4) 814	Mohan, T.	(4) 905
Lizzio, A. A.	(4) 862	Mojelsky, T. W.	(3) 526
Llerena, R.	(3) 727	Mojelsky, T. W.	(4) 917
Lobban, L. L.	(3) 490	Moliner, R.	(4) 857
Lona Batista, L. M. F.	(3) 616	Morales, A.	(3) 521
Lona Batista, L. M. F.	(3) 621	Moriya, T.	(3) 741
López-Linares, F.	(3) 563	Mota, J. P. B.	(3) 601
Lown, E. M.	(4) 917	Nagaishi, H.	(3) 426
Machín, I.	(3) 678	Neathery, J. K.	(4)1010
Maciel Filho, R.	(3) 616	Negulescu, I. I.	(4)1075
Magnoux, P.	(3) 626	Ng, F. T. T.	(3) 456
Maier, W. F.	(3) 534	Nishimiya, K.	(4)1125
Majors, R. K.	(4) 975	Norman, P. R.	(4) 885
Mallinson, R. G.	(3) 490	Nowlan, V.	(4) 929
Man, C. K.	(4)1138	Nunhez, J. R.	(3) 649
Mangun, C.	(4) 880	Odintsov, B. M.	(4) 955
Marasteanu, M. O.	(4)1069	Okuyama, Y.	(3) 707
Markowitz, B. L.	(3) 585	Olah, G. A.	(3) 526
Maroto-Valer, M. M.	(4)1014	Olson, E. S.	(3) 447
Marran, D. F.	(4)1005	Olson, E. S.	(4) 867
Marsh, N. D.	(4) 990	Orikasa, H.	(4) 852
Marshall, W. E.	(4) 805	Ovalles, C.	(3) 521
Marshall, W. E.	(4) 810	Páez, D. E.	(3) 563
Martin, D.	(3) 626	Painter, P. C.	(4) 913
Martin, S.	(3) 538	Palit, A. K.	(3) 392
Martinez-Alonso, A.	(4) 829	Panthaky, M.	(4) 844
Mathews, J. P.	(3) 611	Pantoja, F.	(3) 431
Matos, J.	(4)1112	Parfitt, D.	(3) 717
Matsubara, K.	(3) 707	Park, C.	(3) 368
Matsuoka, K.	(4) 852	Parker, R. J.	(4) 933
Mayes, A. M.	(3) 606	Parra, J. B.	(4)1120
McCormick, C. J.	(4) 985	Parra, J. B.	(4)1133
McFarland, S. J.	(4)1090	Patwardhan, S. R.	(4) 765
McFarlane, R. A.	(3) 496	Paul, S. F.	(3) 373
McFarlane, R. A.	(4) 933	Payzant, J. D.	(3) 526
McGreavy, C.	(3) 635	Peixoto, S. M. C.	(3) 649
McGreavy, C.	(3) 653	Peng, P.	(4) 917

AUTHOR INDEX, VOLUME 43, (ISSUE NUMBER) PAGE NUMBER

Perot, G.	(3) 547	Satou, M.	(3) 426
Pickard, M. A.	(3) 515	Scaroni, A. W.	(3) 611
Pignon, H.	(4) 970	Schaefer, J. L.	(4)1010
Pilawa, B.	(4) 909	Schobert, H. H.	(3) 461
Pis, J. J.	(4) 820	Schobert, H. H.	(3) 538
Pis, J. J.	(4)1120	Schukin, L. I.	(4) 838
Pis, J. J.	(4)1133	Schwarz, J. A.	(4) 833
Plummer, M.	(3) 538	Scott, C. E.	(3) 521
Plummer, M. A.	(3) 552	Serio, M. A.	(3) 585
Poon, R.	(3) 451	Serio, M. A.	(4)1005
Poonphatanaricha, P.	(3) 490	Sharma, A.	(4) 960
Popper, G. A.	(3) 441	Sharma, R. K.	(4) 801
Prada, V.	(4) 941	Sharma, R. K.	(4) 867
Prakash, G. K. S.	(3) 526	Shen, R.	(3) 481
Que, G.	(3) 481	Shi, B.	(3) 558
Que, G.-H.	(3) 486	Shim, H.-S.	(4) 965
Que, G.-H.	(3) 530	Shimizu, K.	(3) 699
Que, G.-H.	(3) 558	Siddiqui, M. N.	(4)1063
Que, G.-H.	(3) 758	Silveston, P. L.	(4) 844
Quin, J. L.	(4) 900	Simons, G. A.	(3) 585
Rahimi, P.	(3) 476	Singh, H. K.	(3) 447
Rahimi, P.	(4) 929	Slattery, D. K.	(3) 378
Rathbone, R. F.	(4) 975	Sobkowiak, M.	(4) 913
Renou-Gonnord, M. F.	(4) 890	Song, C.	(3) 552
Reucroft, P. J.	(4) 785	Soo, P. P.	(3) 606
Revette, J. A.	(3) 563	Soong, Y.	(3) 645
Rivin, D.	(4) 785	Stalzer, R. H.	(3) 441
Robbins, J. L.	(3) 388	Stastna, J.	(4)1026
Robl, T. L.	(4) 985	Steinberg, M.	(3) 412
Rodriguez, N. M.	(3) 368	Stella, A.	(3) 580
Rolle, J. G.	(3) 727	Stencel, J. M.	(3) 591
Rood, M. J.	(3) 596	Stencel, J. M.	(4)1010
Rood, M. J.	(4) 814	Strausz, O. P.	(3) 526
Rostam-Abadi, M.	(3) 596	Strausz, O. P.	(4) 917
Rostam-Abadi, M.	(4) 871	Su, M.	(4)1053
Rubel, A. M.	(3) 591	Subrenat, E.	(4) 875
Rubiera, F.	(4)1120	Subrenat, E.	(4) 970
Rubiera, F.	(4)1133	Subrenat, A.	(4) 875
Rudina, N. A.	(4) 946	Suelves, I.	(4) 857
Russell, N. V.	(4)1000	Suganuma, A.	(3) 699
Russell, N. V.	(4)1138	Sugaya, M.	(3) 635
Sadoway, D. R.	(3) 606	Sugaya, M.	(3) 653
Saito, I.	(3) 699	Sugaya, M.	(3) 684
Sakanishi, K.	(4) 848	Sun, J.	(3) 596
Salanov, A. N.	(4) 946	Suuberg, E. M.	(4) 980
Sanada, Y.	(3) 543	Takahashi, S.	(3) 741
Sanada, Y.	(3) 735	Takanohashi, T.	(3) 712
Sánchez-Delgado, R.	(3) 563	Tam, M. S.	(4) 825
Sardesai, A.	(3) 722	Tan, C. D.	(3) 368
Sasaki, M.	(3) 552	Tanner, D.	(3) 476
Sasaki, S.	(3) 699	Tascon, J. M. D.	(4) 829
Sato, M.	(3) 735	Taulbee, D. N.	(4)1014
Sato, Y.	(3) 658	Taylor, R.	(4)1031
Sato, Y.	(3) 703	Thomas, A.	(3) 466
Sato, Y.	(3) 707	Tierney, J. W.	(3) 421

AUTHOR INDEX, VOLUME 43, (ISSUE NUMBER) PAGE NUMBER

Timpe, R. C.	(4) 801	Yoneda, T.	(3) 735
Toles, C. A.	(4) 805	Yoshida, T.	(3) 426
Toles, C. A.	(4) 810	Yoshikawa, M.	(4) 848
Tomita, A.	(4) 852	Young, B. C.	(3) 407
Tomita, A.	(4) 960	Youtcheff, J.	(4)1037
Trahan, A. D.	(4) 796	Yu, Z.	(4) 905
Vartapetjan, R. S.	(4) 838	Zanzotto, L.	(4)1026
Vassilev, S.	(4) 857	Zarochak, M. F.	(3) 645
Vayenas, C. G.	(3) 663	Zhai, H.	(4)1041
Verkade, J. G.	(4) 905	Zhan, X.	(3) 501
Vladea, R. V.	(4) 844	Zhang, H.-Y.	(3) 486
Vogel, C.	(3) 403	Zhang, H.-Y.	(3) 530
Walsh, P. M.	(3) 611	Zhang, J.	(3) 746
Wang, Z.-X.	(3) 486	Zhang, S.	(3) 421
Wang, Z.-X.	(3) 530	Zheng, H.	(3) 668
Wang, Z.-X.	(3) 758	Zhou, P.	(3) 441
Warzinski, R. P.	(3) 694	Zondlo, J.	(4) 790
Wender, I.	(3) 421		
Wertz, D. L.	(4) 796		
Wertz, D. L.	(4) 900		
White, R.	(3) 727		
Wieckowski, A. B.	(4) 909		
Williams, C.	(4)1037		
Williamson, J.	(4)1000		
Williamson, J.	(4)1138		
Wójtowicz, M. A.	(3) 585		
Wójtowicz, M. A.	(4)1005		
Wornat, M. J.	(4) 990		
Wu, Q.	(3) 515		
Xiao, X.	(3) 421		
Xu, C.	(3) 668		
Xu, C.	(3) 673		
Xu, C.	(3) 746		
Xu, C.	(3) 751		
Xu, X.	(3) 363		
Xu, Y.	(4) 790		
Yagelowich, M.	(3) 447		
Yamaguchi, H.	(3) 703		
Yamaguchi, H.	(3) 707		
Yamane, T.	(4)1125		
Yang, C.	(3) 668		
Yang, C.	(3) 673		
Yang, C.	(3) 746		
Yang, C.	(3) 751		
Yang, M.-G.	(3) 471		
Yang, N.	(4) 965		
Yao, D.	(4)1053		
Yasutake, A.	(4) 848		
Yatsunami, S.	(4) 848		
Yee, E. C.	(4)1115		
Yeh, P.-H.	(4)1075		
Yermakov, D. Yu.	(4) 946		
Yermakova, M. A.	(4) 946		
Yiokari, C. G.	(3) 663		
Yoneda, T.	(3) 543		